DISS. ETH NO. 26408

TRACING SURFACE WATER-GROUNDWATER INTERACTIONS WITH IN-SITU NOBLE GAS ANALYSIS

A thesis submitted to attain the degree of
DOCTOR OF SCIENCES of ETH ZURICH
(Dr. sc. ETH Zurich)

presented by

ANDREA POPP

M.Sc. Hydrology, Albert-Ludwigs-Universität Freiburg

born on 07.09.1988

citizen of Germany

accepted on the recommendation of

Prof. Rolf Kipfer, examiner
Prof. Bernard Wehrli, co-examiner
Dr. Jörg Lewandowski, co-examiner

2019

Für meine Eltern.

ACKNOWLEDGMENTS

Writing this thesis would not have been possible without the support of many people to whom I am very grateful. First, I want to thank my advisor, Rolf Kipfer, for giving me a lot of freedom and allowing me to stir my research in the directions I am most excited about. Thank you for your trust and guidance.

Second, I would like to thank the co-referees of my dissertation—Bernhard Wehrli and Jörg Lewandowski. Thank you for taking the time to review and evaluate my work. A special thank-you goes to Jörg for hosting me at IGB Berlin and for leading the E.U. project "HypoTRAIN", which financed the main part of my thesis and which provided countless opportunities for me to grow as a scientist.

I am grateful to many of my colleagues, who supported me during my PhD: Andreas Scheidegger, Oliver Schilling, Christian Möck, Henner Busemann and Colin Maden, as well as various people from University of Neuchâtel (Álvaro Pardo-Álvarez, Morgan Peel, Philip Brunner), University of Bern (Stéphanie Musy, Roland Purtschert) and UBC (Cara Manning, Julia Soares, Jessy Tse-Hua, Roger Beckie). Thank you for many insightful discussions and for giving me the opportunity to learn from you. Sincere thanks also go to the students and technicians involved during field work: Wendelin Wild, Benjamin Plüss, Reto Britt, Jonas Zbinden, Laurent Marguet, Roberto Costa, Kay Fries and Andreas Raffainer. Thank your for your support!

Additionally, I want to thank my fellow students and colleagues from Eawag and ETH, who contributed to a pleasant and stimulating working environment. Special thanks go to the UI group members Elaheh, Edith, Alex, Uli, Yama and Lina. I am also grateful to the extended Eawag group: Maricor, Nicole, Max, Robin, Sandra, Andres, Ishaan, Erfan, Jagannath, Silvan, Johanna, Nicolas, Marianne, Matthew, Giorgia, Isabell and Susan—thanks for your support, interesting conversations and many laughs during the last four years!

Special thanks go to everyone involved with the Young Hydrologic Society and the EGU hydrology division community. I am particularly grateful for my friends Stefanie and Tim, who helped me in various ways to become a better scientist and always fostered my self-confidence! A big thank-you also goes to Sina, Harsh, Nilay, Wouter B., Wouter K., Shaun, Hannes, Lina, Alex and Caitlyn for all your enthusiasm and the fun times we have together—I am glad to be part of such an inspiring early-career community and hope we will continue working together! Thanks are

also in order for the great support EGU and AGU provide for initiatives by early-career scientists (special thanks to Claudia Jesus-Rydin, Barbara Ferreira and Alberto Montanari as well as countless people behind the scenes).

Also, I want to acknowledge a few key people, who sponsored me earlier in or during my career: Christoph Külls for his ingenious ideas and enlightening conversations about stable water isotopes, Thomas Harter, who showed me what excellent teaching looks like and inspired me to pursue hydrogeology, Mario Schirmer for his mentoring and guidance and Kamini Singha for being an awesome role model—thank you all, truly!

I also thank the friends I met en route of this PhD and who contributed in one way or another to its success: Mikhail, Skuyler, Jannes, Imanol, Ralf, Chiara, Andrea, Matt, Rozemarijn, Robin, DJ, Lex, Dominic, Alan, Julia and Josh. Thanks for your inspiration and enthusiasm!

I would also like to express my gratitude to my friends from home and university, different orchestras and Ultimate Frisbee teams: thank you for the many hours of distraction and fun!

I owe a debt of gratitude to my sister Lisa and my extended family, especially Christine, Christa, Adelheid and Reinhold. Thank you for your unconditional kindness and support!

Lastly, my deepest gratitude goes to my parents Klara and Johann Popp, and my partner Jendrik for always believing in me and all their support. I am very lucky to have you in my life.

SUMMARY

The interactions between surface water (SW) and groundwater (GW) are critical for the quality and quantity of both water resources as they influence each other. SW–GW exchange patterns are governed by river discharge, groundwater pumping, and the heterogeneity of the streambed and the aquifer. The interplay of these drivers can lead to complex feedback mechanisms that remain poorly understood, mainly due to insufficient data availability. To better understand how and when these processes affect the quality and quantity of shallow groundwater, appropriate data with a high spatio-temporal resolution are needed.

This thesis furthers the understanding of SW-GW exchange dynamics by addressing the following questions: (1) how do recently infiltrated river water and regional groundwater mix in complex aquifer systems?, (2) how dynamic are the groundwater fractions of river water and its travel times in an alluvial aquifer?, and (3) how variable are spatio-temporal dynamics of denitrification in riparian groundwater? These questions are tackled by employing (noble) gas tracers analyzed in-situ in different groundwater systems.

Dissolved noble gases are an ideal, yet often untapped tool to gain a better understanding of SW–GW interactions. Noble gases are ubiquitous in natural waters and chemically inert. Therefore, their fractionation and concentrations contain rich information that can shed light on groundwater recharge and travel times. A combined analysis of noble and reactive gases can also be used to study biogeochemical reactions such as denitrification or oxygen turnover in groundwater.

In this thesis, the in-situ use of a portable mass spectrometry system enabled high-resolution sampling of groundwater to acquire either spatially and/or temporally resolved (noble) gas data. The insights obtained from the (noble) gas data combined with other methods helped to derive the following key contributions of this thesis:

(1) On-site ^{4}He analysis combined with a Bayesian modeling framework can identify previously unknown groundwater sources in hydrogeologically complex groundwater systems.

(2) Combined in-situ analyses of ^{4}He and ^{40}Ar concentrations, and ^{222}Rn activities show that about two thirds of alluvial groundwater originate from recently infiltrated river water, which exhibits minimum travel times of 7 to 15 days.

(3) In-situ, continuous (noble) gas analysis (N_2, ^{4}He, ^{40}Ar, ^{84}Kr) can be used to quantify N_2 originating from denitrification showing that denitrification in riparian groundwater is highly variable in space and time.

Overall, this thesis illustrates the need for high-resolution data to accurately delineate the complex nature of SW–GW interactions.

ZUSAMMENFASSUNG

Der Austausch von Fluss- und Grundwasser hat eine grosse Bedeutung für die Qualität und Quantität beider Wasserressourcen, da diese sich gegenseitig beeinflussen. Fluss-Grundwasserinteraktionen werden durch den Abfluss, Grundwasserentnahme und die Heterogenität des Flussbettes und des Aquifers kontrolliert. Die Wechselwirkungen dieser Faktoren kann zu komplexen Rückkopplungsmechanismen führen, die schwer zu erfassen sind. Um zu verstehen wie diese Prozesse die Qualität und Quantität von Grundwasser beeinflussen, sind Daten mit einer hohen zeitlichen und räumlichen Auflösung nötig.

Diese Arbeit fördert das Verständnis der Austauschdynamik von Fluss- und Grundwasser durch die Bearbeitung folgender Fragen: (1) Wie mischen sich kürzlich infiltriertes Flusswasser und regionales Grundwasser in komplexen Aquiferen?, (2) wie dynamisch sind die Grundwasseranteile von infiltriertem Flusswasser und deren Verweilzeiten innerhalb eines alluvialen Aquifers?, und (3) wie variabel sind die zeitlichen und räumlichen Dynamiken von Denitrifizierung in flussnahem Grundwasser? Diese Fragen werden beantwortet durch den Einsatz von in-situ analysierten (Edel-)Gas-Tracern.

Gelöste Edelgase sind ein ideales, jedoch selten angewandtes, Werkzeug, um ein besseres Verständnis von Fluss-Grundwasserinteraktionen zu gewinnen. Edelgase sind allgegenwärtig im Wasser und chemisch inert. Deshalb beinhalten gelöste (Edel-)Gase wertvolle Informationen, die Aufschluss über Grundwassererneuerung und Verweilzeiten liefern. Kombiniert man die Analyse von Edelgasen mit reaktiven Gasen, wie O_2 oder N_2, können auch biogeochemische Reaktionen wie Sauerstoffumsetzung und Denitrifizierung im Grundwasser untersucht werden.

Der Vor-Ort-Einsatz eines portablen Massenspektrometer-Systems ermöglichte eine zeitlich und/oder räumlich aufgelöste Aufnahme von (Edel-)Gas-Daten in verschiedenen Grundwassersystemen. Die aus den (Edel-)Gas-Daten in Kombination mit anderen Methoden gewonnenen Erkenntnisse halfen die folgenden Beiträge dieser Arbeit abzuleiten:

(1) Vor Ort analysiertes ^{4}He kombiniert mit einem Bayesschen Model kann die Beimischung von unbekanntem Grundwasser in hydrogeologisch komplexen Grundwassersystemen aufzeigen.

(2) Eine kombinierte in-situ Analyse von ^{4}He, ^{40}Ar und ^{222}Rn Daten zeigt, dass circa zwei Drittel alluvialen Grundwassers von kürzlich infiltrier-

tem Flusswasser stammt, das eine Fliesszeit zwischen 7 und 15 Tagen aufzeigt.

(3) Eine kontinuierliche, Vor-Ort-Analyse von (Edel-)Gasen (N_2, ^{4}He, ^{40}Ar, ^{84}Kr) kann dazu genutzt werden, um von der Denitrifizierung stammendes N_2 zu quantifizieren. Diese Analyse zeigte, dass Denitrifizierung in flussnahem Grundwasser zeitlich und räumlich variabel ist.

Insgesamt verdeutlicht diese Arbeit die Notwendigkeit von räumlich und zeitlich hoch aufgelösten Daten, um die Komplexität von Fluss–Grundwasserinteraktionen besser verstehen zu können.

CONTENTS

Part I

INTRODUCTION

1

OUTLINE

This thesis consists of four parts subdivided into eight chapters:

- **Part i** gives an overview about the motivation of this work and provides theoretical background information about the principles of gas exchange processes that determine gas concentrations of groundwater investigated in this thesis. These principles in turn allow to study the main research questions addressed in this thesis: 1) groundwater mixing and travel times and 2) the quantification of denitrification in groundwater.
- The following parts—**Part ii and Part iii**—comprise the three main studies conducted within this PhD work:
  - Part ii focuses on groundwater mixing between recently infiltrated river water and regional groundwater as well as groundwater travel times elucidated by a combined approach of in-situ (noble) gas analysis and Bayesian and numerical modeling, respectively.
  - Part iii presents a new method to study the spatio-temporal dynamics of denitrification in riparian groundwater using in-situ noble gas analysis.
- All major conclusions and their implications for surface water-groundwater systems originating from this thesis are summarized in **Part iv**. This final part concludes with recommendations and potential future research ideas for the application of in-situ noble gas analysis at the intersection of hydrology, hydrogeology and biogeochemistry.
- The Appendix A includes a list of other peer-reviewed research articles that were realized within this PhD.

2

MOTIVATION

This thesis sheds light on the complex physical and biogeochemical processes occurring in shallow aquifers, that are strongly influenced by water exchange with surface water.

In the past, surface water (SW) and groundwater (GW) have long been seen and addressed as two separate resources, while they are, in fact, two interconnected components of the water cycle (e.g., Winter 1995, 1999). Nowadays it is widely recognized that any impact on the quality and quantity of either one resource will inevitably affect the other (e.g., Boano et al. 2014; Brunner et al. 2017).

Globally, shallow groundwater (e.g., river bank filtrate) represents a key water source for drinking water supply and irrigation (e.g., Aeschbach-Hertig et al. 2012; Oki et al. 2006). Shallow groundwater systems are, however, highly susceptible to human interactions and climate change impacts—both of which are projected to negatively affect water resources due to the contamination with known and emerging pollutants as well as extreme events such as droughts and floods (Abbott et al. 2019; Blöschl et al. 2019; Jasechko 2019).

A substantial portion of the renewable water in the hydrologic cycle is diverted for human use (Abbott et al. 2019; Ferguson et al. 2012). Due to a ever growing world population, the human interference with the water cycle is anticipated to intensify in the future (Ferguson et al. 2012). Additionally, climate change will considerably alter the timing and magnitude of water availability in rivers and groundwater (Blöschl et al. 2019; Holman 2006). In many regions in Europe, for instance, dry summers will diminish river discharge (Blöschl et al. 2019), which, in turn, results in an increased load of pollutants (e.g., nutrients, bacteria, pharmaceuticals) that will eventually be transported to aquifers (e.g., C. Sprenger et al. 2011). For a safe supply of potable water and to guarantee sustainable water governance, we need an improved understanding of the complex exchange processes between surface water and groundwater, and how these interactions affect groundwater recharge, travel times and the fate of pollutants.

Although SW–GW interactions have been studied intensely over the last two decades (Brunner et al. 2017), a sound characterization of the spatial and temporal dynamics of water exchange processes and their effects on contaminants remains elusive, due to a lack of efficient methods to address the highly anisotropic and heterogenous subsurface properties as well as the temporal dynamics between SW and GW. Thus, most current tech-

niques used to identify and quantify SW-GW interactions are too costly or time-consuming to obtain highly resolved data-sets that could illuminate the complex nature of groundwater systems (Schilling et al. 2019). Consequently, there is a need for novel, more efficient measurement techniques that allow for high resolution sampling (Brunner et al. 2017; Schilling et al. 2019; M. Sprenger et al. 2019).

Recently, fast and (semi-)autonomous in-situ methods have been developed that can be deployed directly in the field and thus, enable highly resolved data-sets (Brunner et al. 2017; M. Sprenger et al. 2019). One such method is based on in-situ (noble) gas spectrometry consisting of a portable Gas Equilibrium Membrane Inlet Mass Spectrometer (GE-MIMS) that can analyze (noble) gas concentrations in gas or other fluids (Brennwald et al. 2016).

Dissolved noble gases in water serve as ideal tracers to tackle physical as well as biogeochemical groundwater processes because they are biogeochemically inert (e.g., Kipfer et al. 2002). Since noble gases are ubiquitous in the environment, their fractionation and concentration carry valuable information about physical flow paths and travel times of water (Aeschbach-Hertig et al. 1999; Kipfer et al. 2002). Noble gases can also be used to constrain biogeochemical processes occurring in groundwater as they allow physical processes to be separated from biogeochemical reactions: by a combined analysis of noble gases and reactive gases any deviation of the expected reactive gas concentration determined by air/water partitioning during groundwater recharge can be attributed to biogeochemical mechanisms such as oxygen turnover or denitrification in groundwater (Mächler et al. 2013a). Consequently, noble gases allow to assess and quantify the fate of reactive gas species such as O_2 or N_2 (e.g., Kipfer et al. 2002; Mächler et al. 2013a).

The objective of this PhD thesis is to characterize surface water–groundwater interactions, and their implications on biogeochemical processes on various spatial and temporal scales by deploying (noble) gas data analyzed on-site, combined with different modeling approaches.

3

CONCEPTUAL ASPECTS AND RESEARCH QUESTIONS

In this multidisciplinary thesis a variety of methods (i.e., tracers, Bayesian and numerical modeling) were combined to investigate physical and biogeochemical aspects of surface water-groundwater interactions. Every method used to address each specific research question is explicitly described in the respective chapters (Chapters 4 to 6).

The core method employed in this thesis is in-situ (noble) gas analysis in groundwater using a portable Gas Equilibrium Membrane Inlet Mass Spectrometer (GE-MIMS) system (Brennwald et al. 2016). This system allows for fast and efficient measurements of (noble) gases dissolved in water (mainly N_2, O_2, He, Ar, Kr).

This section gives a brief introduction about the physical key gas exchange mechanisms between the atmosphere and (ground)water (as illustrated in Fig. 3.1), and how (noble) gases can be used to elucidate physical (i.e., mixing and travel times; Fig. 3.2) and biogeochemical (i.e., denitrification; Fig. 3.3) processes occurring in surface water–groundwater systems.

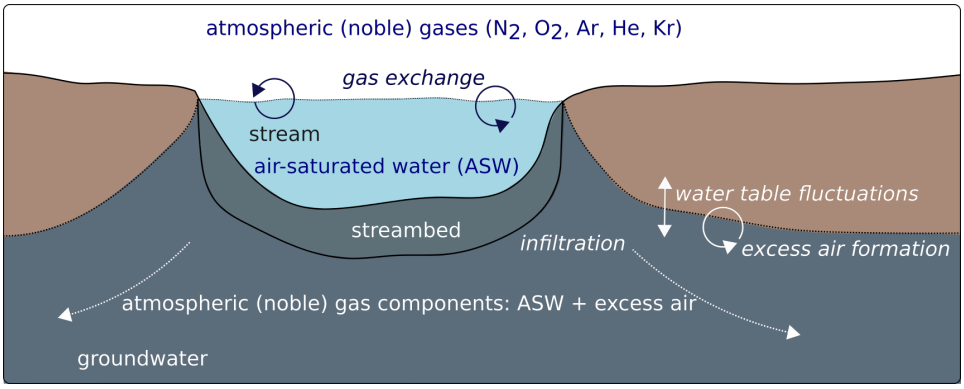

Figure 3.1: Conceptual model showing the two major gas partitioning processes affecting noble gas concentrations in groundwater: (i) air-saturated water (ASW) and (ii) excess air formation during groundwater recharge. Processes affecting gas partitioning are shown in italic.

3.1 Dissolved (Noble) Gases in Water

In surface waters, gas exchange occurs at the interface between the atmosphere and water bodies (Kipfer et al. (2002); see Fig. 3.1). Commonly,

dissolved gases in well mixed surface waters reach an equilibrium with atmospheric gases according to Henry's Law:

$$C_{gas}^{ASW} = \frac{p_{gas}^{atm}}{H_{gas}(T_w, S_w)}, \tag{3.1}$$

where C_{gas}^{ASW} is the gas concentration of a gas species in air-saturated water (ASW), p_{gas}^{atm} is the partial pressure of a gas species in dry air, and H_{gas} is the Henry coefficient of a gas species at a specific temperature (T_w) and salinity (S_w) of the water (e.g., Kipfer et al. 2002). Once surface water infiltrates, the abundance of gases in groundwater changes: reactive gas species typically increase due to gas production (e.g., N_2, CO_2) or the admixture of groundwater containing radiogenic gases (e.g., ^4He), or decrease due to gas depletion (e.g., O_2). Excess air formation—the partial dissolution of entrapped air bubbles due to water table fluctuations and groundwater recharge (Fig. 3.1)—affects both reactive and noble gases and can supersaturate groundwater in dissolved gases by up to 50% (Heaton et al. 1981; Kipfer et al. 2002). Moreover, excess air is typically fractionated (Aeschbach-Hertig et al. 1999; Holocher et al. 2003; Kipfer et al. 2002), which means that during excess air formation the composition of the dissolved gas and the remaining gas phase differs from that of free atmospheric air. Therefore, to reliably study processes such as denitrification through N_2 production, excess air formation including fractionation patterns needs to be quantified accurately.

Aeschbach-Hertig et al. (2000) introduced a widely accepted model on excess air formation (CE model), which assumes that the dissolved gases are in solubility equilibrium with the gases in the bubble at an enhanced hydrostatic pressure. The dissolved gas concentration in groundwater (C_{gas}) of a gas species at a given temperature (T_w; assuming salinity to be zero) and ambient atmospheric pressure (P) can be parameterized by the CE model as follows:

$$C_{gas}(T_w, P, A, F) = C_{gas}^{ASW}(T_w, P) + \frac{(1-F)Az_{gas}}{1 + F\frac{Az_{gas}}{C_{gas}^{ASW}(T_w)}}, \tag{3.2}$$

where A represents the amount of dry air per unit mass of water initially entrapped in the water and z_{gas} is the volume fraction of the gas in dry air; F describes the degree of fractionation of the dissolved bubbles, with $F \approx 0$ implying that all entrapped air bubbles are completely dissolved and $F \approx 1$ implying that basically no entrapped air is dissolved in the surrounding groundwater; $F > 0$ means that only a partial dissolution of entrapped air in favor of the more soluble gas species occurred, causing a fractionation with respect to the complete dissolution of air. In this case, the heavier (i.e., more soluble) gases are relatively more enriched in the water phase.

From a mechanistic, physically-based point of view, only the CE-model is able to accurately describe the gas fractionation that occurs due to a partial dissolution of entrapped air (e.g., Holocher et al. 2003; Klump et al. 2008). Consequently, only the CE-model can accurately quantify excess air formation—a crucial aspect when mass-balance equations are used to separate atmospheric-derived gases from biogeochemical-derived or radiogenic-derived gas components. All other available models for excess air formation are lumped-parameter models whose parameters cannot be interpreted as a physically-based mechanism.

As introduced in Chapter 3, the—for this thesis—relevant processes affecting gas concentrations in groundwater are gas partitioning during groundwater recharge as well as denitrification and the addition of radiogenic ^{4}He from admixing old (i.e., helium-rich) groundwater. Consequently, any deviation of the expected (noble) gas concentrations due to gas partitioning during groundwater recharge (as illustrated in Fig. 3.1) can be attributed to other processes: 1) groundwater mixing of recently infiltrated river water and regional groundwater can be inferred by any excess of helium that originates from the admixture of an old, regional groundwater source (Fig. 3.2) and 2) denitrification can be quantified by any excess of N_2 originating from denitrification in groundwater (Fig. 3.3).

Chapters 4 to 6 examine each of these fundamental processes individually in order to address the following research questions.

3.2 Research Question A

How do surface water and groundwater interact?
Groundwater contains in addition to atmospheric-derived helium, non-atmospheric helium, which indicates the presence of an old groundwater source (e.g., Cook et al. 2000). The ^{4}He concentration in groundwater ($^4He_{GW}$; Fig. 3.2) is given by:

$$^4He_{GW} = {}^4He_{ASW} + {}^4He_{EA} + {}^4He_{RAD} \tag{3.3}$$

where $^4He_{ASW}$ is the helium concentration from equilibrium with the atmosphere at the temperature, pressure, and salinity prevailing during recharge, $^4He_{EA}$ is the helium added through excess air formation, and $^4He_{RAD}$ is helium primarily originating from α decay of Uranium and Thorium in aquifer materials. Thus, ^{4}He concentrations in groundwater increase the longer the water is in contact with the aquifer's matrix (e.g., Cook et al. 2000).

Consequently, for Part ii of this thesis, elevated ^{4}He concentrations are used to indicate the mixing of recently infiltrated river water (no $^4He_{RAD}$) and older, regional groundwater.

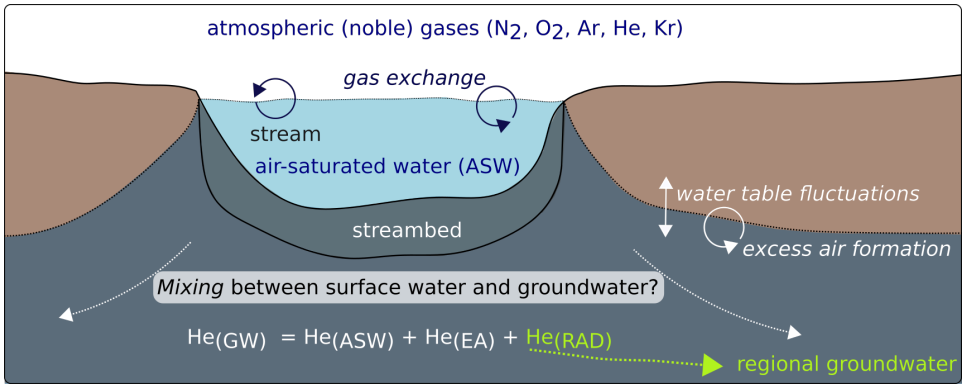

Figure 3.2: Conceptual model illustrating the atmospheric-derived noble gas components (i.e., ASW and excess air) as well as the addition of radiogenic helium from old groundwater.

3.3 Research Question B

How variable is denitrification in riparian groundwater?
Complete denitrification adds elemental N_2 to the already present gas composition in groundwater (e.g., Korom 1992). Consequently, the total amount of $N_{2(GW)}$ dissolved in groundwater originates not only from atmospheric sources but also from the reaction of nitrate and other reactive N-species. The N_2 concentration in groundwater ($N_{2(GW)}$; Fig. 3.3) is given by:

$$N_{2(GW)} = N_{2(ASW)} + N_{2(EA)} + N_{2(DEN)} \tag{3.4}$$

where $N_{2(ASW)}$ represents the air-saturated water concentration (ASW) of N_2 due to the equilibration with the atmosphere at the atmospheric pressure and recharge water temperature (with salinity assumed to be negligible), $N_{2(EA)}$ is the amount of N_2 due to excess air formation and $N_{2(DEN)}$ represents N_2 production due to complete denitrification.

To infer $N_{2(DEN)}$, the atmospheric N_2 components need to be determined reliably. To this end, noble gases (He, Ar, Kr) can be used as measure for atmospheric N_2 as they cover all the physical properties of atmospheric gases, which allows the calculation of the concentration of any atmospheric-derived gas species in groundwater (i.e., for N_2 the sum of $N_{2(ASW)}$ and $N_{2(EA)}$). Knowing the atmospheric N_2 gas components consequently allows to quantify N_2 stemming from denitrification.

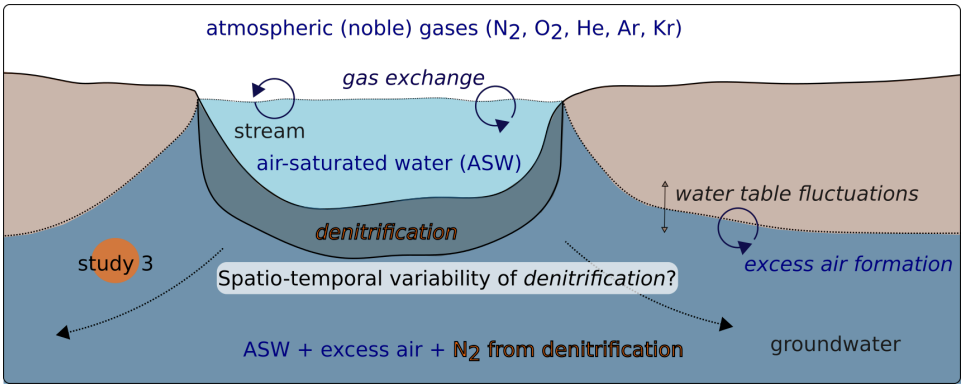

Figure 3.3: Conceptual model illustrating the different atmospheric N_2 components as well as N_2 originating from denitrification in groundwater.

Part II

QUANTIFYING GROUNDWATER MIXING AND TRAVEL TIMES

4

INTEGRATING BAYESIAN GROUNDWATER MIXING MODELING WITH ON-SITE HELIUM ANALYSIS TO IDENTIFY UNKNOWN WATER SOURCES

Chapter 4 has been published as: Popp, A.L., Scheidegger, A., Moeck, C., Brennwald, M.S. and Kipfer R. (2019), Integrating Bayesian groundwater mixing modeling with on-site helium analysis to identify unknown water sources, *Water Resources Research*, 55, https://doi.org/10.1029/2019WR025677.

Abstract

Analyzing groundwater mixing ratios is crucial for many groundwater management tasks such as assessing sources of groundwater recharge and flow paths. However, estimating groundwater mixing ratios is affected by various uncertainties, which are related to analytical and measurement errors of tracers, the selection of end-members and finding the most suitable set of tracers. Although these uncertainties are well recognized, it is still not common practice to account for them. We address this issue by using a new set of tracers in combination with a Bayesian modeling approach, which explicitly considers the possibility of unknown end-members while fully accounting for tracer uncertainties. We apply the Bayesian model we developed to a tracer set which includes helium (^{4}He) analyzed on-site to determine mixing ratios in groundwater. Thereby, we identify an unknown end-member, that contributes up to 84 ± 9% to the water mixture observed at our study site. For the ^{4}He analysis, we use a newly developed Gas Equilibrium Membrane Inlet Mass Spectrometer (GE-MIMS), operated in the field. To test the reliability of on-site ^{4}He analysis, we compare results obtained with the GE-MIMS to the conventional lab-based method, which is comparatively expensive and labor intensive. Our work demonstrates that (i) tracer-aided Bayesian mixing modeling can detect unknown water sources, thereby revealing valuable insights into the conceptual understanding of the groundwater system studied and ii) on-site ^{4}He analysis with the GE-MIMS system is an accurate and reliable alternative to the lab-based analysis.

4.1 Introduction

A groundwater sample usually consists of a mixture of water sources with different renewal rates such as fossil groundwater, decadal-age groundwater or recently infiltrated river water (e.g., Turnadge et al. 2014). The degree of mixing mostly depends on the aquifer's heterogeneity and the extent of the well screen (e.g., Jasechko 2016). Quantifying mixing ratios is key for assessing groundwater recharge (e.g., Beyerle et al. 1999) and groundwater vulnerability to pollution (e.g., Jasechko 2016), and is thus essential to manage water resources sustainably (Pelizardi et al. 2017).

Groundwater mixing models rely on known concentrations of conservative tracers to quantify the fractions of different water sources contributing to a water sample (e.g., Barthold et al. 2011; Carrera et al. 2004; Cook et al. 2019). Mixing ratios are estimated by comparing tracer concentrations in the sampled mixture with the concentrations of previously determined end-members (i.e., signatures of different water sources) by means of a mass balance approach (e.g., Christophersen et al. 1990; Hooper et al. 1990; Sanborn et al. 2016). In a bivariate tracer-tracer plot, end-members represent the most extreme values, with the sampled mixtures lying in between the end-member data points (Fig. S1 in the Supporting Information).

The first step to estimate groundwater mixing ratios is to determine end-members. This is mostly a conceptual step based on a sound understanding of the respective groundwater system e.g., through previous research or water table heads (e.g., Rueedi et al. 2005). It can, however, be aided by methods based on Principal Component Analysis (PCA), which find the minimum number of end-members to sufficiently explain the observed variability of a given tracer set (Christophersen et al. 1992; Pelizardi et al. 2017; Valder et al. 2012). The second step consists of calculating the mixing ratios for the identified end-members based on the tracer concentrations of each sample using a mass-balance approach (in which by definition the fractions of each end-member for a mixed sample have to add up to 1).

Previous research has demonstrated that estimated mixing ratios derived from different tracers are not necessarily consistent (e.g., Carrera et al. 2004)—an issue which is usually handled by employing a least-squares approach to find the best fit of estimated mixing ratios (e.g., Christophersen et al. 1990). It has also been shown that tracer set size and composition as well as the correct identification of end-members have a substantial influence on the derived mixing ratios and that, in general, larger tracer sets yield more robust estimates (Barthold et al. 2011; Delsman et al. 2013).

Such discrepancies stem not only from uncertainties related to inconsistencies in sampling and measurement procedures (i.e., during field work and with regard to analytical measurement precision), but also from the

underlying assumptions regarding conventional end-member mixing itself. These assumptions include that: (i) a water sample can be explained as a linear mixture of end-members (e.g., Delsman et al. 2013), (ii) the tracers behave conservatively, at least in the sense that any chemical reaction is much slower than the mixing process itself (e.g., Valder et al. 2012), (iii) tracer signals of each species are sufficiently distinct (e.g., Pelizardi et al. 2017), (iv) the chemical signatures of end-members are constant over time (e.g., Hooper et al. 1990), and (v) all end-members are identified correctly (Carrera et al. 2004; Delsman et al. 2013). These assumptions must either be justified or systematic uncertainties must be accounted for (in addition to tracer-related uncertainties). Although it is widely acknowledged that mixing ratios are associated with high uncertainties (e.g., Carrera et al. 2004; Delsman et al. 2013; Hooper 2003; Rueedi et al. 2005), few attempts have been made to account for them. Hooper et al. (1990) calculated the uncertainty of the mixing ratios based on linear approximation. Brewer et al. (2002) build a hierarchical Bayesian model that allows us to infer the tracer uncertainty of the end-member concentrations. The approach of Delsman et al. (2013) is similar, however, it is based on an informal likelihood function, which is constructed based to the measurement uncertainties. In contrast, Christophersen et al. (1990) and Hooper (2003) tested by means of a PCA if a data set could be at all explained by a mixing model (without defining the end-members). This can be seen as a test of the fifth assumption. Neglecting systematic uncertainties related to the assumptions mentioned above leads to overconfident estimates of groundwater mixing ratios, which can result in false and unreliable conclusions. While assumptions (i)–(iv) can typically be well defended, assumption (v) is most critical.

Besides traditional end-member mixing models, different Bayesian approaches have evolved in isotope hydrology and geochemistry to constrain source contributions of various Earth surface processes (e.g., Arendt et al. 2015; Blake et al. 2018; Davis et al. 2015; Erhardt et al. 2013; Parnell et al. 2019; Soulsby et al. 2003).

We present a newly developed Bayesian groundwater mixing model that builds on existing Bayesian approaches by adding two new features to better represent and describe the aforementioned uncertainties: first, our model explicitly considers uncertainties originating from sampling and measuring of tracer species; second, the model accounts for the possibility of principally unknown end-members (from here on referred to as *residual end-member*). Not only can our approach express the resulting uncertainties of the estimated end-member mixing ratios, it also allows to quantify the mixing ratios of the residual end-member and its tracer concentrations. Separating these two error sources is important for the interpretation, as otherwise any model mismatch would be "explained" by poor

measurements alone. While it is possible to reach similar conclusions by carefully interpreting residuals of traditional end-member mixing models (e.g., Hooper 2003), more indirect reasoning is required to weight the observation errors accurately.

In addition to the development of the Bayesian mixing model, we introduce the use of ^{4}He analyzed on-site as a tracer to estimate groundwater mixing ratios. The inert biochemical nature of the noble gas helium (mainly ^{4}He) makes it an ideal tracer to study groundwater dynamics, e.g., such as recharge and surface water–groundwater interactions (e.g., Batlle-Aguilar et al. 2017; Gardner et al. 2011; Kulongoski et al. 2008; Marty et al. 1993; Müller et al. 2016; Price et al. 2003). Typically, conventional lab-based ^{4}He analysis is costly and labor-intensive, therefore, only a few specialized laboratories can carry out such analyses on a routine basis. Here, we use ^{4}He data analyzed in the field with a recently developed portable mass spectrometry system (Brennwald et al. 2016) to estimate mixing ratios. Moreover, to test and validate the suitability of the new system, we compare ^{4}He concentrations obtained in the field with concentrations analyzed at the noble gas laboratory of the Swiss Federal Institute of Technology in Zurich, Switzerland.

Our study aims (i) to derive a novel methodology for estimating groundwater mixing ratios by explicitly accounting for the potential presence of unknown end-members and tracer uncertainties and (ii) to assess the suitability of on-site ^{4}He analysis using a portable mass-spectrometry system by comparing it to conventional lab-based noble gas analysis.

4.2 Site Description and Conceptual Model

Our study site, the Hardwald, is located in north-western Switzerland in close proximity to the Rhine river and the city of Basel and covers about 10 km^2 of mainly urban and industrial areas (Fig. 5.1).

The conceptual hydrogeological model (based on previous research; Moeck et al.; Moeck et al., 2016; 2017) assumes two main aquifers at the site (Fig. 4.2): an unconfined Quaternary sand-gravel aquifer, which is overlying a karstified Upper Muschelkalk aquifer (Moeck et al. 2016). The former consists of unconsolidated, highly conductive (k$\sim$270 m/d), fluvial Quaternary sediments (Spottke et al. 2005). The latter mainly consists of low-conductive limestone (k$\sim$10 m/d), is fractured and partly confined (Moeck et al. 2016; Spottke et al. 2005). In both aquifers, groundwater generally flows from southeast to northwest in the direction of the Rhine River. Towards the Rhine, an impermeable boundary formed of limestone of the Middle Muschelkalk exists (Moeck et al. 2016). This boundary fosters up-welling of groundwater from the Upper Muschelkalk aquifer into the Quaternary sand-gravel aquifer towards the northern

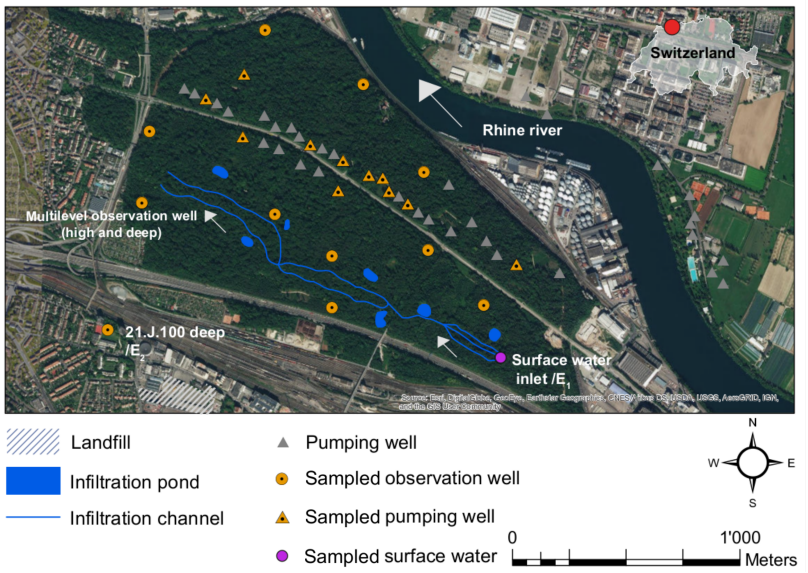

Figure 4.1: Study site showing the Hardwald with the infiltration system of channels and ponds (blue), and its surrounding area. Sampling points are marked as symbols containing black dots, the point in magenta indicates the inlet of Rhine water to the infiltration system.

part of the study area (see Spottke et al., 2005 and Moeck et al., 2016 for more details). Moreover, groundwater mixing between both aquifers is most likely amplified by groundwater pumping (Moeck et al. 2017c). The Upper Rhine Graben—a highly deformed flexure zone—constitutes the western boundary of the study area (Moeck et al. 2019). There the complex hydrogeological features (i.e., fault zones and fractures) result in high uncertainties in the hydraulic conductivity distribution (Moeck et al., 2019; see Fig. S2 for a simplified illustration of the bedrock units mentioned above).

Since the 1950s, groundwater has been abstracted from a pumping well field (Fig. 5.1) within the Hardwald site to produce drinking water. In response to an increased water demand caused by a growing population and industry, managed aquifer recharge (MAR) was introduced in 1958 by taking raw water from the Rhine and diverting it through channels and ponds (Figs. 5.1 and 4.2). From there the water naturally infiltrates into the underlying Quaternary aquifer with an average rate of 95 000 m^3/day. As the artificial recharge exceeds the water withdrawal by a factor of two, a local groundwater mound forms at the recharge site (Fig. 4.2; Moeck et al., 2017). This groundwater mound serves as a natural barrier against water inflow from upstream areas by reversing the natural groundwater flow direction—a crucial feature to protect the drinking water production

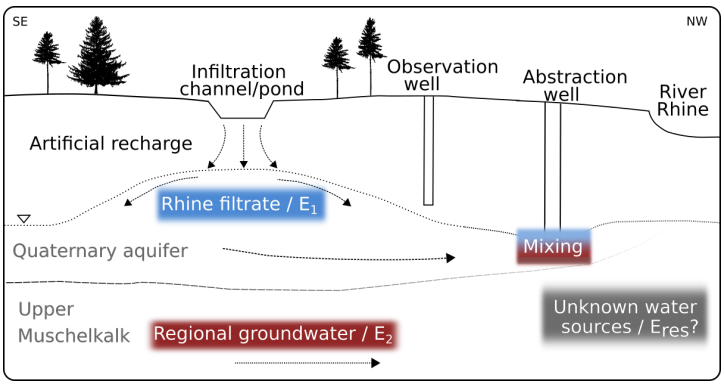

Figure 4.2: Conceptual model of the hydrogeological setting and flow system showing the local groundwater mound caused by the artificial infiltration, and the mixing between recently infiltrated Rhine water (i.e., end-member 1, E_1 in blue), regional groundwater (i.e., end-member 2, E_2 in red) and potential unknown water sources (i.e., residual end-member, E_{res} in gray).

area as the upstream region is exposed to several potential sources of contamination (e.g., surrounding industry; Fig. 5.1).

Figure 4.2 also shows potential mixing pathways between the artificially infiltrated water (i.e., Rhine water, E_1), unknown end-members (E_{res}) and regional groundwater (E_2), which is known to contain certain contaminants (Moeck et al. 2017c). Traces of these contaminants can be found in the abstracted drinking water (Moeck et al. 2016). The admixture of undesirable regional groundwater to the abstracted drinking water is likely to occur given the hydrogeological setting and groundwater withdrawal. The fraction of regional groundwater admixed to the abstracted drinking water might differ, though, depending on the specific well location. Therefore, a spatially resolved, quantitative assessment of the admixture of regional groundwater in the abstracted water is key for the future management of this MAR site, which provides drinking water for more than 200 000 people living in the agglomeration of Basel.

4.3 Material and Methods

To determine groundwater mixing ratios, we analyzed a set of environmental tracers. From August 15^{th} to August 25^{th} in 2016, we sampled 20 groundwater observation and pumping wells all over the study area as well as the infiltration channel from which the Rhine water is being distributed (Fig. 5.1). On December 5^{th} 2017, we sampled another three pumping wells within the study area for the same parameters. For sampling, we either used already pre-installed pumps at the pumping wells

or a submersible pump (MP1, Grundfos) for the observation wells. We started sampling after purging all wells three times according to their volume and after field parameters (O_2, EC, temperature, pH) had reached a stable level (i.e., at least three consecutive measurements with same concentrations within analytical uncertainty; analyzed with a calibrated HACH HQ40D portable multi meter). Details for the sampling procedure for the individual tracers are given below and in the Supporting Information. All tracer data, well locations and well depths are available in the Supporting Information (Dataset S1).

During our sampling campaigns, the MAR system was operated under standard conditions (i.e., average water infiltration and abstraction rates which govern the hydraulic head distribution). Thus, hydraulic conditions representative for the standard operation of the MAR site were guaranteed.

4.3.1 *Hydro-Chemical Parameters*

Rock-water interactions lead to an increase in hydro-chemical species (Ca^{2+}, Mg^{2+}, Na^{+}, K^{+}, Cl^{-}, H_4SiO_4, SO_4^{2-}, EC, alkalinity, total hardness and pH) in groundwater with respect to precipitation, which leave characteristic chemical fingerprints (Cook et al. 2000; Piper 1944). These fingerprints render such hydro-chemical species suitable to identify water flow paths and mixing of waters of different origin (e.g., Currell et al. 2011; Dogramaci et al. 2012; Skrzypek et al. 2013). We acknowledge that the parameters EC, pH, alkalinity and total hardness are correlated with the concentrations of dissolved ions present in a solution. They were, however, analyzed independently (see Table S2), and are thus accounted for as individual tracers.

We collected samples to analyze all hydro-chemical parameters as unfiltered water samples in one liter Schott glass flasks. The flasks were immediately cooled after sampling and analyzed the following day at Eawag (for methods, limits of quantification and analytical errors please see Table S2).

4.3.2 *Analysis of ^4He*

Helium is a noble gas, which has often been used to quantify groundwater residence times and aquifer recharge (e.g., Batlle-Aguilar et al. 2017; Gardner et al. 2011; Kulongoski et al. 2008; Müller et al. 2016). ^4He is slowly produced by α decay of ^{238}U, ^{235}U and ^{232}Th in the rock matrix and continuously accumulates in groundwater, which makes it an excellent indicator of long groundwater residence times, in the order of several hundreds to

thousands of years, depending upon aquifer material and geology (e.g., Gardner et al. 2011). Please see Texts S2.1 and S2.2 of the Supporting Information for a description about the on-site and lab-based ^{4}He analyses.

4.3.3 *Selection of End-Members*

The commonly used end-member mixing analysis—EMMA—was first presented for estimating mixing ratios in stream waters (Christophersen et al. 1990) and is still mainly applied in surface water studies (e.g., Barthold et al. 2011; Bernal et al. 2006; Hooper 2003; Valder et al. 2012). EMMA often involves PCA to elucidate the minimum number of end-members of a water sample. However, PCA is not appropriate for a small number of samples, which is often the case for groundwater studies.

In groundwater samples, the identification and selection of potential end-members is commonly better constrained than in surface waters due to the dampening effect of temporal tracer variations within an aquifer (Carrera et al. 2004). Thus, tracer concentrations in groundwater systems show less temporal variability compared to tracer concentrations in surface waters. We therefore argue that for estimating mixing ratios in groundwater, identifying potential end-members based on expert knowledge such as a conceptual model (e.g., pre-existing data or previous studies) and by screening through bivariate tracer-tracer plots is a valid and robust approach.

Consequently, we selected end-members according to our conceptual model of the field site, which is based on previous research conducted in this area (Moeck et al. 2016, 2017c; Spottke et al. 2005). Our selected end-members generally confirmed our conceptual model by representing the most extreme values in bivariate tracer-tracer distribution for most tracers used in this study (Fig. S1). We thereby identified two end-members: end-member E_1, which represents the infiltrated Rhine water (sample taken from the channel from which the Rhine water is distributed), and end-member E_2, which represents regional groundwater being sampled from observation well *21.J.100_deep* (Fig. 5.1). This well is located in the south-western area of the study site, which is hardly affected by the artificial infiltration and is therefore representative for the regional groundwater component (Fig. 4.2).

Although most samples fall well within the linear mixing lines of the two pre-defined end-members (Fig. S1), we principally cannot exclude the presence of an unknown water source. In cases where the data are not well reproduced by binary mixing of the two end-members considering tracer uncertainties, our model assigns a residual end-member component (E_{res}) to explain the observed tracer concentrations (see next section for a comprehensive description).

4.3.4 *Bayesian Mixing Model*

Conventional end-member mixing models (e.g., Christophersen et al. 1990) estimate the concentration $C[t]$ of a tracer substance t at a given well as a mixture of M pre-selected end-members E_m, with corresponding concentrations $C_{E_m}[t]$:

$$C[t] = r_1 C_{E_1}[t] + \cdots + r_M C_{E_M}[t] + \epsilon_t, \quad t = 1 \ldots T \tag{4.1}$$

where r_m, $m = 1 \ldots M$ are non-negative mixing ratios that sum up to one, and T is the number of tracer substances. The mixing rations are usually estimated by minimizing the errors ϵ_t with a non-negative least-squares approach. We emphasize that this error term allows no direct interpretation because it lumps together all sources of uncertainties.

To achieve an explicit handling of uncertainties, we extend the classical model (Equation 5.2) by first incorporating observational errors due to tracer-related uncertainties, and by second accounting for systematic biases due to potentially unobserved end-members.

4.3.4.1 *Observation Errors*

All measured tracer concentrations are subject to errors. The characteristics for these errors for any tracer species can be described by means of an *observation model*, $p(C^{\text{obs}} \mid C)$, which is the conditional probability distribution of the observed but erroneous concentrations C^{obs} if one knew the true observation C. Such distributions are either derived from repeated measurements or expert knowledge (i.e., a realistic estimation of the overall tracer uncertainty of a sample). For this study we defined the observation model as

$$p(C^{\text{obs}} \mid C) = N(C, \rho\, C)$$

i.e., a normal distribution with a standard deviation of ρ times the mean. This is a very simplistic choice. However, other—potentially non-Gaussian—observation models can readily be used instead.

With the help of the observation model the "true" but unknown concentrations C are inferred from the tracer data. To achieve this, the true concentrations C are treated as additional model parameter, similar to the Bayesian total error analysis approach from surface hydrology (Kavetski et al. 2006). The observation model is part of the likelihood function and accounts for all tracer-related uncertainties. The advantage of this approach is that for the rest of the model derivation we can pretend to know the true, error-free concentration C.

In our case, we assume an overall tracer uncertainty of $\rho = 10\%$ for each individual tracer concentration based on an analytical error of 1-5%

(depending on the tracer species) plus uncertainties due to inconsistencies in the sampling and analytical procedure. For end-member E_1 (Rhine water) we assume an overall tracer uncertainty of 20% due to the higher variability of tracer concentrations in surface water relative to groundwater. This assumption is corroborated by the variance of time series data of hydro-chemical tracers (i.e., major ions, pH, EC, total hardness, alkalinity) observed at the Rhine monitoring station (located about 7 km downstream of our study area): time series data that most likely represent the time frame of infiltration (i.e., the last 3 months before our sampling took place) show a mean variance of tracer concentrations between 10% and 15% (in 2016 and 2017, respectively).

4.3.4.2 *Residual End-Member*

As described above, total tracer-related uncertainties are 10% (20% for E_1, respectively) accounting for sampling and measurements errors. Even if tracer concentrations were error free, we would not expect the classical model to perfectly match our observations due to the systematic bias of not accounting for all end-members present in a system.

To avoid this strong assumption of perfect end-member identification, we introduce a hypothetical *residual* end-member (E_{res}). One can easily imagine that a number of unknown end-members actually exist in any complex environmental system. Therefore, we extend the mixing model (5.2) with a residual end-member:

$$C[t] = r_1\, C_{E_1}[t] + \cdots + r_M\, C_{E_M}[t] + r_{M+1}\, C_{E_{\text{res}}}[t], \quad t = 1 \ldots T \tag{4.2}$$

As the concentrations $C_{E_{\text{res}}}[t]$ of the unknown end-member cannot be observed, they are treated as additional model parameters. This approach has the advantage that not only the fraction r_{M+1} is acquired but also the concentration profile of E_{res} is revealed, which might allow to identify the hydrogeological origin of E_{res}.

It is important to notice that Equation 4.2 only makes use of the true (inferred) concentrations so that the residual end-member corrects for systematic deviations that cannot be explained by tracer-related uncertainties.

4.3.4.3 *Parameter Inference*

The introduction of the observation model and the residual end-member considerably increase the number of parameters to estimate, so that in a frequentist setting (e.g., with maximum likelihood estimation) no unique best parameter values can be determined. However, well defined parameter distributions can still be inferred with Bayesian inference by using weak and intuitive prior distributions.

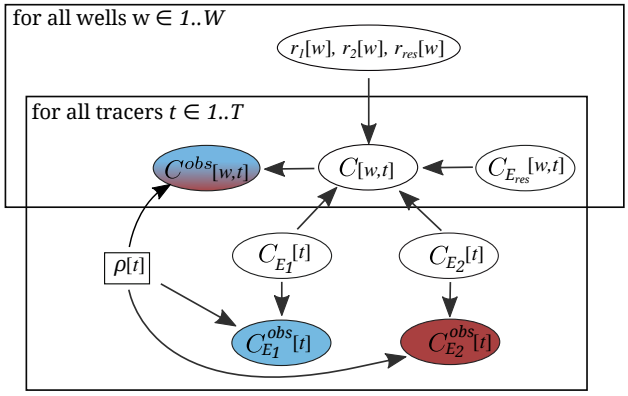

Figure 4.3: Graphical representation of the probabilistic mixing model for two end-members (E_1 and E_2). Round nodes represent random variables, the square node a constant value, and the boxes repetition over the index. The colored nodes are observations on which the other random variables are conditioned on.

Figure 4.3 provides a conceptual overview of the dependency of the involved quantities: all round nodes represent random variables whose distribution are defined by the model according to the values of the incoming nodes. For the colored nodes observations are available on which all the other nodes are conditioned (i.e., inferred) on. The boxes denote repetitions over the index. For example different "true" concentrations of the two end-members are estimated for each tracer. A separate concentration of the residual end-member is inferred for every tracer and well. The complete mathematical derivation of the corresponding likelihood function used for Bayesian inference can be found in the Supporting Information Text S2.

Additional prior distributions are required for the inference of the unknown quantities. We define the following prior distributions: (i) a non-informative, flat prior $U(0, \infty)$ for the true end-member concentrations, (ii) a Dirichlet$(1, \ldots, 1)$ distribution for the mixing ratios, which defines an uninformative distribution over a simplex that guarantees $\sum_{m=1}^{M+1} r_m = 1$ and $0 \leq r_m,\ m = 1, \ldots, M+1$ (see Delsman et al., 2013), and (iii) an informative prior for the residual end-member concentrations. For the latter, we selected uniform distributions with the lower and upper limits being $\pm 20\%$ of any observed tracer concentration.

4.3.4.4 *Implementation*

The model was implemented in STAN (Carpenter et al. 2017)—a probabilistic programming language well suited for Bayesian inference. We gen-

erated three independent Monte Carlo Markov Chains (Kruschke 2015) with a length of 15 000, discarding the first 5 000 samples as burn-in. We pre-processed and visualized all data using R (R Core Team 2018).

4.4 Results

4.4.1 *Comparison between On-Site and Laboratory-Based ^{4}He Analysis*

Due to the time demanded for the lab-based ^{4}He analysis, we limited the analysis of copper tube samples to a subset (n=17) of the 23 wells analyzed in this study. With the GE-MIMS system, however, we analyzed ^{4}He at all 23 wells. We compared the two methods to test whether the GE-MIMS system can reliably substitute the lab-based ^{4}He analysis. The high linear correlation (adjusted R^2=0.98, RMSE=2.4e-8, p <0.001; n=16 after neglecting one outlier, with outlier adjusted R^2=0.94, p <0.001) between the ^{4}He analyses demonstrates that the GE-MIMS is well suited for high precision ^{4}He analysis under field conditions (Fig. 4.4; data are available in Table S1). Overall, these results show that the two methods yield similar concentrations, which consequently allows for the use of on-site analyzed ^{4}He concentrations as tracer to estimate groundwater mixing ratios.

4.4.2 *Model Sensitivity Analysis using Different Tracer Sets*

Theoretically, any set of conservative tracers to calculate mixing ratios can be used. Given the various tracers obtained by us, we explore the effect of different—in number and composition—sets of tracers to test their influence on the estimated mixing ratios. In particular the contribution (r_{M+1}) of the residual end-member (E_{res}) is of fundamental interest, because it can be interpreted as a measure of how internally consistent a tracer set is with regard to the assumed binary mixing hypothesis.

Table 4.1 specifies all the different tracer set sizes and compositions we assessed. The tracer sets differ from "easy to measure" tracers (i.e., feasible to obtain data with a hand-held probe) such as pH and EC (tracer set 1: *TS1*), to more advanced sets consisting of standard hydro-chemical tracers such as major ions, alkalinity and total hardness (*TS2*–*TS4*).

We also tested one tracer set (*TS5*) that includes all tracers obtained including ^{4}He but also less conservative species (i.e., nitrate and sulfate), which are sometimes used to calculate mixing ratios (e.g., Delsman et al. 2013; Moeck et al. 2017b; Soulsby et al. 2003). *TS6* consists only of ^{4}He concentrations determined in the field. Finally, *TS7* includes all tracers except for nitrate and sulfate.

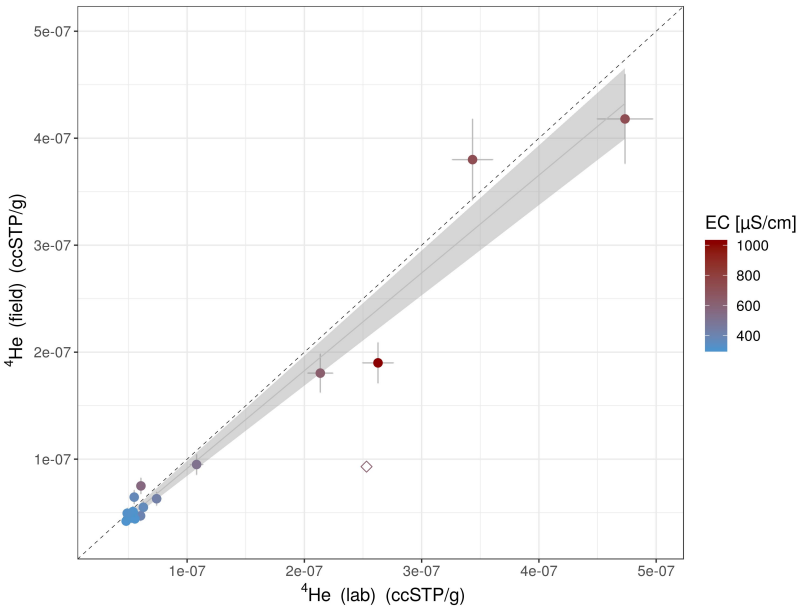

Figure 4.4: Comparison between lab-based and on-site analysis of ^{4}He concentrations. The gray band shows the 95% confidence interval of a linear regression (neglecting one outlier marked as a diamond); error bars represent analytical measurement uncertainties. The data indicate, that ^{4}He and EC concentrations increase simultaneously, suggesting higher mineralization with increasing residence time.

Table 4.1: Mixing model sensitivity analysis by testing different tracers sets. The mean estimated ratio of an unknown end-member (E_{res}) indicates the goodness of fit of the mixing model depending on the respective tracer set.

Tracer Set	Used Tracers	Number of Tracers
TS1	pH, EC	2
TS2	hydro-chemical species (Ca^{2+}, Mg^{2+}, Na^{+}, K^{+}, Cl^{-}, H_4SiO_4)	6
TS3	pH, EC, hydro-chemical species	8
TS4	pH, EC, hydro-chemical species, alkalinity, total hardness	10
TS5	pH, EC, hydro-chemical species, alkalinity, total hardness, nitrate, sulfate, **^{4}He**	13
TS6	**^{4}He**	1
TS7	pH, EC, hydro-chemical species, alkalinity, total hardness, **^{4}He**	11

The results of this sensitivity analysis using different tracer sets demonstrate that model uncertainties (i.e., amount of E_{res}) vary depending on the tracer set used (Fig. 4.5). These findings indicate that, in general, uncertainty tends to decrease with increasing numbers of tracers. This is, however, only true as long as the tracers are consistent, which is not the case for *TS5*.

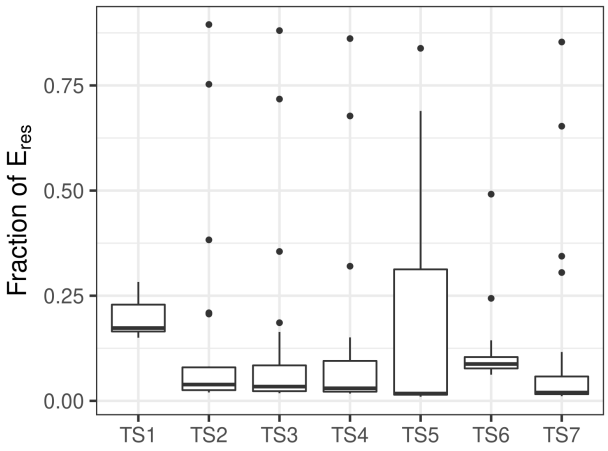

Figure 4.5: Sensitivity test of different sets of tracers shown in box plots: lower fractions of E_{res} indicate a better explanation of the available data with two end-members (i.e., E_1 and E_2) only (see Table 4.1 for information on the tracer sets and Fig. S4 for labels on all data points).

The simplest tracer set (*TS1*) has, with about 20%, the highest average contribution of E_{res}. Using more than two tracers (e.g., *TS2*) or adding more tracers to *TS1* (*TS3–4*) considerably decreases the model uncertainty. *TS5* reveals that including the less conservative species nitrate and sulfate results in higher model uncertainties.

Only using ^{4}He concentrations as a single tracer (*TS6*) shows that despite a low variability in E_{res}, the mean fraction of E_{res} is higher than in *TS2-4*. Overall, *TS7* yields the most robust results: it can explain most data by binary mixing of E_1 and E_2 and allocates higher fractions of an unknown end-member (31$\pm$8–84$\pm$9%) only to four wells (Fig. 4.5). Consequently, we used *TS7* to estimate the mixing ratios given its apparent robustness compared to other tracer sets.

When comparing *TS4* (no ^{4}He) and *TS7* (TS4 + ^{4}He), one could argue that both yield similarly acceptable results and that *TS4* is a reasonable approximation to estimate mixing ratios. However, when looking at specific wells (e.g., *21.C.206*, first column in Fig. 4.6), we note that including ^{4}He concentrations actually results in a considerably higher fraction of E_{res}. For the other two wells illustrated in Figure 4.6, adding ^{4}He concentrations only has a marginal effect. Figure 4.6 also clearly indicates that

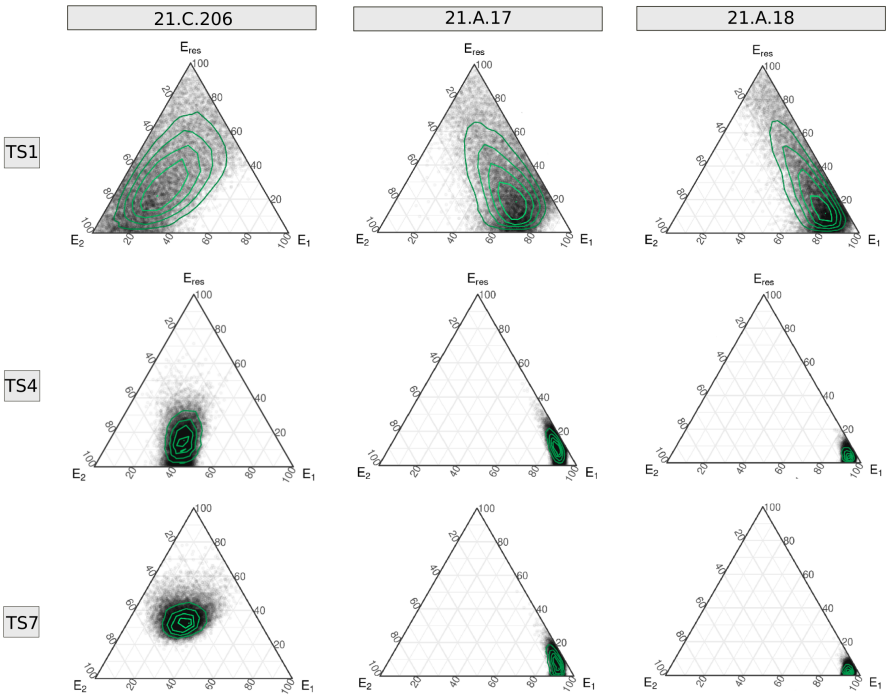

Figure 4.6: Ternary diagrams of the mixing ratios (%) of three different wells (*21.C.206*, *21.A.17*, *21.A.18*) for *TS1*, *TS4* and *TS7*, (representing tracer sets with increasing complexity, see Table 4.1). The assessment shows that with increasing tracer set size (from TS1 to TS4 to TS7) model uncertainty is reduced. Green contour lines show the probability density representing the estimated uncertainty.

even though wells *21.A.17* and *21.A.18* are located adjacent to each other, their respective mixing ratios differ. Please see Figures S5 to S7 for the ternary diagrams showing mixing ratios of all wells for tracer sets 1, 4 and 7.

4.4.3 *Estimated Mixing Ratios and their Uncertainties*

Figure 4.7 illustrates the spatial distribution of estimated fractions of end-members (E_1, E_2 and E_{res}) based on *TS7*. As expected, most wells in proximity to the infiltration area show a large fraction of recently infiltrated Rhine water (E_1, e.g., up to 97±1% at *21.C.215*; Fig. 4.7). Further away from the artificial recharge area, e.g., at pumping well *21.A.16*, the fraction of Rhine filtrate slightly decreases to 94±2%. Interestingly, the close-by pumping well *21.A.17* shows with 88±4% a comparatively low fraction of recently infiltrated water.

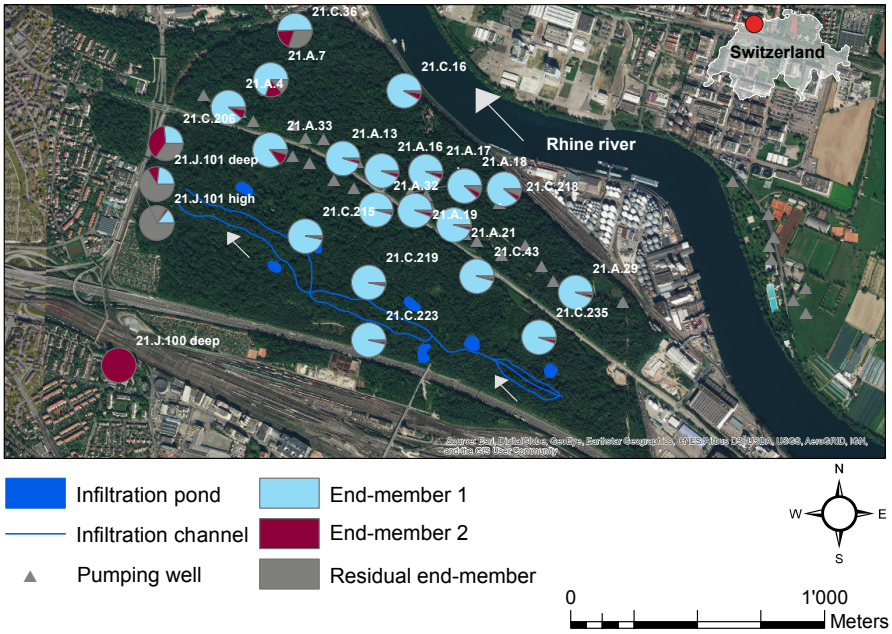

Figure 4.7: Spatial distribution of estimated mixing ratios. Blue represents end-member E_1, red end-member E_2, and grey stands for the residual end-member E_{res}, i.e. an unknown water source.

Towards the western border of the study area, which is (according to previous studies, Moeck et al.; Moeck et al., 2016; 2017) less impacted by the artificial recharge, the fraction of Rhine filtrate further decreases (e.g., *21.A.7* with 70±4% or *21.A.33* with 85±3% of E_1). Observation well *21.C.206*—located at the western border of the study area—shows with 27±7% an exceptionally low fraction of E_1 (compared to surrounding wells like *21.A.4* with 89±2%) but simultaneously also has a relatively high fraction (36±7%) of an unknown end-member (E_{res}). The by far highest fractions of E_{res} were detected in wells *21.J.101_high* (84±9%) and *21.J.101_deep* (66±12%). The mixing model attributed higher fractions of E_{res} only to one other well (*21.C.36* with 31±8%). All wells with a considerable fraction of E_{res} are being located at the western border of the study area.

Apart from these wells, three other wells (*21.A.17*, *21.A.7*, *21.C.218*) show moderate contributions (6±5%–12±8%) of an unknown water source. The remaining wells exhibit only small fractions of E_{res} (≤4±4%). All estimated mixing ratios and their uncertainties are illustrated in Figure S3 (based on Dataset S2). Overall, for most tracer species model-based estimates of tracer concentrations are in good agreement with the measured concentrations (see Fig. S8).

4.5 Discussion

4.5.1 *Substituting Lab-Based with On-Site ^{4}He Analysis*

The two methods compared for analyzing ^{4}He differ regarding sampling volume and technique, analytical procedure, calibration and data processing. Thus, the assumption that both methods yield in fact comparable results for ^{4}He concentrations is not straightforward.

Nonetheless, the statistically significant correlation between the two ^{4}He concentration data sets demonstrates that the results of the simple GE-MIMS system are as satisfying as those of the highly sophisticated lab-based method. Thus, these findings validate the accuracy and suitability of ^{4}He analysis using the GE-MIMS system and confirm that on-site methods can reliably substitute for conventional lab-based ^{4}He analysis, which is comparatively time demanding and labor intensive.

Moreover, we would like to highlight that during field work the portable MS guided the selection of the most interesting wells in quasi real-time, which allowed for very efficient sampling of an access restricted area.

4.5.2 *Tracer Set Selection, Validity of Mixing Model and Study Limitations*

We assessed the sensitivity of the mixing model outcome by testing different tracer sets. This approach shows that the most consistent results (i.e., most data can be explained by our selected end-members E_1 and E_2) are obtained by applying all analyzed tracers (including ^{4}He), except for the less conservative ones (nitrate and sulfate). These results highlight once more that using a combination of multiple, diverse tracers with different geochemical behavior is the most robust approach to quantify water mixing (e.g., Abbott et al. 2016; Tetzlaff et al. 2015). Thus, using a combination of geochemically different tracers is crucial to evaluate whether a mixing model yields meaningful and robust results. Furthermore, our findings show that less conservative tracers should strictly be avoided when calculating mixing ratios because their use tends to increase mixing model uncertainties.

The ability of our mixing model to estimate the contribution of unknown residual end-members (E_{res}) and to account for tracer uncertainty separately turned out to be valuable. We acknowledge, however, that the implementation of such a Bayesian model also requires more assumptions to be pre-described explicitly. For example, uncertainties for each individual tracer analyzed at each individual well have to be determined and a prior distribution for the concentrations of the residual end-members must be defined. We explicitly state that these assumptions are to some degree subjective. However, they increase transparency and avoid over-

interpretation of the results, and allow to test different assumptions. For instance, in our study, the concentrations of the residual end-members were not fixed across the wells allowing for the mixing model to estimate E_{res} and its geochemical composition for each well independently. We chose this approach because we had no expectation regarding the number of unobserved end-members present in our system.

By ascribing an overall tracer concentration uncertainty of 10% (and 20% for the infiltration water), we believe to conservatively account for all associated uncertainties including systematic biases, from sampling in the field to the final concentrations. A limitation of this study is that due to access restrictions to the drinking water protection site, we sampled the tracers only once. Thus, we have to assume that the temporal variability of tracer concentrations is neglectable or accounted for within the ascribed uncertainties. Since the attributed overall uncertainties are rather conservative, the estimated fractions of E_{res} also represent rather conservative estimates of unknown water sources present in our system. Moreover, we argue that the sampled tracer concentrations are representative as the site is artificially controlled by managed aquifer recharge and was sampled under standard operating conditions. To entirely rule out the possibility of time variable end-members, one would need to acquire time series data of the groundwater end-members, which is beyond the scope of this study.

4.5.3 *Adjustment of the Conceptual Model*

In principle, our results are in line with previous studies conducted at the study site. By means of a cluster analysis, Moeck et al. (2016) identified observation well *21.C.206* to have a distinct geochemical signature that could not be classified with any other investigated well. Likewise, our assessment shows that *21.C.206* has an exceptional geochemical signature compared to most other wells (see Figs. 4.6 and 4.7). However, we can now explain these different geochemical characteristics by the presence of a high ratio (36±7%) of a previously unknown water source.

Moreover, pumping well *21.A.17* was found to exhibit a different hydrogeochemistry and higher micro-pollutant concentrations compared to most other wells in its vicinity and to be hydraulically connected to the underlying aquifer (Moeck et al. 2016, 2017c). According to our analysis, these differences might originate from a higher fraction of regional groundwater (E_2) (6±2%) relative to the surrounding wells *21.A.16* and *21.A.18* (both 4±2%).

Although Moeck et al. (2017b) report similar mixing ratios (based on the same selected end-members) compared to our study, they neglect the possibility of unknown end-members, which results in high standard deviations (more than 35%) in their estimated mixing ratios.

Thus, we demonstrate that the existing conceptual model of binary mixing of two water sources (i.e., E_1 and E_2) is not valid for the entire system. These findings require an adjustment of the conceptual model by acknowledging the contribution of unknown water sources (E_{res}), which were previously neglected.

Since E_{res} fractions are highest in the west (Fig. 4.7), we hypothesize that water of unknown origin occurs in the Hardwald site at its western boundary. The local presence of E_{res} can therefore be interpreted as a third end-member and not as various different unknown water sources. As the Rhine Graben forms the western boundary of the study area (Fig. S2), it becomes apparent that E_{res} reflects water from this flexure zone, which provides a pathway for groundwater of deeper strata to ascend (Fig. 4.2). This conclusion is further reinforced since deep groundwater is expected to be high in helium (e.g., Stute et al. 1992a). Wells (i.e., 21.C.36, 21.A.7, 21.C.206, 21.J.101.h, 21.J.101.d, 21.A.7, 21.C.36, 21.C.206; see Dataset S1) located at the western edge of the study area show indeed elevated ^{4}He concentrations.

In conclusion, water mixing through the flexure zone might be of greater importance for the water management of the Hardwald site than previously assumed. Consequently, water mixing at the study site can only be explained by at least three groundwater components and not by two as previously assumed.

4.6 Conclusions

According to Tetzlaff et al. (2015), there is an urgent need for a "more economic analysis of large sample numbers in conjunction with novel, tracer-aided modeling approaches" to improve our understanding of hydrological processes. By demonstrating the suitability of the portable GE-MIMS system as a substitute for the conventional lab-based analysis of ^{4}He (Fig. 4.4), we are able to introduce a new, more efficient method for dissolved (noble) gas analysis. Beyond proving the suitability of on-site ^{4}He analysis, our study shows that ^{4}He is as an excellent tracer to estimate groundwater mixing ratios and can help to reduce model uncertainty and to identify unknown water sources, e.g., water mixing through fault zones (Figs. 4.5 and 4.6).

Moreover, our sensitivity analysis emphasizes that mixing model uncertainties decrease with increasing numbers of conservative tracers (Fig. 4.5). By combining the most robust tracer set (TS7) with a Bayesian modeling framework, we can identify the presence of a previously unknown water source and thereby improve our conceptual understanding of our study site (Figs. 4.7 and S3).

4.7 Outlook

The compact size of the portable GE-MIMS system allows for efficient (noble) gas analyses at remote locations (e.g., northern catchments, high altitudes) with a high spatio-temporal resolution. Therefore, it has great potential for a widespread application in locations where tracer data resolution is usually scarce due to time and cost limitations as well as access restrictions.

Although, we applied the Bayesian mixing model presented in a groundwater context, it is generally applicable to a variety of mixing-related research questions, e.g., stream water mixing on a catchment scale. We hope that the available data set and source code will serve as a template for future studies to facilitate reliable estimates of groundwater mixing and ultimately improve water management.

Acknowledgments

All data and code used in this study can either be found in the Supplementary Information or are available online: `https://doi.org/10.25678/000183`. We thank Richard P. Hooper, two anonymous reviewers and the associate editor for their constructive comments and suggestions that helped to improve the manuscript. We also thank Benjamin Plüss, Reto Britt and Jonas Zbinden for their help in the field. Furthermore, we are grateful for technical support in the ETH Noble Gas laboratory provided by Henner Busemann and Colin Maden, and the assistance provided by Edith Horstmann and Alexandra Lightfoot. The AUA laboratory at Eawag is thanked for the analysis of the hydro-chemical data. A.L.P. gratefully acknowledges financial support for this work from the EU Framework Programme for Research and Innovation Horizon 2020 ITN "Hypotrain" (Marie Sklodowska-Curie grant agreement No. 641939) and Eawag.

4.8 Supporting Information

This Supplementary Material includes

- Text S1 explaining why we did not use the other obtained dissolved gas data in this study.
- Text S2 describing on-site and lab-based ^{4}He analyses.
- Text S3 explaining the likelihood function and Bayesian inference of the model we present.
- Figure S1 showing examples of bivariate tracer-tracer plots to graphically support the description of the Introduction (manuscript).

- Figure S2 showing a simplified geological map of the study site with the main bedrock units.
- Figure S3 illustrating the estimated fractions and uncertainties of end-members based on the model results (Dataset S2) using tracer set *S7*.
- Figure S4 showing the results of the sensitivity test with labels on all data points.
- Figures S5 to S7 showing estimated mixing ratios at all investigated wells calculated for tracer sets 1, 4 and 7.
- Figure S8 comparing model-estimated and measured tracer concentrations.
- Table S1 containing the data on which Figure 4 (manuscript) is based on.
- Table S2 describing the instruments used, parameter units, LOQ and measurement uncertainties for the major ion data and other hydrochemical parameters.

Datasets S1 (containing information about sampling locations and all tracer input data) and S2 (model results) as well as the model Source Code S1 are available online: `https://doi.org/10.25678/000183`.

Text S1

Other (noble) gases analyzed with the GE-MIMS could not be used to estimate mixing ratios since they were either not conservative (N_2, O_2) or did not yield distinctive differences in their concentrations between end-members (^{40}Ar, ^{84}Kr).

Text S2.1: On-Site ^4He Analysis

With the GE-MIMS system operated in the field, we analyzed partial pressures of ^4He together with a set of other (noble) gases (N_2, O_2, Ar, Kr, not further discussed, see Text S1). The abstracted water was pumped through a membrane module (3M Liqui-Cel 2017), where the dissolved gases are extracted into a head space until a gas-equilibrium between the dissolved and the free gas phase is established (Brennwald et al. 2016). The solubility equilibrium guarantees that the partial pressures of the analyzed gas species are proportional to the concentrations in water. The module is connected via a small capillary to a Quadruple Mass Spectrometer for

final gas analysis. Air-water equilibrium within the membrane module is reached after ∼15 minutes with a determined water flow rate of about 1.5 to 1.8 L/min.

With a second capillary we sampled for ambient air, which we used as standard. Gas calibration was then performed by comparing peak heights between ambient air and the sampled gases. Each measurement cycle (including all aforementioned gas species) for either an air standard or dissolved gas measurement takes about 8–9 minutes. We conducted four cycles per well and two air standards (as first and last measurement), which results in an overall sampling time with the GE-MIMS of approximately 60 minutes at each well (including about 2 minutes waiting time to purge the capillary after switching from a water sample to an air sample).

Water temperature was continuously recorded before the membrane module (temperature probe DS18B20 Maxim) allowing the conversion of the determined gas partial pressures into dissolved gas concentrations according to Henry's law solubility constants at the respective water temperature assuming zero salinity (Kipfer et al. 2002). For a more comprehensive description of gas analysis using the GE-MIMS system, see Brennwald et al. (2016).

Text S2.2: Laboratory-Based ^{4}He Analysis

After the GE-MIMS analysis we collected samples for laboratory-based noble gas analysis as water samples in copper tubes sealed with pinch-off clamps following standard procedure (Beyerle et al. 2000).

We analyzed ^{4}He, ^{3}He and other gases (not further discussed) at the ETH noble gas lab in Zurich, as described by Beyerle et al. (1999). The gas free copper tubes were stored to allow for ^{3}He in-growth for later tritium analysis (Tolstikhin et al. 1969). Tritium, however, turned out to be an unsuitable tracer to analyze water mixing at this study site due to the unsteady tritium release from several nuclear power plants located upstream of the study area. Due to the highly variable input signal of tritium concentrations into our groundwater system, we consequently excluded tritium as a tracer.

Text S3: Likelihood function and Bayesian inference

The introduction of the observation model and the residual end-member considerably increase the number of parameters to be estimated. However, by using weak and intuitive prior assumptions, Bayesian inference still guarantees the parameter identifiability. To derive the required likelihood function, we first introduce a vector notation. In all equations below

we assume that the tracer substances are indexed with $t = 1 \dots T$, the selected end-members with $m = 1 \dots M$, and the wells with $w = 1 \dots W$. Let $\boldsymbol{r}[w] = (r_1[w], \dots, r_{M+1}[w])$ be the vector of all mixing ratios for wells w, and $\boldsymbol{r} = (\boldsymbol{r}[1], \dots, \boldsymbol{r}[W])$ the set of all mixing ratios. Similarly, the end-member concentrations are $\boldsymbol{C}_E = (\boldsymbol{C}_E[1], \dots, \boldsymbol{C}_E[T])$ with $\boldsymbol{C}_E[t] = (C_{E_1}[t], \dots, C_{E_M}[t])$ and the residual end-member concentrations are $\boldsymbol{C}_{\text{res}} = (\boldsymbol{C}_{\text{res}}[1], \dots, \boldsymbol{C}_{\text{res}}[W])$ with $\boldsymbol{C}_{\text{res}}[w] = (C_{E_{\text{res}}}[w, 1], \dots, C_{E_{\text{res}}}[w, T])$ at wells w. The concentrations of the non-end-member wells (i.e., mixtures) are summarized as $\boldsymbol{C} = (\boldsymbol{C}[1], \dots, \boldsymbol{C}[W])$ with $\boldsymbol{C}[w] = (C[w, t], \dots, C[w, T])$.

The observation model and the mixing model (Equation 2) specify the likelihood function for the mixture concentrations. The parameters are the mixing ratios, but also the (true) end-member concentrations, and the residual end-member concentrations:

$$p(C^{\text{obs}}[w, t] \mid C[w, t]) = p(C^{\text{obs}}[w, t] \mid \boldsymbol{C}_E[t], C_{\text{res}}[w, t], \boldsymbol{r}[w]) \,.$$

If we further assume that the observation errors are independent, we can write

$$p(\boldsymbol{C}^{\text{obs}} \mid \boldsymbol{C}_E, \boldsymbol{C}_{\text{res}}, \boldsymbol{r}) = \prod_{w=1}^{W} \prod_{t=1}^{T} p(C^{\text{obs}}[t, w] \mid \boldsymbol{C}_E[t], C_{\text{res}}[t, w], \boldsymbol{r}[w]) \,.$$

By combining this result with the observation model for end-members we obtain the complete likelihood function:

$$p(\boldsymbol{C}^{\text{obs}}, \boldsymbol{C}_E^{\text{obs}} \mid \boldsymbol{C}) = p(\boldsymbol{C}^{\text{obs}} \mid \boldsymbol{C}_E, \boldsymbol{C}_{\text{res}}, \boldsymbol{r})\, p(\boldsymbol{C}_E^{\text{obs}} \mid \boldsymbol{C}_E).$$

The parameters $\{\boldsymbol{r}, \boldsymbol{C}_E, \boldsymbol{C}_{\text{res}}\}$ are not identifiable in a frequentist maximum likelihood setting. Therefore, we define the following prior distributions: (i) a non-informative, flat prior $p(\boldsymbol{C}_E) = U(0, \infty)$ for the true end-member concentrations, (ii) a Dirichlet distribution $p(\boldsymbol{r}[w]) = \text{Dirichlet}(1, \dots, 1)$ for the mixing ratios, which defines an uninformative simplex that guarantees $\sum_{m=1}^{M+1} r_m = 1$ and $0 \leq r_m,\ m = 1, \dots, M+1$ (the same choice was made by Delsman et al., 2013), and (iii) an informative prior for the residual end-members. For the latter we used uniform distributions with lower and upper limits selected so that they are 20% less/more extreme than any observed tracer concentrations.

With these prior distributions and the likelihood function, we define the posterior distribution as

$$p(\boldsymbol{C}_E, \boldsymbol{C}_{\text{res}}, \boldsymbol{r} \mid \boldsymbol{C}^{\text{obs}}, \boldsymbol{C}_E^{\text{obs}}) \propto p(\boldsymbol{C}^{\text{obs}}, \boldsymbol{C}_E^{\text{obs}} \mid \boldsymbol{C}_E, \boldsymbol{C}_{\text{res}}, \boldsymbol{r})\, p(\boldsymbol{C}_E)\, p(\boldsymbol{r})\, p(\boldsymbol{C}_{\text{res}}) \,. \tag{4.3}$$

The proportional relationship is sufficient to sample from this distribution, for example with Monte Carlo Markov Chain methods (Kruschke 2015).

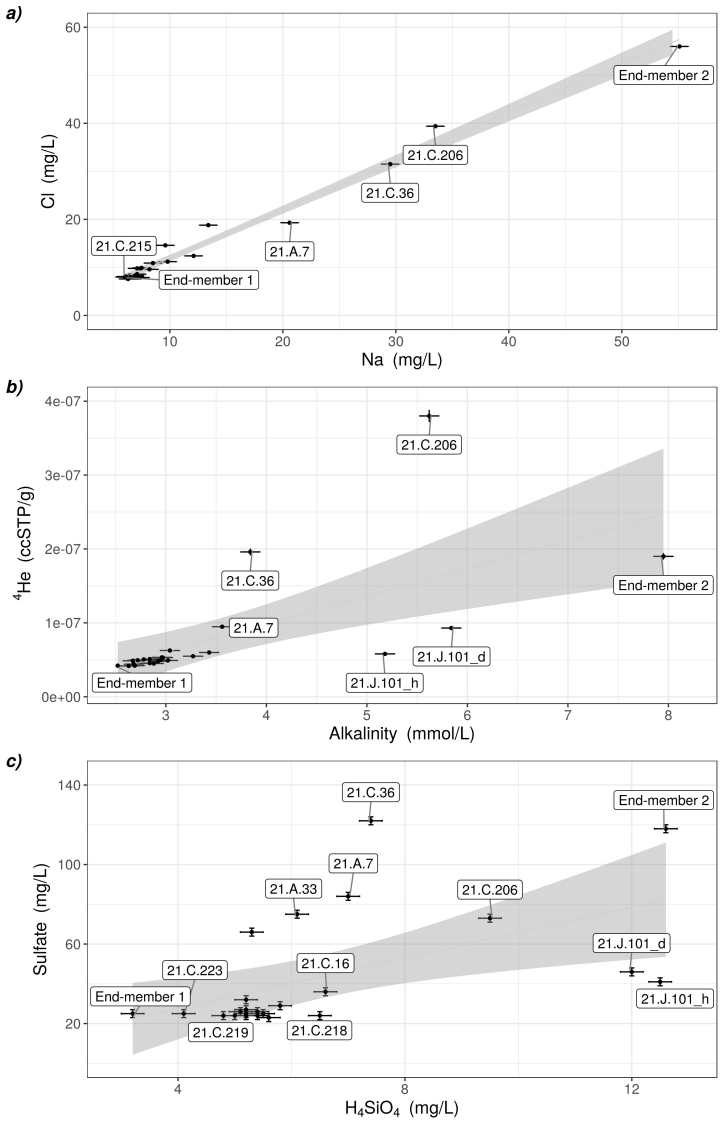

Figure S1: Exemplary bivariate tracer-tracer plot with a) showing natrium (Na) vs. chloride (Cl), b) showing alkalinity vs. helium (^{4}He) and c) showing silica (H_4SiO_4) vs. sulfate for the two pre-selected end-members and the sampled mixtures. The gray bands indicate the 95% confidence intervals of the linear regressions; error bars represent analytical uncertainties.

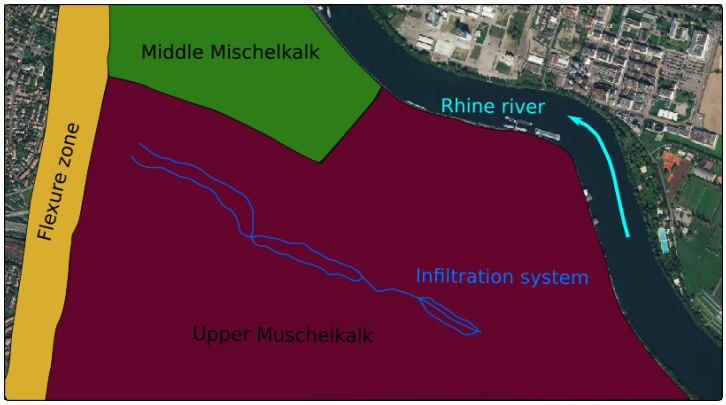

Figure S2: Simplified geological map showing the main known bedrock units at the study site. The overlying Quaternary deposits are not shown.

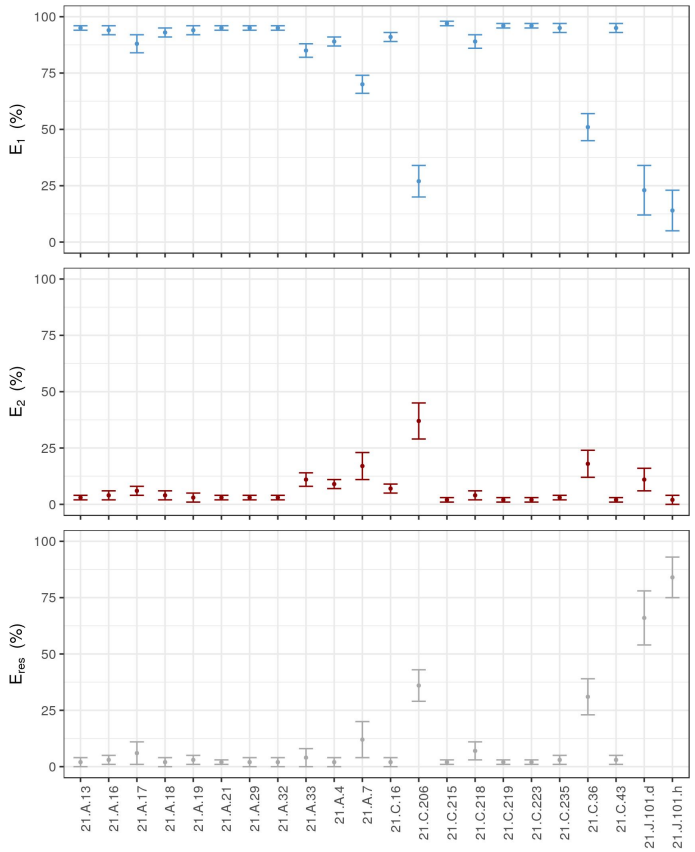

Figure S3: Estimated fractions of end-members (E_1, E_2 and E_{res}) and their uncertainties (using TS7 and Source Code S1).

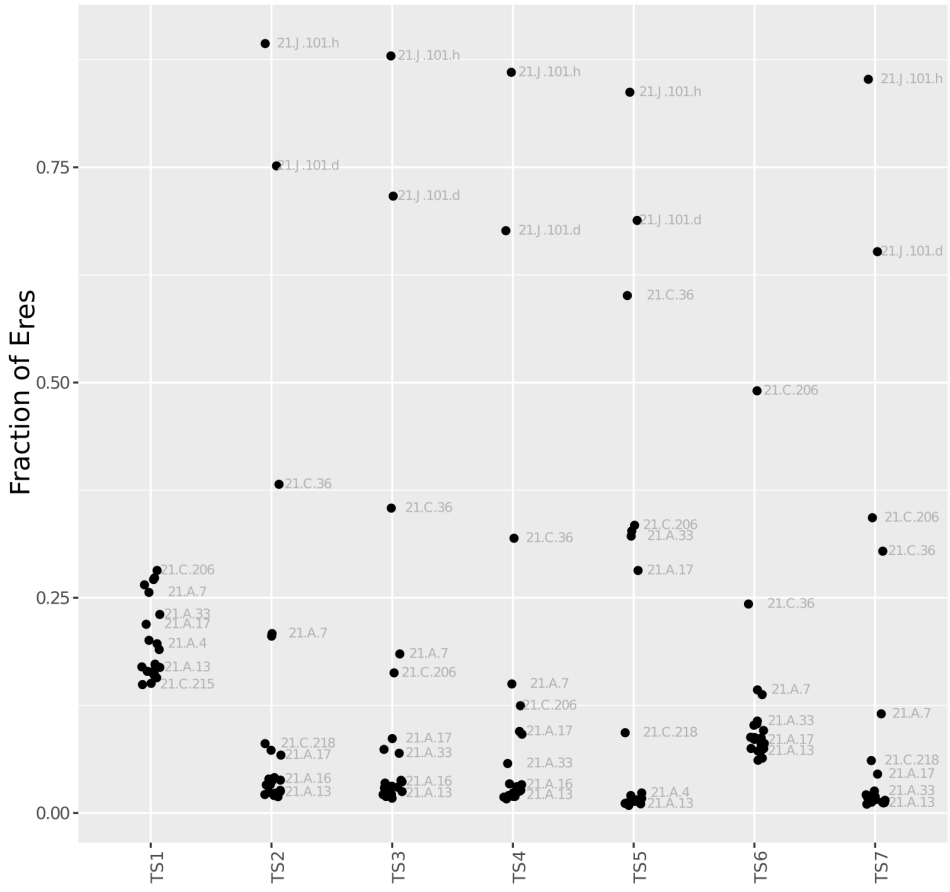

Figure S4: Sensitivity test of different tracer sets.

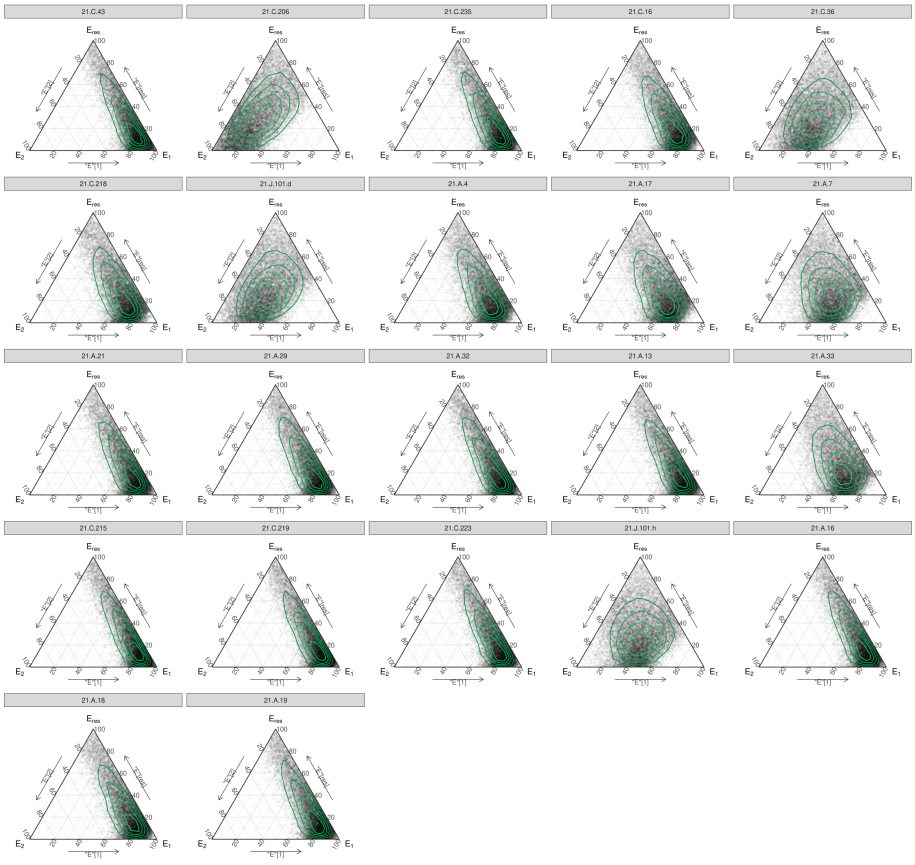

Figure S5: Ternary diagrams showing mixing ratios of all wells using tracer set 1.

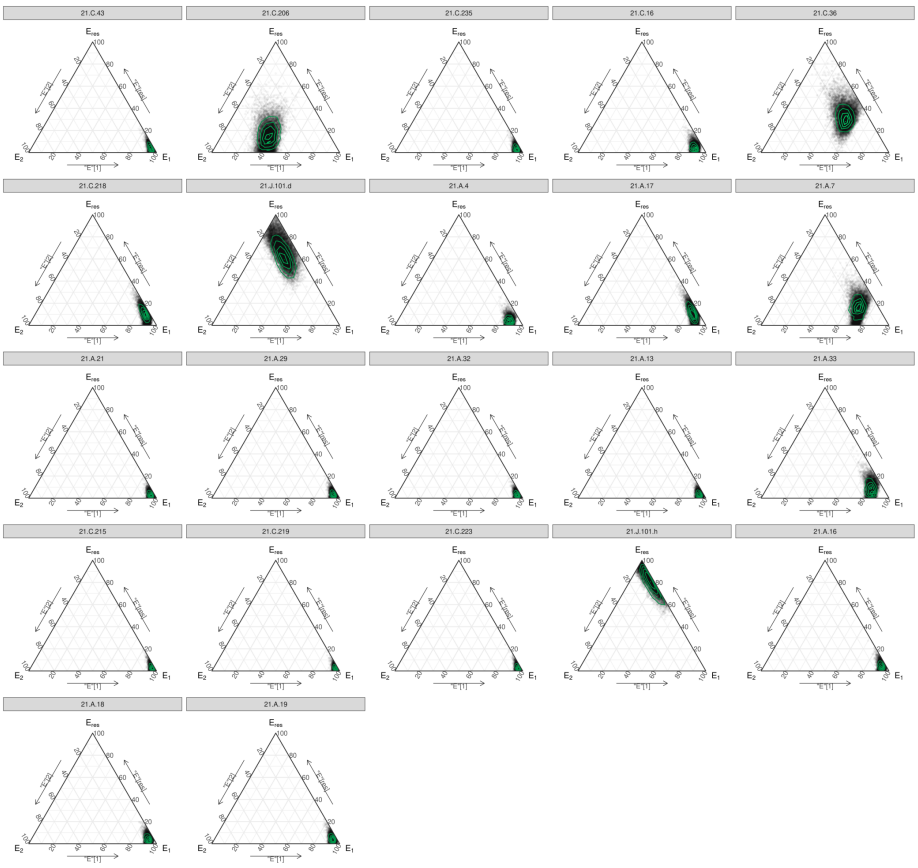

Figure S6: Ternary diagrams showing mixing ratios of all wells using tracer set 4.

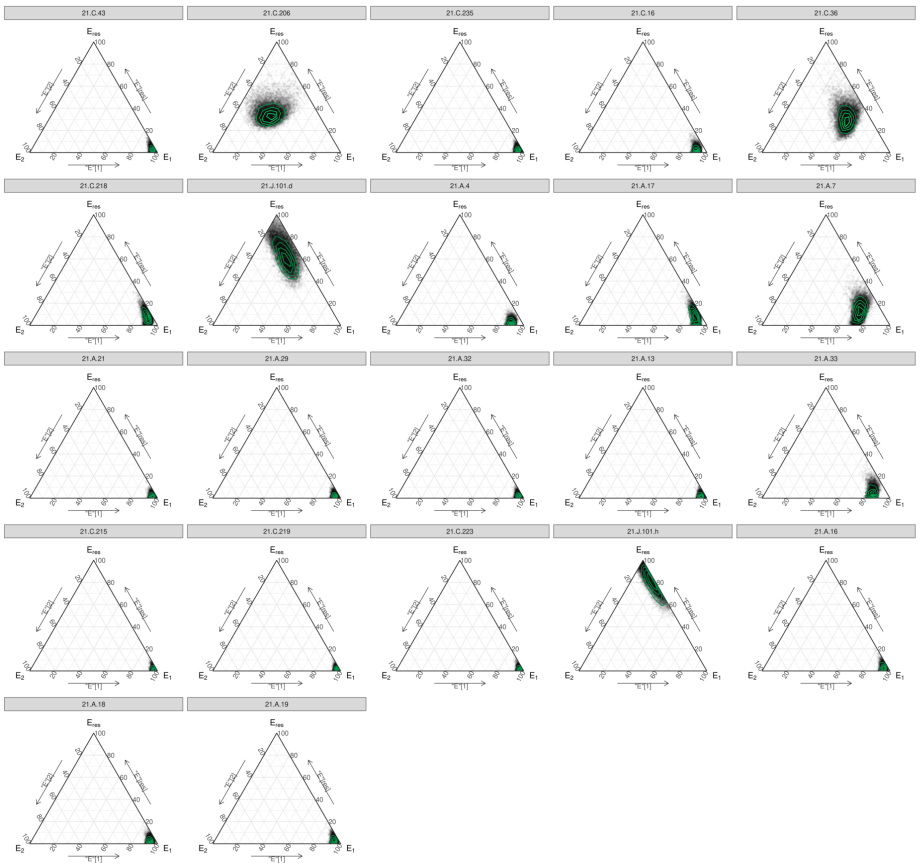

Figure S7: Ternary diagrams showing mixing ratios of all wells using tracer set 7.

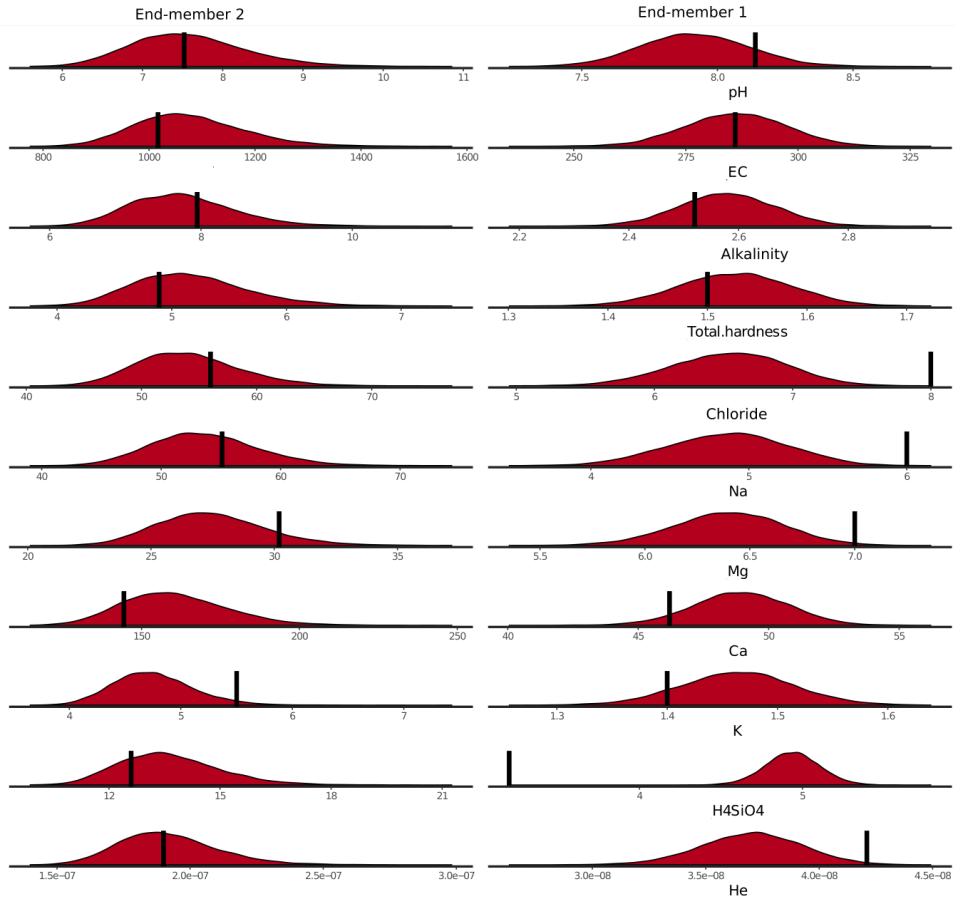

Figure S8: Comparison between model-estimated (red) and measured end-member (black) concentrations of end-members 1 and 2.

Table S1: Data for comparison between on-site and lab-based ^{4}He concentrations (ccSTP/g) (including analytical errors) as well as EC concentrations (μS/cm) of the respective wells studied.

Well ID	^{4}He (lab)	Err ^{4}He (lab)	^{4}He (on–site)	Err ^{4}He (on–site)	EC (μS/cm)
21.C.206	3.43E-07	1.72E-08	3.80E-07	3.80E-08	723
21.C.36	2.03E-07	1.01E-08	2.00E-07	2.00E-08	627
21.A.4	6.27E-08	3.14E-09	5.50E-08	5.50E-09	365
21.A.17	6.03E-08	3.02E-09	4.70E-08	4.70E-09	404
21.A.7	1.08E-07	5.40E-09	9.50E-08	9.50E-09	510
21.A.29	5.42E-08	2.71E-09	5.00E-08	5.00E-09	323
21.A.32	5.38E-08	2.69E-09	5.10E-08	5.10E-09	315
21.A.13	5.24E-08	2.62E-09	4.50E-08	4.50E-09	322
21.A.33	7.40E-08	3.70E-09	6.30E-08	6.30E-09	433
21.J.100_deep	2.63E-07	1.31E-08	1.90E-07	1.90E-08	1017
21.J.101_high	6.06E-08	3.03E-09	7.50E-08	7.50E-09	566
21.C.36	2.14E-07	1.07E-08	1.80E-07	1.80E-08	627
21.C.206	4.73E-07	2.37E-08	4.18E-07	4.18E-08	723
21.A.17	5.49E-08	2.74E-09	6.45E-08	6.45E-09	371.9
21.A.18	4.89E-08	2.45E-09	4.94E-08	4.94E-09	324.7
21.A.16	4.80E-08	2.40E-09	4.21E-08	4.21E-09	311.4
21.A.19	5.55E-08	2.78E-09	4.42E-08	4.42E-09	311.8

Table S2: Information about instruments used, parameter units, LOQ and measurement uncertainties for major ions and other physico-chemical parameters. LOQ and measurement uncertainties (±) are given in the respective parameter unit.

Parameter	Instrument	Method	Units	LOQ	±
Total hardness	Metrohm 809 Titrando	Titration with Titriplex III (0.1 mol/L); Metrohm Ion Selective Electrode	mmol/L	0.2	0.1
Alkalinity	Metrohm 809 Titrando	Titration with HCl (0.1 mol/L); Metrohm pH-electrode	mmol/L	0.2	0.1
pH	Metrohm 809 Titrando	Metrohm pH-electrode	–	–	0.05
EC	Metrohm 712 Conductometer	Metrohm conductivity-measuring flow-through cell, combined with Pt 1000 temperature detection	μS/cm	–	2
NO_3-N	Metrohm 761 Compact IC with chem. suppression	Column: Metrohm Metrosep A Supp 5 100/4 mm	mg/L	0.25	0.1
H_4SiO_4	Skalar San++ Autoanalyzer	Spectrophotometric determination after the reaction to silicon molybdenum blue complex	mg/L	0.5	0.2
SO_4	Metrohm 761 Compact IC with chem. suppression	Column: Metrohm Metrosep A Supp 5 100/4mm	mg/L	5	2
Na	Metrohm 761 Compact IC	Column: Metrohm C4-100/4.0	mg/L	2.5	0.8
K	Metrohm 761 Compact IC	Column: Metrohm C4-100/4.0	mg/L	1	0.3
Mg	Metrohm 761 Compact IC	Column: Metrohm C4-100/4.0	mg/L	2.5	0.8
Ca	Metrohm 761 Compact IC	Column: Metrohm C4-100/4.0	mg/L	5	1.7
Cl	Metrohm 761 Compact IC with chem. suppression	Column: Metrohm Metrosep A Supp 5 100/4mm	mg/L	0.5	0.2

5

UNTANGLING GROUNDWATER MIXING AND TRAVEL TIMES WITH NOBLE GAS TIME SERIES AND NUMERICAL MODELING

Chapter 5 is in preparation for publication as: Popp, A.L., Álvarez, Á., Schilling, O., Musy, S., Scheidegger, A., Peel, M., Purtschert, R., Brunner, P., Kipfer R., Untangling transient groundwater mixing and travel times with noble gas time series and numerical modeling.

Abstract

The quality and quantity of alluvial groundwater in mountainous areas are particularly susceptible to the effects of climate change, as well as increasing pollution from agriculture and urbanization. Understanding the mixing between surface water and groundwater as well as groundwater travel times in such systems is thus crucial to sustain a safe and sufficient water supply. We used a novel combination of real-time, in-situ noble gas analyses of helium-4 (^{4}He) and radon-222 (^{222}Rn) to quantify groundwater mixing of recently infiltrated river water (F_{rw}) and regional groundwater, as well as travel times of F_{rw} during a two-month groundwater pumping test carried out at a drinking water wellfield in a prealpine valley in Switzerland. Transient groundwater mixing ratios were calculated using ^{4}He concentrations as tracer combined with a Bayesian end-member mixing model. Having identified the groundwater fraction of F_{rw} consequently allowed us to infer the travel times from the stream to the wellfield, estimated based on ^{222}Rn activities of F_{rw}. Additionally, we compared and validated our tracer-based estimates of F_{rw} using a calibrated surface water-groundwater model. Our findings show that (i) travel times of F_{rw} are in the order of two weeks, (ii) during most of the experiment, F_{rw} is substantially high ($\sim$70%), and (iii) increased groundwater pumping only has a marginal effect on groundwater mixing ratios and travel times. The high fraction of F_{rw} and its short travel times emphasize the vulnerability of mountainous regions to present and predicted environmental changes.

5.1 Introduction

Surface water (SW) and groundwater (GW) are one single water resource, thus any impact on the quality and quantity of one component will in-

evitably affect the other (e.g., Winter 1995; Winter et al. 1998). Climate change is predicted to disproportionately alter the seasonality and quantity of water resources in mountainous regions such as Switzerland (Addor et al. 2014; Henne et al. 2018; Michel et al. 2020; Rössler et al. 2014; Rössler et al. 2012) by affecting snow accumulation and melting (e.g., T. R. Green et al. 2011; Maxwell et al. 2008) as well as river discharge (e.g., Addor et al. 2014; Blöschl et al. 2019). Such changes will, in turn, profoundly influence groundwater recharge and storage in mountainous environments (Rössler et al. 2014). Therefore, an improved understanding of SW-GW interactions under changing environmental conditions is highly relevant for sustainable water governance and water-dependent ecosystems in sensitive regions (e.g., Holman 2006; Krause et al. 2014).

Within the last two decades, studies on SW-GW exchange dynamics have substantially improved the understanding of the drivers and controls of water exchange patterns and their impact on biogeochemical cycling of solutes in SW-GW systems. However, spatiotemporal dynamics remain elusive due to a lack of high-resolution data that yield insight into transient SW-GW processes (Barthel et al. 2016; Boano et al. 2014; Brunner et al. 2017; Krause et al. 2014). Consequently, further progress for an improved conceptual understanding as well as model development which depends on high-resolution data for model calibration and/or validation is limited by the quantity and quality of data available (e.g., Barthel et al. 2016; Paniconi et al. 2015; Schilling et al. 2019).

Environmental tracers such as stable water isotopes or dissolved noble gases have been proven to be highly beneficial to study groundwater flowpaths, travel times and water source partitioning (e.g., Cook et al. 2000; Jasechko 2019). These tracers deliver an integrated signal over the entire catchment and thus carry important information on groundwater flow paths on larger scales (e.g., Jasechko 2019; M. Sprenger et al. 2019). Therefore, recent review papers (Brunner et al. 2017; Jasechko 2019; Schilling et al. 2019; M. Sprenger et al. 2019) emphasize the need for novel, more efficient isotope tracer measurement techniques to advance the understanding of complex feedback mechanisms occurring in river-aquifer systems. Fortunately, recent advances in hydrological modeling (e.g., Schilling et al. 2017) have proceeded synchronously with rapid methodological developments in tracer hydrology (Brunner et al. 2017; Paniconi et al. 2015)—the latter allowing for high-resolution, on-site sampling of stable water isotopes (e.g., Herbstritt et al. 2019) or noble gases (e.g., Mächler et al. 2012). One such technique enabling high-resolution (noble) gas analysis is a recently developed Gas Equilibrium-Membrane Inlet Mass Spectrometer (GE-MIMS, Brennwald et al., 2016) system, which can analyze a multitude of gas species such as the noble gas ^{4}He. The noble gas ^{222}Rn is another ideal and often used tracer to study stream-groundwater interactions (e.g.,

Gleeson et al. 2018). With a half-life of 3.8 days, ^{222}Rn can be used to assess travel times of up to $\sim$15 days of infiltrating river water to groundwater (e.g., Hoehn et al. 1989).

Accurately interpreting age dating tracer such as ^{222}Rn activities is, however, inherently challenging because every water sample typically consists of a mixture of waters with various ages (e.g., Jasechko 2019; M. Sprenger et al. 2019). Thus, disentangling major flow paths and identifying groundwater mixing processes is key to allow for an interpretation of travel times using age tracer data (e.g., M. Sprenger et al. 2019).

The main aim of the present study is to enable the interpretation of ^{222}Rn activities of a groundwater fraction by first determining groundwater mixing between recently infiltrated river water (F_{rw}) and older, regional groundwater: We first determined transient groundwater mixing ratios of F_{rw} and regional groundwater using ^{4}He concentrations as tracers in a binary end-member mixing model; second, we inferred transient travel times of F_{rw} employing ^{222}Rn activities. To this end, we analyzed dissolved (noble) gases (^{4}He, ^{222}Rn) on-site in quasi-real-time at two locations during a two-months pumping test conducted at an important wellfield used for drinking water supply of Bern, Switzerland. Finally, to test made assumptions as well as validate the tracer-based results, we compare groundwater mixing ratios obtained from the noble gas analysis with those derived from a fully-coupled and calibrated numerical SW-GW model of the wellfield built in *HydroGeoSphere* (HGS; Aquanty Inc., 2015).

5.2 Materials and Methods

5.2.1 *Site Description*

This study was conducted in the alluvial catchment of the Emmental, located at the northern margin of the Swiss Alps (Fig. 5.1). We focus on the lower part of the catchment, which consists of the river Emme and the underlying alluvial aquifer. The river exhibits a coarse gravel and sand riverbed with a very dynamic discharge, which is usually highest during snowmelt from April to May (Käser et al. 2015).

The alluvial aquifer has an average thickness of about 25 m but can extend up to 46 m. At our study location, the valley is between 200 m and 400 m wide (Würsten 1991). The upper part of the aquifer is predominantly unconfined, being filled with coarse sandy gravel and cobbles with variable fractions of silt. The saturated hydraulic conductivity of the alluvial aquifer is relatively high ($\sim 5 \times 10^{-3}$ m/s). The lower part of the alluvium overlying the bedrock consists of up to 3 m thick silty material, which hydraulically disconnects the bedrock from the alluvial aquifer (Blau et al. 1997).

A wellfield consisting of 8 wells (Br1–Br8), aligned in parallel to the river Emme (Fig. 5.1) abstracts on average a total of 24 000 L/min of groundwater. Wells Br1 to Br3 pump water from 10 m depth, whereas wells Br4 to Br8 withdraw water from 15 m depth (Käser et al. 2015).

Determining groundwater residence times at this wellfield is particularly important in the context of environmental changes, such as climate change and increasing water pollution. Michel et al. (2020), for example, found that the annual discharge of the Emme between 1999 and 2018 decreased each decade by 12±4% due to climate change impacts. Additionally, Addor et al. (2014) showed that stream discharge in the Emmental catchment is projected to decrease by 25–45% in summer (for the years 2070-2099) in response to future climate change impacts. A changing stream discharge naturally also impacts groundwater recharge pattern and most likely the groundwater quality. Consequently, predicted environmental changes are expected to negatively affect the drinking water production of the study area.

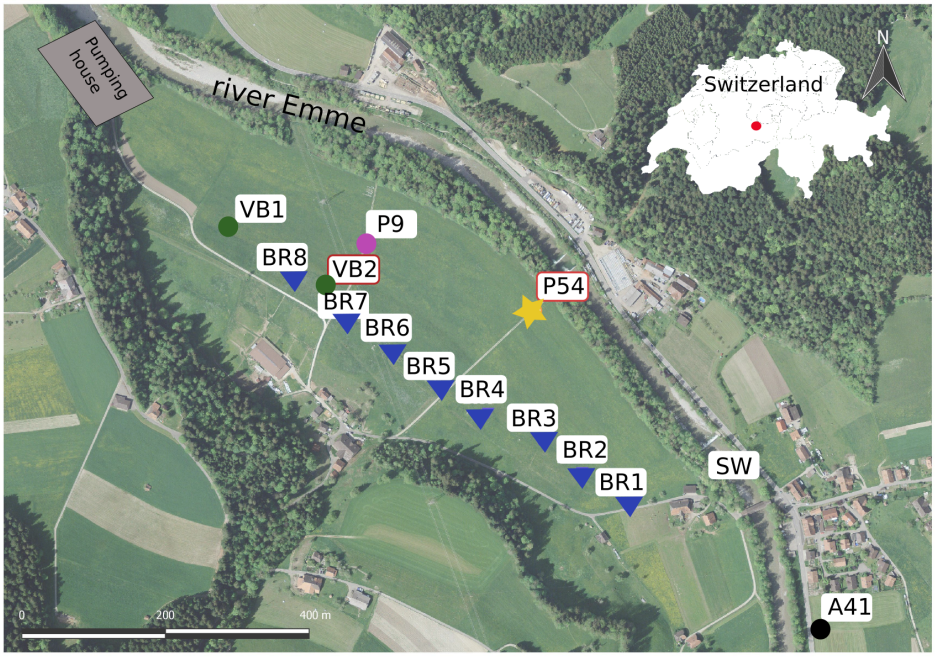

Figure 5.1: Study area showing the pumping well gallery (BR1–BR8 in blue), the newly installed wells (VB1 and VB2 in green), the location of the pumping house as well as the piezometers P54 (orange), P9 (magenta) and A41 (black). The red dot on the Swiss map indicates the location of the study site.

5.2.2 *Controlled Forcing of the System through a Pumping Test*

From January 15 to February 26, 2019, a pumping test was conducted, primarily using two newly installed wells (VB1=41 m deep and VB2=26 m deep, screened from 6 m depth to the bottom of the borehole) as well as existing wells (Br1–Br8; Fig. 5.1).

Panels a) and b) of Figure 5.2 show the dynamics of the prevailing hydraulic conditions during the pumping test, and Panel d) shows the water temperatures. Panel c) depicts the two main stages of the pumping test: 1) January 15 marks the beginning of the pumping test when pumping started with 16 000 L/min equally withdrawn from VB1 and VB2, and was gradually increased to 26 000 L/min (14 000 L/min from VB1 and 12 000 L/min from VB2) until January 18; 2) from February 12 to 26 pumping was further increased to reach an overall maximum pumping rate of 36 000 L/min by employing BR4 to BR8 (11 000 L/min) in addition to VB1 (14 000 L/min) and VB2 (11 000 L/min). On February 26 the pumping test was completed and the pumping regime at the drinking water production site went back to normal operating conditions (i.e., using Br1–Br8 only). All pumping rate data can be found in Table S1 (supporting information).

5.2.3 *Tracer-Based Approach*

5.2.3.1 *Theory and Dissolved (Noble) Gas Analyses*

The activities of the radioactive noble gas ^{222}Rn increase non-linearly in groundwater and will eventually reach a secular equilibrium after ∼20 days (∼5 half-lives; Hoehn et al.; Krishnaswami et al., 1989; 1982). The Earth's atmosphere has virtually no source of ^{222}Rn, therefore, water in equilibrium with the atmosphere is practically devoid of radon (Cook et al., 2000; Fig. 5.3). The absence of ^{222}Rn in air-equilibrated water and its short half-life render ^{222}Rn an excellent tracer to study surface water-groundwater interactions (e.g., Bourke et al. 2014; Gleeson et al. 2018; Hoehn et al. 1992).

Different to ^{222}Rn, ^{4}He is a stable noble gas, which is either of atmospheric or radiogenic origin (Fig. 5.3). The concentration of ^{4}He dissolved in groundwater ($^{4}He_{gw}$) is given by

$$^{4}He_{gw} = {}^{4}He_{asw} + {}^{4}He_{ea} + {}^{4}He_{rad} \tag{5.1}$$

where $^{4}He_{asw}$ corresponds to the helium in air-saturated water (ASW) at a given water temperature, pressure and salinity, $^{4}He_{ea}$ is helium originating from excess air formation (that is the partial dissolution of air entrapment at recharge and water table fluctuations, Heaton et al., 1981) and $^{4}He_{rad}$

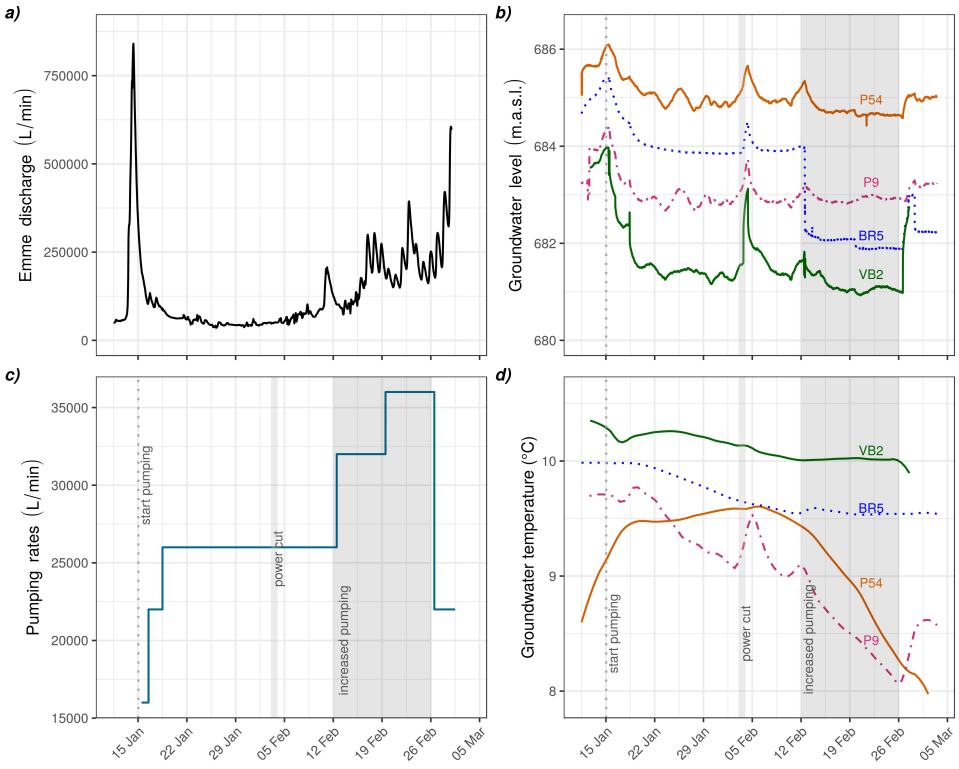

Figure 5.2: Prevailing conditions during the experiment: Panel a) shows the discharge of the Emme (recorded in Emmenmatt ∼6 km upstream of the study site), Panel b) depicts the groundwater levels of P54 (orange), VB2 (green), BR5 (dotted, blue) and P9 (dashed, magenta), Panel c) shows the total sum of groundwater pumped and Panel d) shows the water temperatures of P54, VB2, BR5 and P9. The gray segment indicates the period of maximum pumping (February 12–26). Light gray bands indicate an electric power cut occurring at the study site, which caused a shutdown of all wells from February 3, 7 p.m., to the following morning at 9 a.m.

represents radiogenic helium accumulated underground (e.g., Cook et al. 2000; Kipfer et al. 2002).

Recently infiltrated river water presumably does not contain any $^4He_{rad}$ (Gardner et al. 2011). Thus, any excess in $^4He_{gw}$ (relative to atmospheric-derived ^4He) indicates an admixture of older groundwater that also contains $^4He_{rad}$ due to longer travel times (Fig. 5.3). However, typically one has to account for the formation of excess air to assess whether elevated $^4He_{gw}$ with respect to $^4He_{asw}$ is purely atmospheric or a result of admixing older groundwater containing $^4He_{rad}$. Since we expect to sample a mixture of recently infiltrated river water (no $^4He_{rad}$) and regional groundwater, it is unfeasible to untangle the different atmospheric ^4He components ($^4He_{asw}$ and $^4He_{ea}$). Thus, we only use the concentration differences of ^4He

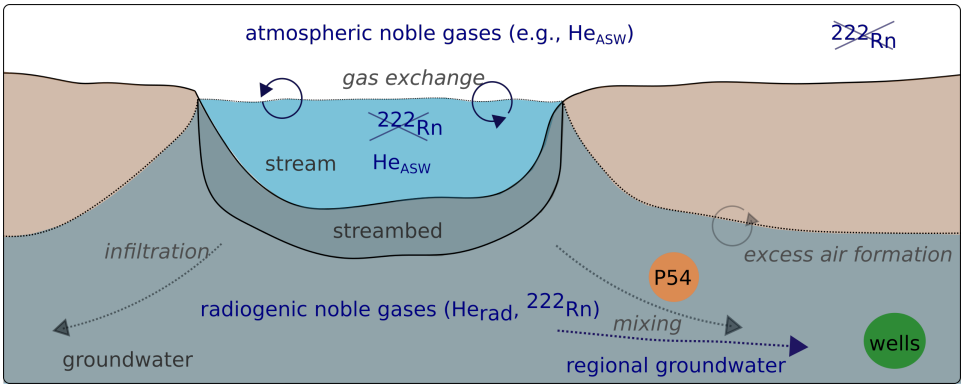

Figure 5.3: Conceptual model of processes (in italic) affecting the noble gas composition of groundwater: the ^{4}He concentration of the stream is solely affected by gas exchange with the atmosphere; once SW infiltrates, ^{4}He is added due to excess air formation. The admixture of $^{4}He_{rad}$ enriched older groundwater causes a further increase in ^{4}He concentrations. ^{222}Rn starts to accumulate once the streamwater is infiltrated.

assuming that both water sources (that is F_{rw} and regional groundwater) are similarly affected by excess air formation.

The dissolved (noble) gases were analyzed at two locations: once in the pumping house, in which we first analyzed water originating from the new Pumping Well VB2 (Fig. 5.1). VB2 is located in about 220 m distance to the stream. Water from VB2 was being abstracted by two submersible pumps (10 m and 8 m below ground) and parts of it were pumped to the pumping house. To increase the pumping rate, the existing Wells Br 5-7 and Br 4-8 were used from February 12 and 19 on, respectively (see Table S1). This water was also transported to the pumping house. This means that from February 12 on the water being analyzed in the pumping house was a mixture of waters pumped from the wellfield (i.e., BR 4-8) (Table S1). From February 12 on, however, the pumped water from VB2 was discharged into the stream (downstream of our study site). Therefore, the water mixture analyzed in the pumping house consisted only of water from BR 4-8.

In the pumping house (Fig. 5.1), we continuously analyzed dissolved ^{222}Rn using a Rad7 instrument (DURRIDGE 2019) as well as ^{4}He employing the GE-MIMS system (Brennwald et al. 2016). The two instruments were operated in parallel by allocating ∼2 L/min of pumped water to each instrument. Sampling resolution was 30 min and ∼10 min for the Rad7 and the GE-MIMS, respectively. For air-water equilibration we used commercially available membrane modules (3M Liqui-Cel 2017) for both instruments.

The second sampling location was piezometer P54 (Fig. 5.1), which is located close to the Emme (∼50 m). There, a submersible pump (Comet ECO-PLUS_20000) abstracted ∼3 L/min from a depth of 6 m (well depth is 8 m with 2 m screen at the bottom). Gas sampling and analysis were conducted in exactly the same way as in the pumping house. More details on continuous noble gas analyses are available in Text S1 and in Popp et al. (2020).

5.2.3.2 *Tracer-Based Mixing Ratios*

As previously shown (e.g., Carrera et al. 2004; Delsman et al. 2013; Hooper 2003; Popp et al. 2019), estimated water mixing ratios based on tracer measurements can exhibit large uncertainties. These uncertainties are still often neglected, which can lead to an erroneous interpretation of tracer-based mixing ratios. To quantify uncertainties and assess the reliability of our approach, we applied the Bayesian groundwater mixing framework presented in Popp et al. (2019). For this study, however, the model was simplified by excluding the possibility of unknown end-members based on expert knowledge from previous studies (Käser et al.; Schilling et al., 2015; 2017; also confirmed by the numerical model, see Section 5.3.2). Similar to Brewer et al. (2002), we assume that for every point in time the following relationship holds:

$$C = F_1\, C_{E_1} + F_2\, C_{E_2} \tag{5.2}$$

where C is the concentration of a tracer (here ^{4}He) observed at a given well, resulting from a mixture of 2 preselected end-members (that is E_1 and E_2), with corresponding concentrations (that is C_{E_1} and C_{E_2}). The non-negative mixing ratios F_1 and F_2 must sum up to one and are estimated for every point in time independently. Deviations from equation 5.2 are assumed to stem from observational errors due to tracer-related uncertainties. These errors were modeled as normal distributions with relative standard deviations. See Popp et al. (2019) for the mathematical formulation and inference of F_1 and F_2. Note that this approach neglects the time lag between observations obtained in P54 and those obtained in the pumping house. We argue that this time lag is expected to be neglectable though given the high groundwater flow velocities inferred from an artificial tracer test (Fig. S2).

First, we defined the most likely end-members present within our studied domain based on the conceptual understanding of the area. Since the alluvial aquifer is expected to be relatively homogeneous, two possible groundwater end-members can be defined: 1) recently infiltrated river water and 2) regional groundwater. Given the proximity of P54 to the stream, we argue that ^{4}He concentrations in this piezometer represent end-member 1 (E_1) (i.e., 100% recently infiltrated river water, containing excess

air but no $^4He_{rad}$)—an assumption that was supported by the numerical model (see Section 5.3.2). End-member 2 (E_2) is represented by piezometer A41 (Fig. 5.1), that previously served as background piezometer for regional groundwater (Schilling et al. 2017). There are no high-resolution time series data available for E_2. However, following Schilling et al. (2017), time series data seem dispensable since this piezometer is most likely not affected by seasonal changes or groundwater pumping.

Employing the Bayesian mixing model, we assumed an overall uncertainty of 5% for E_1 and for each individual measurement of mixed water analyzed at VB2. These uncertainties are based on analytical errors (∼2%) plus ∼3% of noise stemming from inconsistencies in the sampling and analytical procedure. For E_2, we allocated an overall uncertainty of 10% due to the strong assumption of having steady-state conditions at this location (in addition to the aforementioned uncertainties). As tracers the analyzed ^{4}He concentrations were used (n=802 each at P54 and VB2).

This approach consequently allowed us to estimate the water fraction of recently infiltrated water (F_{rw}) observed in the pumping house (see following section).

5.2.3.3 *Estimating Travel Times of F_{rw}*

Having estimated F_{rw}, we were able to determine the radon activities originating from this water fraction ($Rn_{(F_{rw})}$) assuming that ^{222}Rn activities of E_2 (Rn_{E_2}) equal those of the background well:

$$Rn_{(F_{rw})} = \frac{(Rn_{(mix)} - (1 - F_1) * Rn_{(E2)})}{F_1} \tag{5.3}$$

where $Rn_{(mix)}$ is the ^{222}Rn activity of the water mixture analyzed in the pumping house.

Consequently, we estimated TTs in days (d) (n=686) from the point of infiltration to the pumping house using the ^{222}Rn ingrowth curve (Hoehn et al. 1989) (see Fig. S1 for the ingrowth curve):

$$\mathrm{TT} = \lambda^{-1} * ln\frac{(Rn_{E2} - Rn_{river})}{(Rn_{E2} - Rn_{F_{rw}})} \tag{5.4}$$

where λ is the radioactive decay constant (0.183 day^{-1}) (Hoehn et al. 1989) and Rn_{river} corresponds to the mean radon activity analyzed in the river Emme (see Table S2).

5.2.4 *Simulation-Based Approach*

As one objective of this study is to compare and validate tracer-based mixing ratios with those from a numerical model (from here on referred to as

model-based mixing ratios), we used a model built in HGS combined with the *Hydraulic Mixing-Cell* flow tracking tool (HMC; Partington et al., 2011) to determine water mixing throughout the model domain.

HGS is able to simulate both surface water and groundwater flow in a fully-integrated way, that means, precipitation partitions into all parts of the water cycle (e.g., groundwater recharge, snow, streamflow, evaporation) in a physically-based manner, making it unnecessary to artificially impose these components as boundary conditions. HGS solves a modified version of Richard's equation using van Genuchten parametrization, allowing for the simulation of variably saturated subsurface flow, which is particularly important when simulating river-aquifer interactions (Brunner et al. 2012; Schilling et al. 2017).

Different to particle tracking, HMC allows to obtain transient mixing of water from different sources at every model cell with marginal extra computational costs (Partington et al. 2011).

We adopted the existing model built and calibrated by Schilling et al. (2017), which implies that our model setup equals the model described there.

Before the transient simulation of the pumping experiment, a quasi-steady-state simulation with constant forcing for 2 500 days (corresponding to the forcing observed at the beginning of the transient simulation period) was carried out, to obtain an equilibrated initial distribution of water sources for subsequent transient HMC analyses. For the transient simulations, all boundary conditions (that is river discharge, groundwater heads, precipitation, air temperature and snow) were updated according to corresponding values at the time of our experiment. In contrast to Schilling et al. (2017), we explicitly simulated snow accumulation, snowmelt and pore water freeze-thaw (Jonas et al. 2009; Magnusson et al. 2014), because winter conditions were prevalent during a significant part of our experiment. For a detailed description of boundary conditions and model parameters, see Schilling et al. (2017).

5.3 Results

5.3.1 *Continuously Analyzed Dissolved (Noble) Gases*

Figure 5.4 shows the ^{222}Rn activities (Panel a) and ^{4}He concentrations (Panel b) synoptically analyzed at P54 and in the pumping house. As expected, ^{222}Rn activities and ^{4}He concentrations are lower at P54 than the observations made in the pumping house, except for a short period in February (please see earlier discussion about time shift in observed concentrations).

The overall ^{222}Rn activities observed in the pumping house temporarily reached the secular equilibrium (i.e., 12 800±1 000 Bq/m^3 observed at A41, n=7). ^{222}Rn activities recorded at P54, however, have not reached the secular equilibrium, clearly indicating TTs from the stream to P54 of less than two weeks.

Similarly to the ^{222}Rn activities, the ^{4}He concentrations observed at P54 are closer aligned to the ^{4}He concentrations of air-saturated water (ASW) at 3°C, which reflects the ^{4}He concentration of the river Emme for the prevalent mean water temperature.

Although both tracers (^{4}He and ^{222}Rn) exhibit temporal fluctuations, the overall trend shows a decrease in both tracers for the duration of our experiment. Please note that the tracer activity/concentration for end-member 2 (that is the background well) was assumed to be constant over time. Also note that we did not detect any relevant ^{222}Rn activities (mean activity 190±120, n=13) in the river Emme during sporadic sampling.

5.3.2 *Comparing Tracer-Based and Model-Based Mixing Ratios of F_{rw}*

Figure 5.5 shows the estimated fraction of F_{rw} for the wellfield inferred from the tracer-based (green) and the model-based approaches (dashed, dark-red). Generally, both datasets align to a satisfying degree for the majority of the experiment, except for the first ∼10 days. Within the initial phase of the pumping test, F_{rw} calculated from the tracer data shows a sharp increase from about 40% (mean of the first 12 hours of pumping) to a mean value of about 50% within the first three days into the pumping test. The model-based calculations, however, predict an average of 80% of water originating from recently infiltrated river water within the first 12 hours and three days, respectively, which steadily decreases to about 60% until the end of January. These differences most likely arise from the uncertain assumption that had to be made with respect to the initial conditions and hence distribution of the water sources in the model-based approach. However, after the initial mismatch, both estimates are in good agreement in which F_{rw} slowly increases from ∼60% to ∼70% (Fig. 5.5).

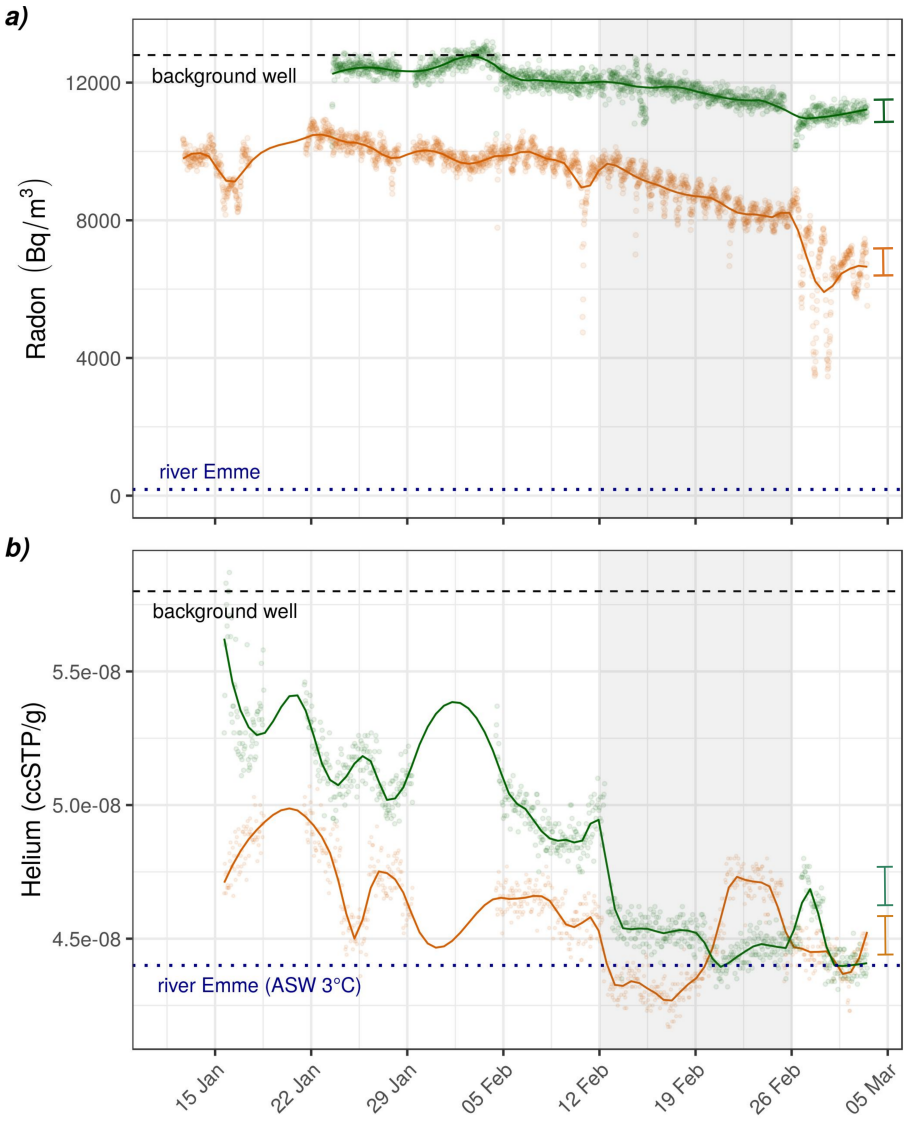

Figure 5.4: ^{222}Rn activities (Panel a) and ^{4}He concentrations (Panel b) continuously analyzed at P54 (orange) and the pumping house (green); the background well (A41, black dashed line) represents regional groundwater; ASW (blue dotted line) represents the average ^{4}He concentration of the stream water. Average uncertainties are indicated as error bars.

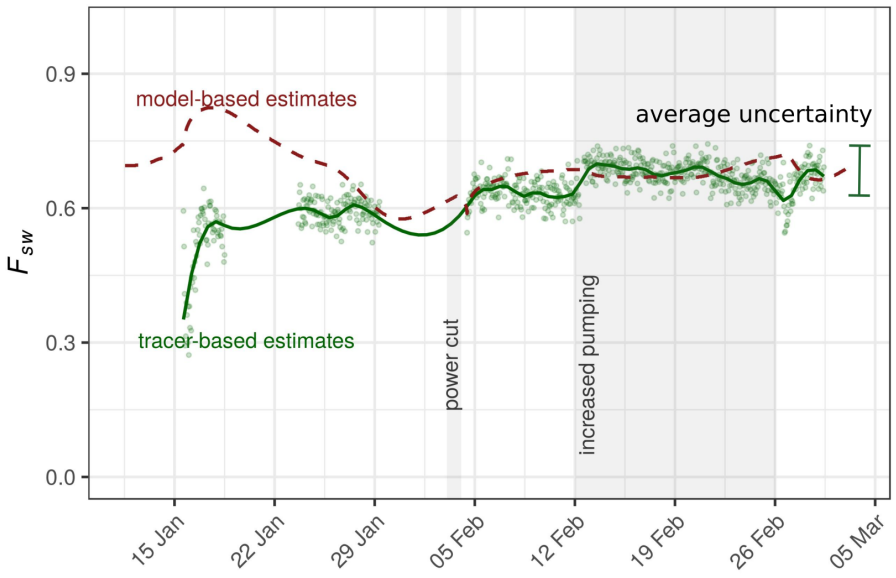

Figure 5.5: River water fractions (F_{rw}) derived from ^{4}He concentrations (green) and from the numerical model (dashed, dark-red line). Error bar indicates average model uncertainty.

Interestingly, F_{rw} shows no considerable influence of increased pumping. Only a marginal increase of ~5% in F_{rw} can be detected in the tracer-based estimates immediately after the pumping rates were increased. On the other hand, the model-based estimates show no effect (Fig. 5.5).

Mixing ratios simulated at P54 confirm that its water consists almost exclusively (~90%) of infiltrated river water. Thus, the assumption to use ^{4}He concentrations of P54 to represent the ^{4}He concentrations of F_{rw} for the groundwater mixing model seems justified.

5.3.3 *Travel Times of F_{rw}*

Knowing the fraction of river water (i.e., F_{rw}) present in the wellfield, we can use the ^{222}Rn activities of F_{rw} to infer the travel times of F_{rw} to the pumping house (see Section 5.2.3.3). Naturally, the estimated TTs show the same decreasing trend over time like the ^{222}Rn activities observed at P54 and the pumping house (Figs. 5.4 and 5.6). On average, the travel time from the stream to the wellfield is 13±2 days, which is relatively short given the potential flow path lengths of several hundred meters. Maximum travels times were recorded at the start of the pumping test until the beginning of February. Afterwards, TTs generally decreased until the end of the experiment. Towards the end of February, minimum travel times of 7±1 days were observed.

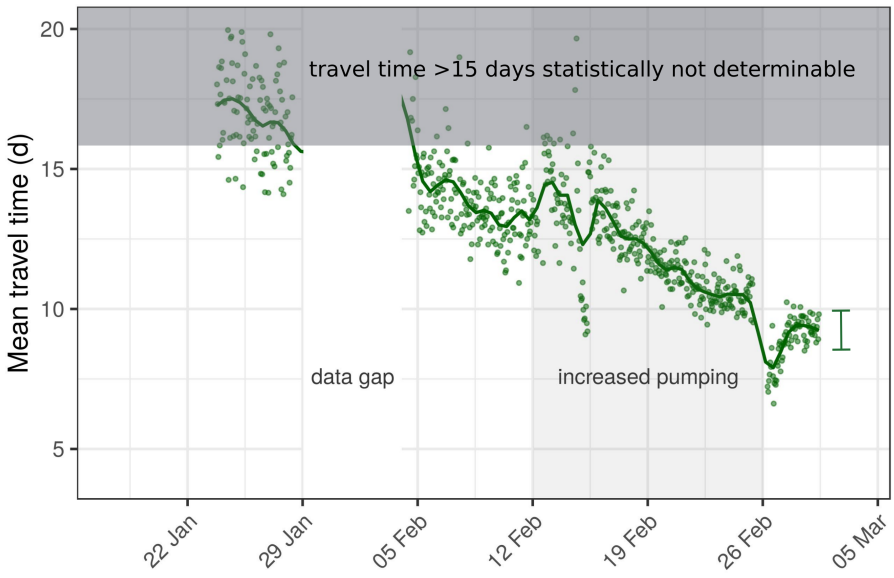

Figure 5.6: Estimated TTs of F_{rw}. Error bar indicates average uncertainty.

Our travel time estimates align well with those obtained through an artificial tracer test (using uranine) conducted as part of the pumping experiment, which revealed a travel time from the injection well (i.e., A41) to VB2 of ∼7 days (Fig. S2). Since the tracer was directly injected into the groundwater, the travel time between the point of injection and VB2 is expected to be lower than the TT of F_{rw} because the river water first has to pass the low hydraulic conductivity zone of the riverbed.

5.4 Discussion

5.4.1 *Validation of Tracer-Based and Model-Based Mixing Ratios*

The estimated mixing ratios of the tracer-based and model-based approach agree acceptably well, considering the given uncertainties related to both approaches (Fig. 5.5). There are, however, distinct discrepancies between the two approaches during the initial phase of the pumping test. These differences most likely reflect the heterogeneity (e.g., preferential flowpaths) of the aquifer, which the model does not adequately reproduce particularly at the beginning of the simulations. This effect also becomes apparent during the increased pumping when only the tracer-based mixing ratios show a slight increase in F_{rw}.

Besides comparing tracer-based and model-based mixing ratios, we can also compare results observed in this study with those obtained by

Schilling et al. (2017). They observed fractions of recently infiltrated river water within a similar range (between 70–80%) at BR7.

Consequently, we can corroborate our estimates of F_{rw} not only through a good agreement between the two independently derived estimates of this study but also by a reasonable match with previous tracer analyses.

5.4.2 *Impact of Controlled Forcing on Groundwater Tables, Mixing Ratios and Travel Times*

Figure 5.2b shows that groundwater pumping clearly has an effect on groundwater levels. Interestingly, we did not observe any major effects of increased pumping within the wellfield on the groundwater mixing ratios or TTs. These findings are, however, in line with previous results (Schilling et al., 2017, considering the uncertainties of their tracer-based estimates).

From previous and our own results, we conclude that groundwater flow paths and travel times exhibit a temporal variability, which does not appear to be governed by groundwater pumping rates. We explain this insensitivity against hydraulic forcing by the relatively high hydraulic conductivity of an aquifer with a large saturated thickness and thus high storage capacity: the high hydraulic conductivity enables large amounts of river water infiltrating at different locations within the catchment, resulting in an overall large ratio of F_{rw} in the groundwater mixture regardless of the intensity of groundwater pumping. Temporal fluctuations (e.g., increase in F_{rw} and decrease in travel times of F_{rw}) seem to be controlled by the rise in river discharge (thereby enhancing infiltration rates) over the duration of this experiment (Fig. 5.2a).

5.4.3 *Limitations of Estimated F_{rw} and Travel Times*

Despite the validation of the groundwater mixing ratios by two independently executed methods, we acknowledge remaining limitations of this study. Since any water sample is principally a mixture of waters with different travel times, any interpretation of tracer data is challenging and potentially erroneous (e.g., M. Sprenger et al. 2019). Ideally, we would have analyzed multiple age-dating tracers (e.g., argon-37 and $^{3}H/^{3}He$) to capture a wide-range of potential water ages. However, such tracer studies cannot be carried out with a high resolution since they are typically costly or difficult to sample. Also, only specialized laboratories are able to conduct such analyses. We acknowledge that our estimated TTs using ^{222}Rn are potentially biased—the actual distribution of travel times of F_{rw} can differ from the possible dating range of ^{222}Rn. At the same time, we

argue that in the context of drinking water production from bank filtrate, the identification of water fractions younger than 15 days is most relevant. This is particularly true for Switzerland because according to Swiss law groundwater used for drinking water production must have a travel time of at least 10 days (Der Schweizerische Bundesrat 2018). Thus, in terms of drinking water supply, a conservative estimate (i.e., lower limit) of water travel times is of highest interest, as provided with the data-set at hand.

5.5 Implications and Conclusions

The generally acceptable agreement of the two methods used to quantify F_{rw} (Fig. 5.5) shows that transient mixing ratios can reliably be determined by quasi-continuous noble gas measurements using ^{4}He concentrations as tracer (Fig. 5.5). Determining groundwater mixing ratios consequently enabled us to interpret the ^{222}Rn activities of the recently infiltrated water fraction as travel times (Fig. 5.6). This approach of first identifying major water sources and second interpreting the age tracer data of the water fraction of interest is, to our knowledge, presented in this paper for the first time. We also demonstrated that high-resolution noble gas analysis in the field enables the investigation of the system response to groundwater pumping in quasi-real time.

Our findings imply that changes in hydraulic forcing in a highly conductive system create a sharp response in hydraulic heads (Fig. 5.2) but groundwater mixing and TTs remain mostly unaffected (Figs. 5.4 and 5.6). Moreover, we highlight that a substantial fraction ($\sim$70%) of abstracted groundwater originates from recently infiltrated stream water that exhibits travel times as low as 7 ± 1 days. These findings imply that the system studied is susceptible to environmental changes, particularly given the disproportionately large impact climate change has on high-elevation terrain.

Acknowledgments

All data and code used in this study can be found in the supplementary information or will be made available in an online repository. We thank Laurent Marguet, Roberto Costa, Reto Britt and Kay Fries for their support in the field. We thank Tracerlabor Dr. Wernli for providing the artificial tracer test data. Moreover, we are grateful for the model input data provided by the Federal Office for the Environment (BAFU), MeteoSwiss and the Canton of Bern. A.L.P. acknowledges funding by the EU Framework Programme for Research and Innovation Horizon 2020 ITN "Hypotrain" (Grant: 641939) and Eawag

5.6 Supporting Information

This Supplementary Material includes

- Text S1 describing the noble gas data collection and handling
- Figure S1 showing the Radon ingrowth curve
- Figure S2 showing the uranine breakthrough observed at VB2
- Table S1 containing data on the pumping rates

All code and remaining data used in this study will be made available in an online repository.

Text S1

Number of observations for ^{4}He n=1045 at P54 and n=922 in pumping house; number of observations for radon-222: n=1092 at P54 and n=907 in pumping house. Differences in number of observations are due to different extents of data cleansing and data gaps.

To compare data obtained with the GE-MIMS and with the Rad7, all data time-series were aggregated to mean bi-hourly data.

Furthermore, we note that the noble gases collected in the pumping house are potentially subjected to degassing: the water pumped from the different wells (i.e., VB2 and BR4–8) was eventually released into a pipe, which was not fully filled with water. Thus, particularly lighter gases (e.g., ^{4}He) might have degassed slightly. A gas-water equilibrium in the not submerged part of the pipe will eventually have been established, which potentially caused a dampening and delaying effect to changes in the gas composition due to changes in pumping. The water flow rate within the pipe, however, was relatively high so that degassing most likely did only occur at the surface of the water within the pipe. We sampled water from the bottom of the pipe, which was most likely not well mixed with the degassed part of the surface.

We calibrated the GE-MIMS measurements by comparing peak heights between ambient air (analyzed as standard) and the gases equilibrated in the head space of the membrane module, thereby receiving partial pressures of the gas species observed. The partial pressures were converted to dissolved gas concentrations according to the gas-specific Henry coefficients at the respective water temperature (recorded with a water temperature probe). For a more detailed description about continuous dissolved (noble) gas analysis using the GE-MIMS see Popp et al. (2020). ^{222}Rn in water activities were calculated according to the recorded water temperature using the software "CAPTURE" provided by Durridge (`https://durridge.com/software/capture/`).

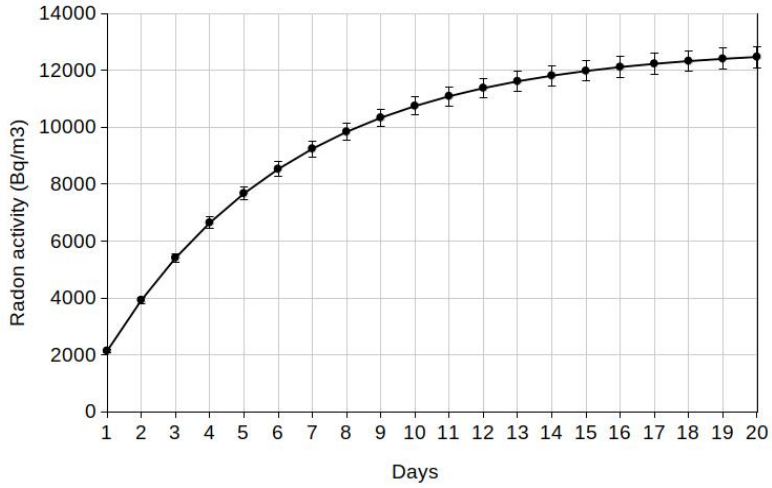

Figure S1: Radon ingrowth curve with the secular equilibrium being 12 800 Bq/m^3 (mean activity observed at the Background Well A41); error bars show analytical uncertainty.

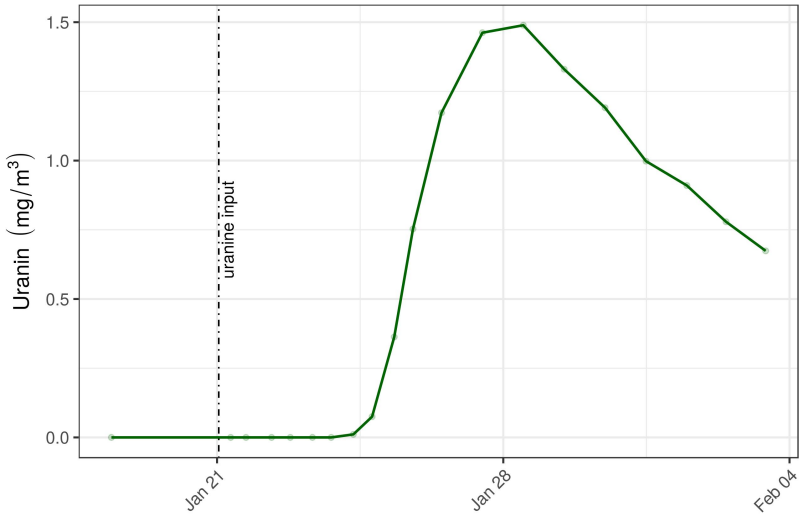

Figure S2: Uranine tracer breakthrough observed at VB2. 1 kg uranine was injected on January, 21, 2019 at 3 p.m. into piezometer A41.

Table S1: Pumping rates (L/min) of the respective wells for the duration of our experiment.

Date	VB1	VB2	Br 5–7	Br 4–8
15.01.19 12:00	8000	8000	0	0
16.01.19 12:00	8000	8000	0	0
16.01.19 12:01	12000	10000	0	0
18.01.19 12:00	12000	10000	0	0
18.01.19 12:01	14000	12000	0	0
12.02.19 12:00	14000	12000	0	0
12.02.19 12:01	14000	11000	7000	0
19.02.19 12:00	14000	11000	7000	0
19.02.19 12:01	14000	11000	0	11000
26.02.19 12:00	14000	11000	0	11000
26.02.19 12:01	0	0	8250	13750
01.03.19 12:00	0	0	8250	13750

Part III

DENITRIFICITATION IN RIPARIAN GROUNDWATER

6

A NEW ON-SITE METHOD FOR TRACING DENITRIFICATION IN RIPARIAN GROUNDWATER

Chapter 6 has been published as: Popp, A.L., Manning, C.C., Brennwald, M.S. and Kipfer R. (2019), A new in-situ method for tracing denitrification in groundwater, *Environmental Science & Technology*, https://doi.org/10.1021/acs.est.9b05393.

Abstract

The spatiotemporal dynamics of denitrification in groundwater are still not well understood due to a lack of efficient methods to quantify this biogeochemical reaction pathway. Previous research used the ratio of N_2 to argon (Ar) to quantify net production of N_2 via denitrification by separating the biologically-generated N_2 component from the atmospheric-generated components. However, this method does not allow to quantify the atmospheric components accurately since the differences in gas partitioning between N_2 and Ar are being neglected. Moreover, conventional (noble) gas analysis in water is both expensive and labor-intensive. We overcome these limitations by using a portable mass spectrometer system, which enables a fast and efficient in situ analysis of dissolved (noble) gases in groundwater. By analyzing a larger set of (noble) gases (N_2, He, Ar and Kr) combined with a physically meaningful excess air model, we quantified N_2 originating from denitrification. Consequently, we were able to study the spatiotemporal dynamics of N_2 production due to denitrification in riparian groundwater over a six-month period. Our results show that denitrification is highly variable in space and time, emphasizing the need for spatially and temporally resolved data to accurately account for denitrification dynamics in groundwater.

6.1 Introduction

One of the most prevalent water quality threats in many parts of the world is excess nitrogen, which primarily results from extensive fertilizer application in agriculture (Mekonnen et al. 2015; Rockström et al. 2009; Stevens 2019). Water quality impacts of excess nitrogen are severe and include, but are not limited to, algae blooms and hypoxia, which in turn can have harmful effects on a variety of ecosystems (Sinha et al. 2017; Stevens 2019).

Excess nitrate (NO_3^-) poses a prevalent and lasting threat to drinking water (WHO 2011). Nitrate pollution of the environment is projected to continue rising due to an increasing population, changing land management practices and climate change (Sinha et al. 2017; Yu et al. 2019). Thus, it is expected that in future more drinking water sources worldwide will have nitrate concentrations exceeding potability limits (e.g., the 50 mg/L nitrate threshold of water potability defined by the E.U. (European Union 1991; Sinha et al. 2017; UNEA 2017).

Denitrification is known as the major biogeochemical reaction pathway attenuating nitrate concentrations in water under anoxic conditions (Davidson et al. 2006; Groffman et al. 2009; Korom 1992; Rivett et al. 2008). This microbially mediated process converts NO_3^- to nitrogen gas (N_2) (Groffman et al. 2006; Saunders et al. 2001; Smith et al. 1991). Denitrification depends on (i) the presence of NO_3^-, an electron donor (most commonly—dissolved organic carbon, DOC) and denitrifying bacteria, (ii) the scarcity of O_2 (i.e., anaerobic conditions under which nitrate becomes the microbially preferred electron acceptor instead of O_2), and (iii) favorable ambient conditions regarding temperature and pH (optimum values lie between 25°C and 35°C, and 5.5 and 8.0, respectively) (Rivett et al. 2008). However, the availability of an electron donor and anaerobic conditions are the most critical factors for denitrification (Rivett et al. 2008).

Well-recognized hotspots for high nitrate removal are riparian zones, which are the dynamic interfaces between streams and shallow groundwater where surface water and groundwater exchange (Gu et al. 2012; Hill et al. 2014; Peter et al. 2012; Ward et al. 2018). Riparian zones deliver a multitude of ecosystem services by retaining and removing pollutants such as nitrate (Krause et al. 2017). In river-aquifer systems, the conditions favorable for denitrification are controlled by the ambient sediment texture (i.e., hydraulic conductivity) and the hydraulic connection between the stream and the surrounding aquifer (Mendoza-Lera et al. 2017; Newcomer et al. 2018; Packman et al. 2003).

Numerous studies have investigated denitrification in (riparian) aquifers at different spatial and temporal scales using a variety of methods (Merill et al. 2014; Ranalli et al. 2010; Rivett et al. 2008). However, despite the importance of denitrification and technological advancements, the spatiotemporal dynamics of this process remain poorly understood. This is because most conventional methods require discrete sample collection and lab-based analyses—thus most methods available are prohibitively costly and labor-intensive (Boyer et al. 2006; Davidson et al. 2006; Groffman et al. 2006; Kolbe et al. 2019). Ignoring the dynamics of denitrification, however, may lead to insufficient groundwater monitoring for nitrate contamination and an erroneous assessment of water quality.

Previous research (Boyer et al. 2006; Davidson et al. 2006; Groffman et al. 2006) stresses that the fundamental problem regarding studying denitrification is the difficulty of quantifying the end-product, N_2, due to its high atmospheric background (78% N_2 in air, Ozima et al., 1984), which makes denitrification "a miserable process to measure" (Groffman et al. 2006).

The atmospheric N_2 component dissolved in groundwater originates from air-water exchange during groundwater recharge which involves gas equilibrium partitioning as well as the ubiquitously observed (partial) dissolution of entrapped air bubbles leading to the formation of excess air (i.e., a surplus of atmospheric gases relative to the atmospheric solubility equilibrium) (Oana 1957). Dissolved atmospheric, noble gases in groundwater are solely affected by physical processes (i.e., groundwater recharge temperature and excess air), whereas reactive gases such as N_2 are not only affected by physical but also by biogeochemical processes (e.g., denitrification) (Kana et al. 1994). Therefore, to quantify N_2 stemming from denitrification in groundwater, one needs to separate the different N_2 components: N_2 resulting from air-water gas exchange during groundwater recharge can be identified and quantified using noble gas measurements to model the physical gas partitioning of N_2. Subsequently, N_2 in excess of the atmospheric components can be attributed to denitrification (Vogel et al. 1981; Wilson et al. 1990).

Previous studies (Blicher-Mathiesen et al. 1998; Böhlke et al. 2009; Eschenbach et al. 2018; C. T. Green et al. 2008; Izbicki et al. 2015; Kana et al. 1994; Kennedy et al. 2009; McAleer et al. 2017; Stenger et al. 2018; Szymczycha et al. 2017; Vogel et al. 1981; Weymann et al. 2008; Wilson et al. 1990) have used a combined analysis of N_2 and the noble gas Ar (i.e., the N_2/Ar method) to account for the atmospheric N_2 component and thereby quantify net denitrification in groundwater. Inherently, this approach assumes that air bubbles dissolve completely during excess air formation. This assumption, however, is physically-incorrect since the hydrostatic pressure necessary for the complete dissolution of entrapped air bubbles is almost never sufficient in natural groundwater systems (Kipfer et al. 2002; Klump et al. 2008). The current scientific consensus on excess air research is that an initially trapped air bubble dissolves only partly, which leads to the formation of excess air that is elementally fractionated (i.e., the water phase is enriched in the heavier, more soluble noble gases with respect to completely dissolved air) (Kipfer et al. 2002; Klump et al. 2008). Therefore, to accurately estimate the atmospheric N_2 components, one needs to quantify i) excess air formation, which is typically fractionated relative to air (Aeschbach-Hertig et al. 1999; Holocher et al. 2003; Kipfer et al. 2002; Klump et al. 2007) and ii) the water recharge temperature which determines the gas solubility equilibrium concentration. The amount and fractionation of excess air, however, can only reliably be

estimated if the concentrations of several noble gas species are available (Aeschbach-Hertig et al. 2008; Kipfer et al. 2002; Klump et al. 2007; Mächler et al. 2013a,b).

Here, we present a new method to overcome the limitations of conventional (noble) gas analysis (i.e., costly and time-consuming) and the commonly used N_2/Ar method (i.e., neglecting excess air fractionation). We employed a recently developed Gas Equilibrium-Membrane Inlet Mass Spectrometer (GE-MIMS) system (Brennwald et al. 2016) to obtain spatially and temporally resolved time series data of dissolved gas concentrations including N_2, O_2 as well as the noble gases Ar, helium (He) and krypton (Kr) in groundwater.

Thereby, we were able to quasi-continuously analyze dissolved gas concentrations directly in the field at three different piezometers located in the riparian zone from January until June 2018. Having the concentrations of three different noble gas species available allowed us to estimate the groundwater recharge temperature as well as the amount and fractionation of excess air. Thereby, we can reliably determine the atmospheric N_2 components using in situ noble gas analysis. With the obtained data-set, we consequently explored the spatiotemporal dynamics of denitrification in groundwater over a six-month period.

Gas analysis was complemented by the analyses of DOC and NO_3^- concentrations, which are key factors for denitrification. Moreover, we observed typical transformation products originating from the conversion of NO_3^- to N_2, which include elevated alkalinity and sulfate ion (SO_4^{2-}) concentrations (requiring electron donors like organic matter and pyrite, respectively) (Hayakawa et al. 2013; Rivett et al. 2008; Uyanik et al. 2011). To determine drivers of spatial variability in denitrification, we also determined the local sediment properties as well as the biological activity. All these chemical and sedimentological parameters govern the ambient conditions for denitrification because the hydraulic conductivity of the porous media and the microbial activity control gas and solute transport and can thereby affect denitrification (Mendoza-Lera et al. 2017).

The key objectives of this study are to use continuous, on-site (noble) gas spectrometry combined with an excess air model to (i) quantify N_2 stemming from denitrification and to (ii) identify spatiotemporal denitrification dynamics and its drivers in riparian groundwater.

6.2 Materials and Methods

6.2.1 *Site Description*

Our study site is located in northern Switzerland in the city of Dübendorf (Fig. 6.1). We conducted our experiments at a restored stream reach of

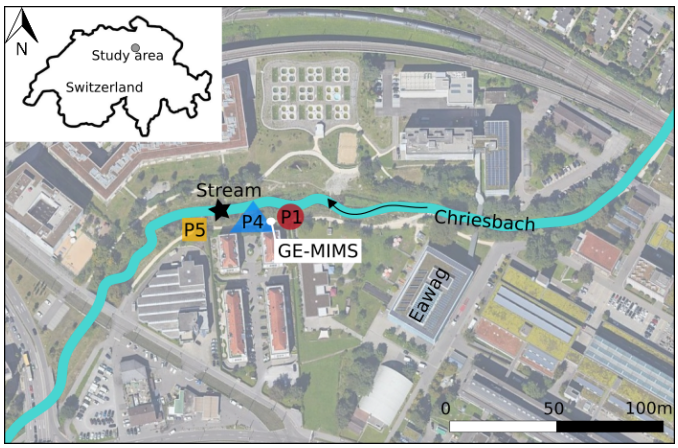

Figure 6.1: Study area showing the approximate locations of the three piezometers (P1 in red, P4 in blue and P5 in orange) as well as the stream sampling location (in black), the installed GE-MIMS and the surrounding urban area.

the Chriesbach—a heavily urbanized, losing stream (Kurth et al. 2015). The majority of its length has been channelized and treated wastewater accounts for up to ∼30% of the discharge (AWEL 2018).

The streambed consists of fine sands and loam (Kurth et al. 2015) and is known to be partially clogged due to the settling suspended matter originating from an upstream wastewater treatment plant (AWEL 2012).

Water from three piezometers (P1, P4 and P5) was weekly (microbiology, water chemistry) and quasi-continuously (gas measurements) analyzed from January until June 2018. The piezometers are located approximately 0.5 m from the stream alongside the streambank (Figs. 6.1 and S3). Each piezometer is 6 m deep and screened over its entire length. Please note that the groundwater studied represents recently infiltrated river water (that is bank filtrate) and therefore any reference to groundwater throughout the text relates to shallow groundwater of a riparian aquifer. For more information about aquifer properties, please see Text S2.

6.2.2 *Estimating the Hydraulic Conductivity of the Streambank*

Stream-aquifer interactions are controlled by hydraulic head gradients and the hydraulic conductivity of the sediments (k) (Mendoza-Lera et al. 2017; Packman et al. 2003). The latter defines how easily a fluid flows through a porous matrix and is determined by the sediment texture (such as grain size distribution and packing) (Bear 1972). To gain insight into the local sediment texture of the streambank at our study site, we conducted slug tests at all piezometers (P1, P4 and P5). Thereby, we estimated the local

hydraulic conductivity of the streambank using the Bower-Rice slug test solution (Bouwer et al. 1976).

6.2.3 *Analysis of Total Cell Concentrations*

The sediment texture governs not only the hydraulic conductivity but also the available area for microbial colonization, thereby impacting the abundance of microbial communities (Mendoza-Lera et al. 2016). Microbes can, in turn, alter the hydraulic conductivity through biofilm growth fostering clogging and affecting water residence times and pollutant turnover (Krause et al. 2017).

Total cell concentrations (TCC) in water were determined as a rough indicator of denitrification potential in all three piezometers and in the stream using flow cytometry (Prest et al. 2013). We sampled TCC as water samples (n=13 at each location from January until June 2018) in 12 ml flasks, which contained para-formaldehyde to fix the microbes. The flasks were cooled immediately after sampling and analyzed the next day at Eawag (see Table S1 for more information).

6.2.4 *Analysis of Key Parameters associated with Denitrification*

Nitrate, DOC and low oxygen concentrations are essential prerequisites for denitrification to occur, whereas the formation of sulfate and bicarbonate ions (i.e., alkalinity) are typical transformation products associated with denitrification (Hayakawa et al. 2013; Rivett et al. 2008; Uyanik et al. 2011).

On a weekly basis we sampled these key parameters at all three piezometers and at the stream (except for O_2 concentrations, which were determined continuously; see next section).

For the determination of NO_3^-, DOC, alkalinity and SO_4^{2-} concentrations we took water samples in 1 L Schott glass bottles, which were stored in a cooling room immediately after sampling. The samples were analyzed the following day at Eawag (see Table S1 for instruments used, limits of quantification and uncertainties). For water sampling of the piezometers we used fixed installed groundwater pumps (see next section), except for the streamwater, which was sampled manually.

6.2.5 *Continuous Dissolved (Noble) Gas Analysis*

For the continuous dissolved (noble) gas analysis we permanently installed a GE-MIMS system (Brennwald et al. 2016) in a wooden box with access to a power supply at the study site (Figs. 6.1 and S3). Three submersible pumps (Comet ECO-PLUS_20000; placed $\sim$3 m below the

groundwater table) continuously abstracted groundwater (∼0.8 L/min) from the three piezometers. To prevent algae growth and atmospheric gas contamination, we used nontransparent, gas impermeable nitrile tubing for water transport from the wells to the GE-MIMS. The tubing was buried about 30 cm below ground to avoid any extreme cooling or heating of the water. The pumped water was first filtered (Nussbaum, chrome-steel, 10 microns) before flowing to commercially available membrane modules (MiniModule 1x5.5, 3M Liqui-Cel, 2017). While water was flowing through the membrane module, a gas equilibrium was established between the gas species dissolved in the sampling water and the gas species in the head space of the module. Through a capillary connecting the head space of the module with the GE-MIMS, a small gas fraction entered the MS for gas analysis (Brennwald et al. 2016). After passing the membrane module, the water was disposed of into the stream downstream of our study area. Each piezometer had its own water filter and membrane module to allow for quasi-continuous gas analysis.

The GE-MIMS features six different gas inlet ports, which allow for quasi-continuous, consecutive sampling of up to six different sampling locations (although one gas inlet port is usually reserved for the calibration of the MS with ambient air). We used four ports in total: one for each piezometer and one for sampling of ambient air. At every piezometer He, Ar, Kr, N_2 and O_2 were alternately analyzed, which took about 8 minutes for each analysis block, plus two minutes of purging for the gas inlet system between switching inlet ports. After repeating the set of water samples twice, one standard was analyzed. By obtaining a standard approximately every 1.5 hours, we were able to correct for instrument sensitivity drifts, e.g., due to air temperature changes.

Water samples were calibrated by comparing peak heights between ambient air and the gases equilibrated in the head space of the membrane module. Thereby, we could calculate the partial pressures of the respective gas species observed. The partial pressures were converted to dissolved gas concentrations according to the gas-specific Henry coefficients at the respective water temperature (recorded with a MAXIM type DS18B20 sensor placed at the membrane module).

For more details on dissolved (noble) gas theory in riparian aquifers, see Text S1. For more technical details regarding the GE-MIMS system, we refer to Brennwald et al. (Brennwald et al. 2016).

6.2.6 *Estimating N_2 Production due to Denitrification*

The total dissolved N_2 (from here on referred to as $N_{2(tot)}$) consists of atmospheric N_2 components and N_2 originating from denitrification:

$$N_{2(tot)} = N_{2(ASW)} + N_{2(EA)} + N_{2(DEN)} \tag{6.1}$$

where $N_{2(ASW)}$ represents the air-saturated water concentration (ASW) due to the equilibration with the atmosphere at the atmospheric pressure and recharge water temperature, $N_{2(EA)}$ is the amount of N_2 due to excess air formation and $N_{2(DEN)}$ corresponds to N_2 stemming from complete denitrification (please see Text S2 and Fig. S1 for an explanation regarding the assumption of complete dentrification).

To obtain the noble gas recharge temperature (NGT), the amount of excess air (A) and the fractionation factor (F) necessary to accurately quantify excess air, we used the "closed-equilibrium" (CE) model (which assumes a concentration equilibrium between the entrapped air and water)(Aeschbach-Hertig et al. 2008, 2000; Klump et al. 2008) by applying an inverse modeling approach(Aeschbach-Hertig et al. 1999; Ballentine et al. 1999) employing the noble gas data (He, Ar and Kr) observed at each piezometer as input parameters (see Text S1). The CE-model is able to account for the continuous and progressive dissolution of entrapped air in porous media and thereby, provides an adequate estimate of excess air formation (Holocher et al. 2003; Klump et al. 2008).

$N_{2(ASW)}$ was calculated for the prevailing ambient pressure and estimated NGTs (Equation S1, Text S1) and $N_{2(EA)}$ was calculated according to the same parameters as well as A und F. Having calculated the atmospheric N_2 components ($N_{2(ASW)}$ and $N_{2(EA)}$), we can subsequently quantify the amount of N_2 produced by denitrification by solving for $N_{2(DEN)}$ (Equation 6.1).

Note that from here on we applied local polynomial regression fitting (i.e., "LOESS") to all data sets shown in Figures 6.3, 6.5, 6.6 to reduce noise and increase readability. LOESS uses a weighted, sliding-window to locally fit conditional means (Jacoby 2000). Please note that this approach smooths out the short-term variability of the data. However, without smoothing the data it would be inherently difficult to detect trends and pattern with the amount of data available. For a detailed discussion regarding issues during field work that let to data gaps, please see the supporting information (Text S2).

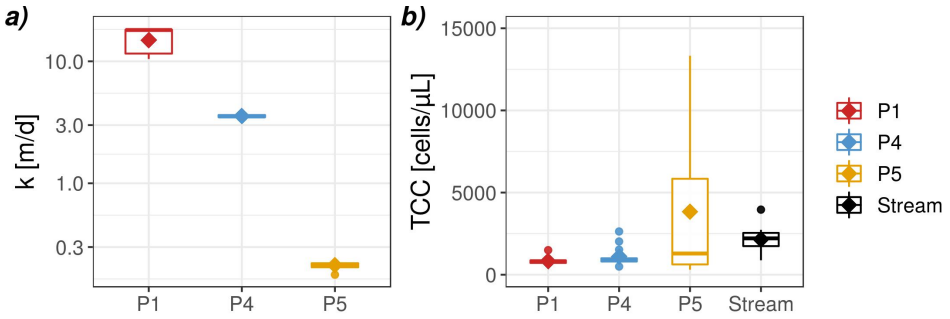

Figure 6.2: a) The hydraulic conductivity (log-scale) analyzed at P1 (n=5), P4 (n=13) and P5 (n=9); b) the total cell concentrations observed at P1, P4, P5 and at the stream (n=13 at each location); diamonds represent mean values.

6.3 Results and Discussion

6.3.1 *Spatial Variations of Hydraulic Conductivity and Total Cell Concentration*

According to the results of the slug tests, hydraulic conductivity varies over two orders of magnitude within the approximately 40 m stream reach studied (Fig. 6.2a): P1 shows, with a mean of 15 ($\pm$4) m/d, the highest hydraulic conductivity, P5 ranks lowest, with 0.21 ($\pm$0.02) m/d, and P4 lies in between P1 and P5, with a mean k of 3.6 ($\pm$0.1) m/d.

The observed spatial differences in hydraulic conductivity seem to be reflected in the observed spatial differences of the total cell concentrations (Fig. 6.2): P1 shows the lowest mean concentration with 830 ($\pm$250), P4 exhibits a mean of 1100 ($\pm$600), and P5 shows the highest mean with 3800 ($+/(-)$4600) TCC (cells/μL) (please note that $\pm$ represents the standard deviation and that from here on $+/(-)$ refers to standard deviations being larger than the mean concentrations).

In contrast to P1 and P4, P5 has a comparatively high variability in TCC. On average, the stream has higher TCC concentrations (2200$\pm$800 TCC cells/μL) than P1 and P4 but, interestingly, a lower mean than P5. The high variability in TCC at P5 also shows that microbial activity can vary over several orders of magnitude within weeks, which most likely also influences nitrate respiration rates.

TCC in all piezometers is unusually high for groundwater—the natural background concentration in groundwater with a residence time longer than a few days is $\sim$10 cells/μL (Besmer et al. 2016). The high TCC concentrations observed in our samples demonstrate that stream water, which typically has higher TCC than groundwater, feeds the underlying groundwater and that travel times from the stream to the groundwater must be

short (i.e., a few days), as also indicated by previous radon measurements (Kurth et al. 2015).

Moreover, our findings indicate that both parameters, k and TCC, are potentially linked: a high hydraulic conductivity appears to correlate to low total cell concentrations (at P1) and vice versa (at P5). These results are in line with previous studies (Mendoza-Lera et al. 2016; Newcomer et al. 2018), which found that microbial abundance greatly varies depending on the sediment texture because the sediment texture governs the available surface area for microbial colonization and advective mass transport of water, solutes and gases.

6.3.2 *Key Parameters associated with Denitrification*

Chemical species associated with denitrification show that the conditions in the riparian groundwater of our study site are favorable for denitrification (Fig. 6.3; n=22 for each parameter and piezometer except for O_2): constantly high nitrate and DOC concentrations in the river guarantee a permanent supply of two key chemical species for denitrification (Fig. 6.3a and 6.3c, respectively). At the same time, the riparian groundwater is well below 10% of oxygen saturation for most of the time of our experiment (Fig. 6.3b). Moreover, nitrate concentrations in all three piezometers are considerably reduced compared to the concentrations in the stream, indicating denitrification (Fig. 6.3a).

P1 exhibits with 7% the highest mean O_2 saturation (i.e., O_2 in respect to $O_{2(ASW)}$), P4 shows a slightly lower mean saturation with 6% and P5 has the lowest mean saturation with 2% (Table 6.1). The locally observed oxygen concentrations seem to correspond to the ambient hydraulic conductivity observed at the respective piezometer: the highest mean O_2 saturation found at P1 indicates that the highest k also results in the best hydraulic connection between the stream and the aquifer, delivering more oxygen rich stream water; whereas the lowest k at P5 leads to the lowest mean O_2 saturation.

The O_2 concentration time series of P4 and P5, however, sporadically show elevated levels, which most likely result from enhanced infiltration of oxygenated stream water to the riparian groundwater (Fig. 6.3b). These more aerobic conditions can inhibit denitrification—however, it has been shown that denitrification can still occur in anoxic microzones of bulk oxic sediments (Briggs et al. 2015).

Also, sulfate and alkalinity concentrations are variable over time and again distinctively different in the three piezometers and the stream (Figs. 6.3d and e). For most of the time, we observed elevated concentrations of sulfate and alkalinity with respect to the stream water

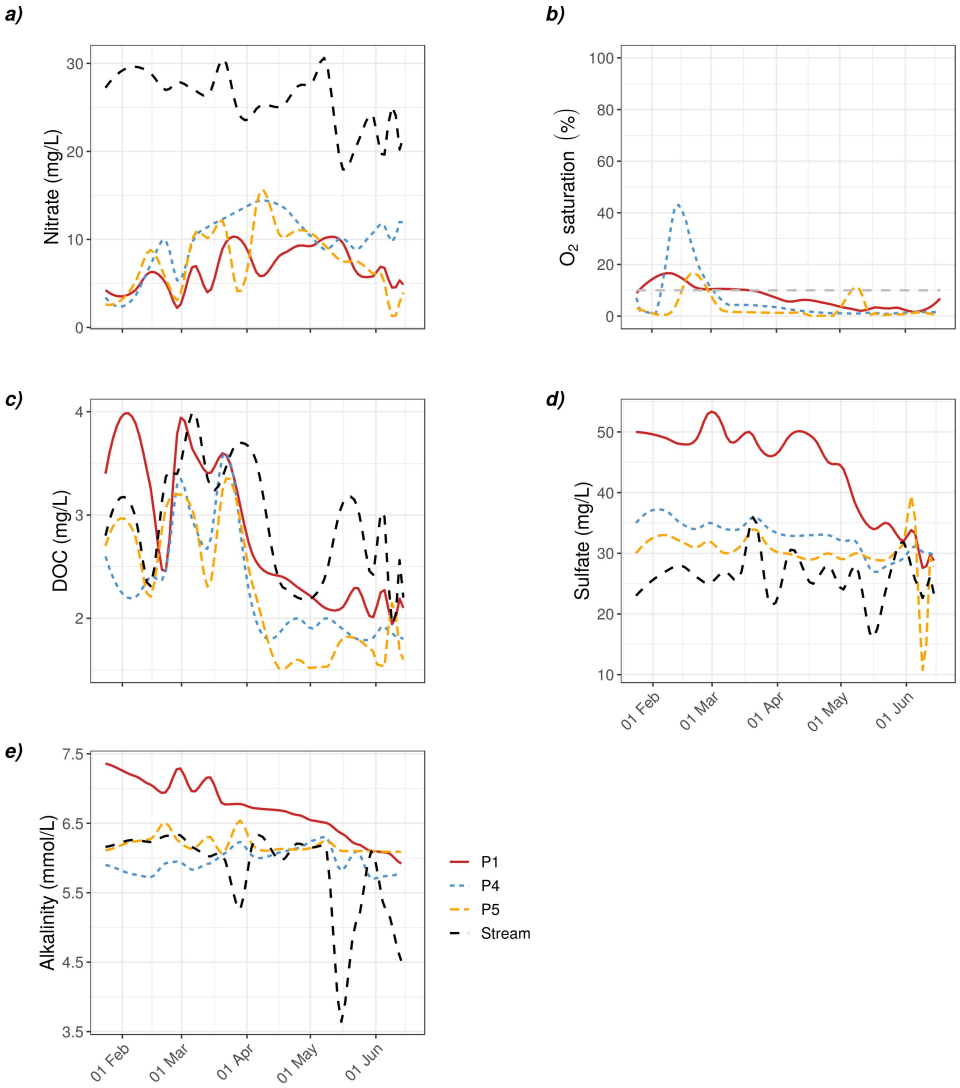

Figure 6.3: Concentrations of key parameters associated with denitrification (panels a–e). Gray dashed line in panel b shows 10% O_2 saturation indicating hypoxic conditions.

Table 6.1: Number of total observations of N_2, O_2 and N_2 excess continuously analyzed at P1, P4, and P5, and their respective mean concentrations ± standard deviations. Number of observations differs between locations due to varying extents of data cleansing. [a] Refers to $N_{2(DEN)} + N_{2(EA)}$ normalized to $N_{2(ASW)}$.

	P1	P4	P5
Number of total observations	4373	3977	2738
N_2 (10^{-5} cm^3_{STP}/g_{water})	156 (±10)	156 (±11)	161 (±13)
O_2 (10^{-5} cm^3_{STP}/g_{water})	5 (±4)	5 (±9)	2 (±3)
O_2 saturation (%)	7 (±5)	6 (+/(−)12)	2 (+/(−)5)
N_2 excess (%)[a]	18 (±4)	19 (±5)	23 (±5)
$N_{2(EA)}$ (10^{-5} cm^3_{STP}/g_{water})	60 (±40)	70 (±60)	80 (±60)

concentrations at all three piezometers, which is a clear indicator of denitrification occurring.

6.3.3 *N_2 Production due to Denitrification*

Previous studies used N_2/Ar to account and correct for N_2 injection due to excess air formation (Blicher-Mathiesen et al. 1998; Böhlke et al. 2009; Eschenbach et al. 2018; C. T. Green et al. 2008; Kana et al. 1994; Kennedy et al. 2009; McAleer et al. 2017; Szymczycha et al. 2017; Vogel et al. 1981; Weymann et al. 2008; Wilson et al. 1990). Thereby it is assumed that the produced excess air has an elemental composition matching that of free unfractionated air presuming the complete dissolution of air bubbles (Heaton et al. 1981; Kipfer et al. 2002). It has been shown, however, that unfractionated excess air has no mechanistic physical basis as entrapped air bubbles almost never completely dissolve at groundwater recharge (Holocher et al. 2003; Klump et al. 2008; Stute et al. 1992b). In contrast, the used CE-model approach to frame excess air formation is capable to correctly describe the partial dissolution of entrapped air in porous media. The conventional N_2/Ar approach would only be applicable if excess air was negligible ($A \sim 0$, $F \sim 0$; Fig. 6.4). At our study site most gas measurements, however, show considerable amounts of excess air being produced which is elementally strongly fractionated (Fig. 6.4). Thus, for the majority of the measurements only the CE-approach leads to a physically acceptable interpretation of excess air formation, which cannot be achieved by the N_2/Ar method.

Figure 6.5 shows that $N_{2(tot)}$ concentrations vary spatially and temporally at all three piezometers and that they are distinctively elevated with respect to $N_{2(ASW)}$ concentrations. At P1, we observe the lowest mean concentration of $N_{2(EA)}$, whereas P5 exhibits on average about 30% more

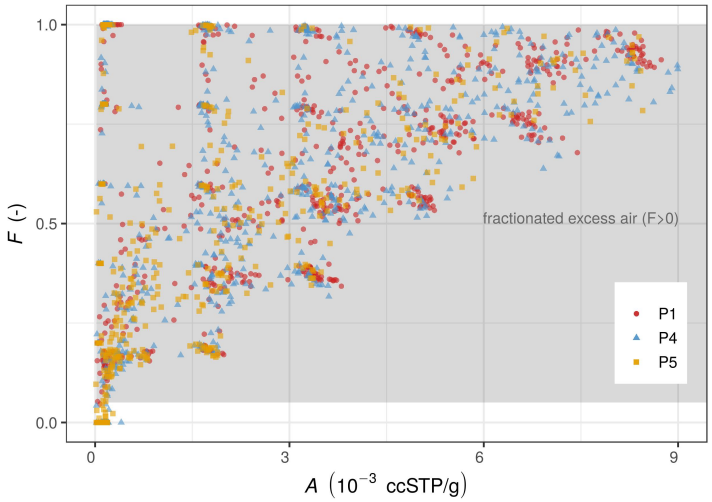

Figure 6.4: Amount of excess air (A) vs. elemental fractionation (F) calculated for the three piezometers using the CE-model. Grey area shows where excess air formation is affected by fractionation.

$N_{2(EA)}$ than P1 (Table 6.1, Fig. 6.5). Generally, $N_{2(EA)}$ decreases at all three piezometers towards the warmer summer months (see difference between black and grey data in Fig. 6.5). This might be related to increased clogging of the riverbed due to an enhanced biofilm growth, which in turn can reduce water infiltration.

$N_{2(EA)}$ concentrations vary to a great extent not only temporally but also spatially within this small scale of about 40 meters (Table 6.1). The lower hydraulic conductivities at P4 and P5 compared to P1 most likely explain the higher excess air content of P4 and P5 because air entrapment and immobilization of air bubbles strongly depend on the local sediment characteristics and are fostered in fine grained sediments (Klump et al. 2007). Thus, we hypothesize that the different sediment textures observed at the three piezometers result in different feedback mechanisms between excess air formation, microbial growth and nutrient delivery, which in turn affect nitrate availability and turnover.

Figure 6.6 shows the prevailing hydraulic conditions (Panels a and b) during our experiment as well as the concentrations of NO_3^- (Panel c) that were estimated to have been denitrified for all three piezometers ($N_{2(DEN)}$, Equation 6.1). For the time of our experiment, an average concentration of 10 mg/L denitrified NO_3^- was present at P1 and P4, and 13 mg/L at P5. The average uncertainty to determine denitrification with the method presented is 2 mg/L NO_3^-. Interestingly, these mean values lie in a similar range at all three piezometers even though external conditions such as hydraulic conductivity and TCC concentrations are distinctively different at each piezometer. Since all piezometers, however, are constantly recharged

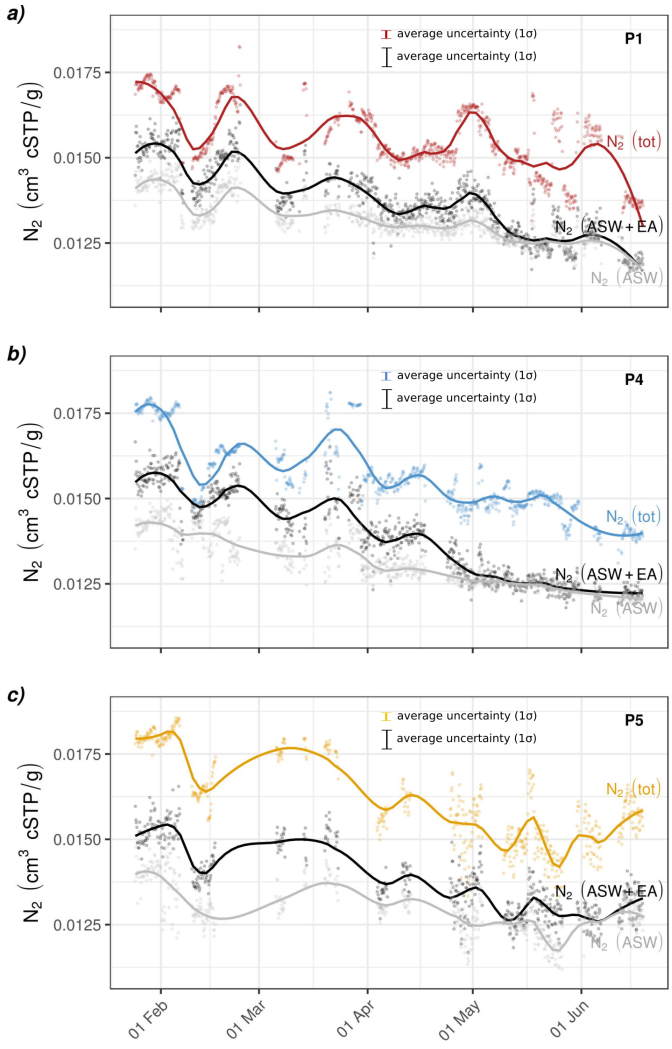

Figure 6.5: Colored lines (panel a in red=P1; panel b in blue=P4; panel c in orange=P5) show the observed $N_{2(tot)}$ concentrations; gray lines show the $N_{2(ASW)}$ concentrations for the respective piezometer; black lines show the sum of $N_{2(ASW)}$ and $N_{2(EA)}$; 1-σ indicates the averaged standard deviation of 5 aggregated data points. The difference between $N_{2(tot)}$ and $N_{2(ASW+EA)}$ represents the amount of N_2 originating from denitrification.

by the same water source (i.e., receiving the same nitrate supply), this similarity can be explained reasonably well. Overall, the highest respiration of nitrate to N_2 observed at P5 can most likely be attributed to the overall lowest O_2 concentrations observed at this piezometer.

Denitrification, however, differs not only spatially but also temporally: from virtually no denitrification in February at P4 when O_2 levels at P4 were relatively high (Fig. 6.3b) to more than 22 mg/L of NO_3^- being respired in June at P1 when O_2 levels in P1 were lowest (Figs. 6.3b and 6.6). Figure 6.6 also demonstrates that the main difference in the concentration of denitrified NO_3^- between P5 and the other piezometers (i.e., P1 and P4) occurred in the colder months, when the latter had temporarily better but still low oxygenated conditions (Fig. 6.3b).

Moreover, piezometers P1 and P4 both show a response to higher discharge events (shown as darker gray segments in Fig. 6.6). Shortly after such events, denitrification in P1 and P4 seems to decrease, whereas P5 appears to remain rather unaffected. While this pattern can again be related to the different hydrogeologic properties, we would like to note that an in-depth interpretation of the relation between hydrological dynamics and denitrification is not possible without knowing the residence time and flow-paths of groundwater (see also Text S2).

The high temporal variability of denitrification most likely results from the dynamic interactions occurring in river-aquifer systems, where the infiltration of oxygenated river water (as sporadically observed at P4 and P5; Fig. 6.3b) reduces or inhibits denitrification. Moreover, the spatial differences in sediment characteristics and microbial activity (Fig. 6.2) are additional factors contributing to differences in space and time as these parameters influence flow paths and reaction rates.

P1 and P4 exhibit comparatively low $N_{2(DEN)}$ concentrations throughout January until mid March, whereas from end of March on, denitrification observed at P1 and P4 approximates that of P5. The overall increase in denitrification observed at P1 and P4 (Fig. 6.6) can be explained by the gradual decrease in O_2 saturation (Fig. 6.3b) and a potentially enhanced nitrate turnover due to higher microbial activities with increasing temperature (Rivett et al. 2008). The slight decrease in denitrification observed at P5 might result from an increased biofilm growth, which in turn can reduce the infiltration rate(Battin et al. 1999) and limit the delivery of nitrate-rich stream water to the riparian groundwater. An enhanced biofilm growth would limit infiltration rates at P5 to a greater extent than at P1 or P4 because of the already low hydraulic conductivity present at P5. The hypothesis of reduced infiltration rates as a consequence of partial clogging of the streambed in warmer summer months is further corroborated by the decline in DOC concentrations over time (Fig. 6.3c). The system studied is, however, apparently not DOC limited because denitrification still

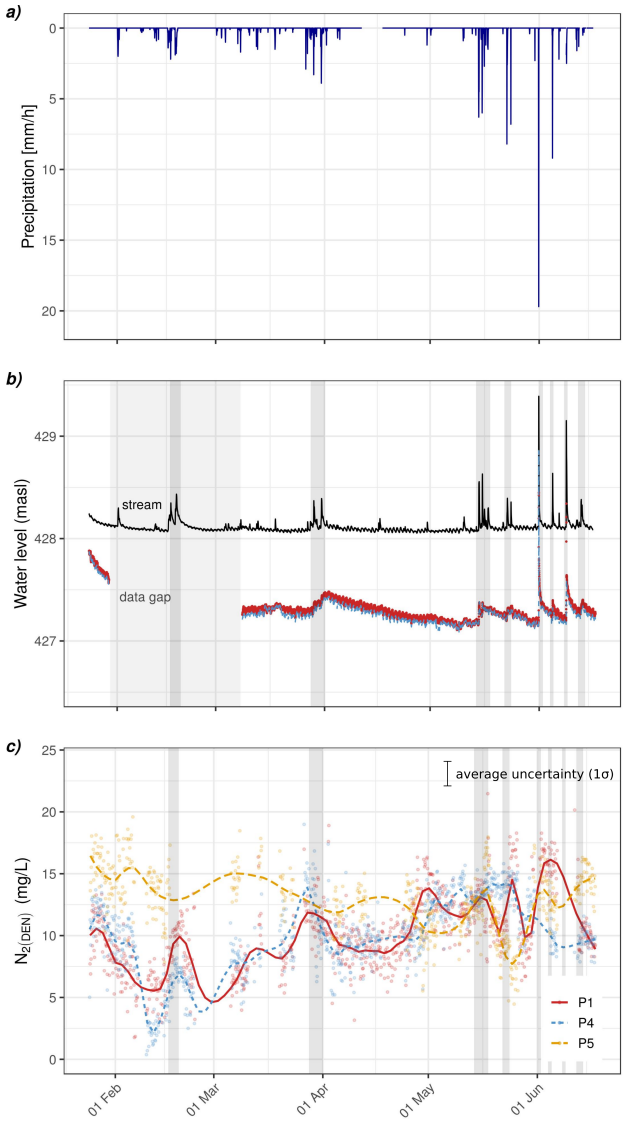

Figure 6.6: Panel a and b show the hydrological conditions for the duration of our experiment: precipitation observed at the study site and water levels of the Chriesbach (black) as well as P1 (red) and P4 (blue, dashed), respectively (data of P5 not available). Panel c illustrates estimated concentrations of N_2 originating from denitrification at P1, P4 and P5; error bar indicates averaged 1-σ uncertainty. Darker gray segments indicate high discharge events.

increases (P1 and P4) or stays the same (P5) despite the decrease of DOC in the warmer summer months.

The highest observed value of respired nitrate (22 mg/L at P1) corresponds to ∼25% of dissolved N_2 originating from denitrification. This result aligns well with estimates of Wilson et al. (1990), who found that denitrification can account for up to 25% of N_2 in a limestone aquifer. Moreover, our results add experimental evidence to model-based findings (Newcomer et al. 2018) demonstrating the enormous capacity of riparian zones to convert nitrate to nitrogen gas and to also store this gas. Our experimental data also underscore previous other model-based findings (Dwivedi et al. 2018) showing that respiration rates in riparian corridors can vary to great extents spatially and temporally and that losing streams can efficiently remove nitrate (Shuai et al. 2017).

We conclude that nitrate respiration to N_2 in riparian groundwater is highly variable in time and space, as denitrification is dependent on competing controls. On the one hand, a well connected stream-aquifer system fosters denitrification by constantly supplying enough nitrate and DOC. On the other hand, it can impede denitrification by also delivering O_2-rich stream water. A combination of a rapid low-cost method like the GE-MIMS combined with a physically meaningful excess air model presents a valuable new tool to study denitrification dynamics in fast-changing groundwater systems.

Acknowledgements

We thank four anonymous reviewers for their constructive feedback, which helped to improve this manuscript. We thank Benjamin Plüss, Wendelin Wild, Jonas Zbinden and Reto Britt for their support in setting up the field experiment. The AUA laboratory at Eawag is thanked for analyzing the water samples for nitrate, DOC, sulfate, alkalinity, nitrite and ammonium concentrations. Moreover, we thank Frederik Hammes and Michael Besmer for discussions about microbes in groundwater systems. Frederik Hammes is acknowledged for analyzing the TCC samples. The Federal Office for the Environment (FOEN) is thanked for providing the precipitation data. A.L.P. acknowledges funding by the EU Framework Programme for Research and Innovation Horizon 2020 ITN "Hypotrain" (Grant: 641939) and Eawag.

6.4 Supporting Information

This Supplementary Material includes

- Text S1 providing background information on dissolved (noble) gas theory;
- Text S2 explaining assumptions and limitations of this study;
- Text S3 stating some field work issues;
- Code S1 providing links to the noble gas data processing scripts;
- Figure S1 showing Nitrite and Ammonium data of P1, P4, P5 and the stream (weekly sampling);
- Figure S2 showing the recorded stream water temperature and estimated NGTs for all piezometers;
- Figure S3 showing a picture of the study site including the stream, the piezometers and the location of the GE-MIMS;
- Table S1 containing information about instruments used, limits of quantification and uncertainties for the data shown in Figure 3 (manuscript);
- Dataset S1 contains (noble) gas data obtained at piezometer P1, P4 and P5;
- Dataset S2 contains the CE-model results and subsequent calculations for piezometer P1, P4 and P5;
- Dataset S3 contains the data for Figure 3 (except for oxygen, which can be found in Dataset_S2), Figure 2 (microbial activity) and Figure S1 for all piezometers;
- Dataset S4 contains the hydraulic conductivity (k) data for all piezometers;
- Dataset S5 contains the stream (Chriesbach) water level data (data source: `http://www.hydrometrie.ch/KundenDaten/EAWAG/HBZHa-558.htm`);
- Dataset S6 contains the groundwater level data of P4 and P5;
- Dataset S7 contains precipitation and air temperature data (data source: `https://bafu.meteotest.ch/nabel/index.php/abfrage/start/english` recorded at station "Dübendorf-Empa".

Datasets S1 to S7 are available online: `https://doi.org/10.25678/0001JD`.

Text S1: Dissolved (Noble) Gas Theory.

In surface waters, gas exchange occurs at the interface between the atmosphere and water bodies (Kipfer et al. 2002). Commonly, dissolved gases in well mixed surface waters reach an equilibrium with atmospheric gases according to Henry's Law (assuming that gases are neither produced nor consumed):

$$C_{gas}^{ASW} = \frac{p_{gas}^{atm}}{H_{gas}(T_w, S_w)}, \tag{6.2}$$

where C_{gas}^{ASW} (cm^3STP/g_{water}) is the gas concentration of a gas species (e.g., N_2) in air-saturated water (ASW), p_{gas}^{atm} is the partial pressure (atm) of a gas species in dry air, and H_{gas} is the Henry coefficient (atm) of a gas species at a specific temperature (T_w, °C) and salinity (S_w, ‰) of the water (Kipfer et al. 2002). Once surface water infiltrates, the abundance of gases in shallow groundwater changes: reactive gas species typically increase due to gas production (e.g., N_2 or CO_2) or decrease due to gas depletion (e.g., O_2); excess air—the dissolution of entrapped air bubbles due to water table fluctuations and groundwater recharge—affects both reactive and noble gases and can supersaturate groundwater in dissolved gases by up to 50% (Heaton et al. 1981; Kipfer et al. 2002). Moreover, excess air is typically fractionated (Aeschbach-Hertig et al. 1999; Holocher et al. 2003; Kipfer et al. 2002), which means that during excess air formation the composition of the dissolved gas and the remaining gas phase differs from that of pure atmospheric air. Thus, to reliably study N_2 production due to denitrification, excess air formation including fractionation patterns need to be quantified accurately.

Aeschbach-Hertig et al. (2000) introduced a widely accepted excess air model (CE model), which assumes that the gas composition in the entrapped gas bubbles and the dissolved gases are in solubility equilibrium with respect to the elevated pressure in the gas phase. Thus, the dissolved gas concentration in groundwater (C_{gas}, cm^3STP/g_{water}) of a gas at a given temperature (T_w; assuming salinity to be zero) and ambient atmospheric pressure (P, atm) can be described by the CE model as follows:

$$C_{gas}(T_w, P, A, F) = C_{gas}^{ASW}(T_w, P) + \frac{(1-F)Az_{gas}}{1 + F\frac{Az_{gas}}{C_{gas}^{ASW}(T_w)}}, \tag{6.3}$$

where A (cm^3STP/g_{water}) represents the amount of dry air per unit mass of water initially entrapped in the water and z_{gas} is the volume fraction of the gas in dry air; F (–) describes the degree of fractionation of bubble dissolution, with F≈0 implying that all air bubbles are completely dissolved and F≈1 implying that basically no entrapped gas is dissolved in

the surrounding groundwater; F>0 means that only a partial dissolution of entrapped air occurred, which favors the more soluble gases causing a fractionation with respect to the complete dissolution of air in which case the heavier, more soluble gases are enriched in the water phase.

Text S2: Assumptions and Limitations.

In this study, we assume that nitrate is fully reduced to N_2 and we neglect other processes that potentially contribute to N_2 dissolved in groundwater such as Anammox. During weekly measurements, we analyzed nitrite and ammonium, but found only very low concentrations (see Fig. S1). These data suggest that nitrification, Anammox, ammonification or nitrate reduction to NH_4^+ (i.e., DNRA) play no important role at our study site. We also checked if nitrogen is bound in intermediate N-species: During sporadic checks the GE-MIMS did not detect any elevated peaks for NO and NO_2, which shows that denitrification appears to be complete. N_2O could not be analyzed as it has the same mass as CO_2.

Moreover, we assume that the helium content of our samples is purely atmospheric (i.e., no terrigenic helium is present) due to the shallow groundwater fed by the stream and the absence of a deep aquifer within the study area. The estimated groundwater thickness at the study location is between 2-20m and the riparian aquifer is unconfined, consisting of unconsolidated rocks.; information source: `https://maps.zh.ch/?topic=AwelGrundWaMWwwwZH&offlayers=bezirkslabels&scale=310000&x=692000&y=252000`, Baudirektion, Amt für Abfall, Wasser, Energie und Luft Abteilung Gewässerschutz, Zürich, CH). We thus use He as input parameter (together with Ar and Kr) to estimate A, F and NGTs.

Figure 6 shows rainfall patterns and the water heads recorded in the stream and the groundwater at our study location. The latter indicates that the stream is indeed a losing stream for the duration of our experiment. Precipitation was recorded at the BAFU station "Dübendorf-Empa", which is ∼450m away from our study site (data source: `https://bafu.meteotest.ch/nabel/index.php/abfrage/start/english`). Stream water heads were recorded ∼200 m upstream of our study site (data source: `http://www.hydrometrie.ch/KundenDaten/EAWAG/HBZHa-558.htm`). All water levels of the piezometers were recorded using Ott CTD probes.

With the methods used in this study we cannot estimate infiltration flow paths or travel times. This would require a hydrogeological model, which is beyond the purpose of this study. However, several factors indicate that the analyzed groundwater is indeed recently infiltrated stream water: e.g., the microbial activity is unusually high for groundwater (Fig. 2b), NGTs correspond well with the recorded stream water temperature (Fig. S2) and groundwater levels respond fast to increases in stream discharge

(Figs. S1 b and c). Thus, we can assume that groundwater flow paths and travel times from the stream to the riparian groundwater are relatively short.

Text S3: Issues during Field Work.

We first intended to analyze dissolved (noble) gases in the stream water as well. However, due to the high load of suspended matter in the stream, which immediately clogged the pump and the water filter, we were unable to proceed with the stream water analysis. Consequently, we could not test whether denitrification already occurs through hyporheic exchange, which would lead to an increase in dissolved N_2 in the stream water. The used filters and membranes for groundwater analyses had to be cleaned or exchanged weekly due to clogging.

Due to the temperature difference of the ambient air (relatively cold) and groundwater (relatively warm) in the colder weeks of our sampling period (mainly February), water condensed inside the membrane module. This does not at first affect the gas measurements, but extensive water condensation inside the membrane module does eventually clog the attached capillary. Under cold ambient air temperatures, we therefore suggest to heat the membrane module and the attached capillary (to decrease the temperature difference between ambient air and sampling water), thus reduce water condensation.

Code S1.

All processing scripts necessary to convert raw data to partial pressure of gas species and gas concentrations are available online (`https://github.com/brennmat/ruediPy`). GNU Octave can be used to run the scripts. The software package NOBLEFIT (`https://github.com/brennmat/noblefit`), containing a χ^2 regression model to estimate the amount of excess air and the noble gas recharge temperature, are also publicly available. Both software packages include examples and manuals to facilitate reproducing our results.

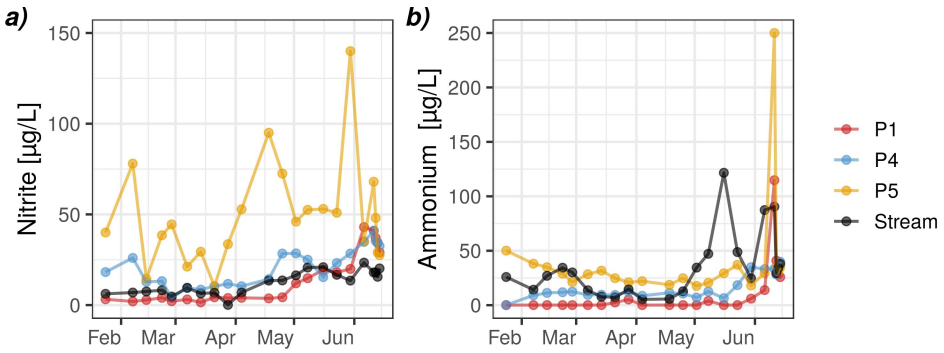

Figure S1: Nitrite (a) and ammonium (b) concentrations of P1, P4, P5 and the stream from weekly sampling.

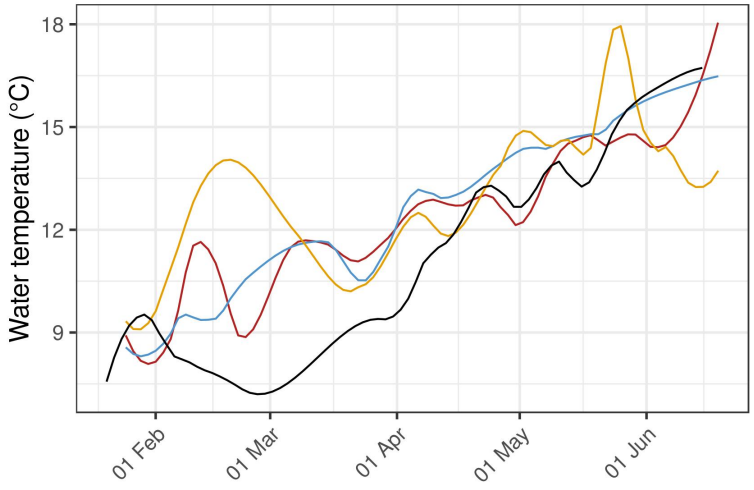

Figure S2: Recorded stream water temperature (black; data source: `http://www.hydrometrie.ch/KundenDaten/EAWAG/HBZHa-558.htm`) and estimated NGTs of P1 (red), P4 (blue) and P5 (orange).

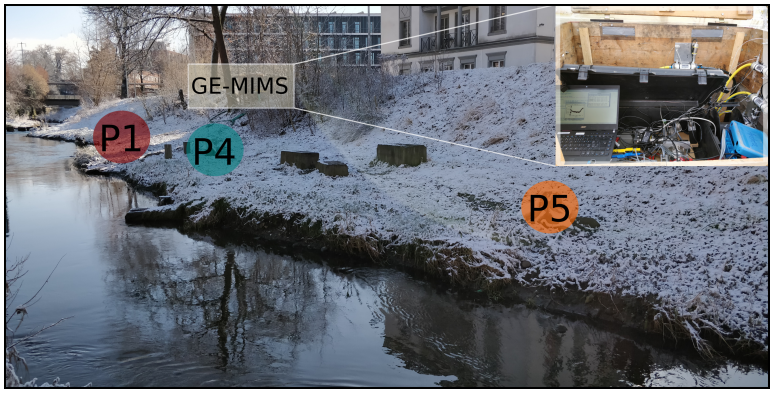

Figure S3: Picture of the study site in February 2018 showing the stream, the piezometers as well as the location of the GE-MIMS.

Table S1: Information about instruments used, parameter units, LOQ and measurement uncertainties for nitrate, sulfate, alkalinity, DOC and TCC concentration data. LOQ and measurement uncertainties are given in the respective parameter unit.

Parameter	Instrument	Method	Units	LOQ	Uncertainty ±
Nitrate	Metrohm 761 Compact IC	Column: Metrohm Metrosep A Supp 5 100/4 mm	mg/L	0.25	0.1
Sulfate	Metrohm 761 Compact IC	Column: Metrohm Metrosep A Supp 5 100/4 mm	mg/L	5	2
Alkalinity	Metrohm 809 Titrando	Metrohm pH-electrode	mmol/L	0.2	0.1
DOC	shimadzu TOC-L CSH	Catalytic incinerator 720 °C (analysis of CO_2 via IR)	mg/L	0.5	0.2
TCC	BD Accuri cytometers, Belgium; (Prest et al. 2013)	Flow cytometric cell counting (not diluted)	cells/μL	–	–

Part IV

CONCLUSIONS AND OUTLOOK

7

SYNTHESIS

The results of this multidisciplinary thesis further the understanding of processes at the intersection of hydrology, hydrogeology and geochemistry. The different research questions introduced in Chapter 3 were addressed by applying a combination of various methods (e.g., environmental tracers, models, hydraulic testing, microbial data) with a focus on in-situ (noble) gas analysis. This chapter summarizes the key outcomes that originate from the main research questions (Fig. 7.1), which were individually answered in Chapters 4 to 6:

Study 1: **Considerable water fractions (up to 84±9%) of groundwater can originate from unidentified water sources in hydrogeologically complex groundwater systems.**
On-site helium analysis integrated with Bayesian end-member mixing modeling enables the identification of previously unknown water components by explicitly accounting for tracer-related uncertainties. This integrated approach improved the conceptual understanding of the studied groundwater system by revealing that a considerable fraction of old groundwater originates from a flexure zone within the study area. This work showed that only the use of conservative tracers, such as the noble gas ^{4}He, can assess the uncertainty of estimated mixing ratios in highly heterogeneous aquifers.

Study 2: **About two third of alluvial groundwater used for drinking water supply originates from recently infiltrated river water that exhibits travel times between 7 to 15 days.**
A combined in-situ analysis of ^{4}He, ^{40}Ar and ^{222}Rn helped to illuminate groundwater mixing and travel times of an alluvial aquifer used for drinking water supply. Our results show that mean travel times from the river to the groundwater wellfield are in the order of a few days (∼7–15 days) and that recently infiltrated river water accounts for ∼70% of groundwater. Moreover, we showed that groundwater pumping in the study area has only a marginal impact on groundwater mixing ratios and travel times. The short travel times and the high groundwater fraction of recently infiltrated river illustrate the vulnerability of the pumped groundwater to climate change and increasing pollution.

Study 3: **Denitrification in riparian groundwater is highly variable in space and time.**
In-situ, continuous (noble) gas analysis (N_2, He, Ar, Kr) enables us to accurately quantify N_2 originating from denitrification by calculating the atmospheric N_2 components using a physically meaningful excess air model. Consequently, the N_2 originating from denitrification and thus the spatio-temporal dynamics of denitrification in riparian groundwater can be determined with a high spatio-temporal resolution.

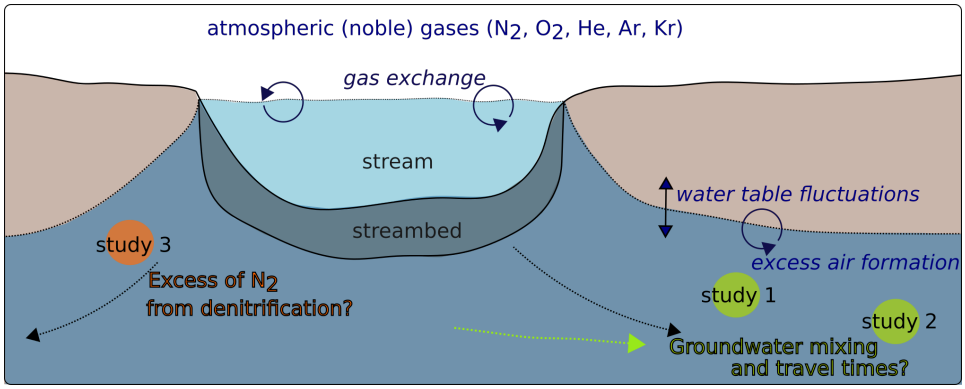

Figure 7.1: Conceptual model illustrating the major research questions addressed in this thesis.

The main results of this thesis highlight that common end-member mixing methods in hydrogeologically complex groundwater systems can lead to an erroneous assessment of groundwater mixing ratios by neglecting potential end-members contributing to the water mixture. Thus, a more sophisticated approach is required such as the Bayesian model framework that explicitly considers uncertainties originating from measuring and analyzing tracer concentrations and simultaneously accounts for the possibility of unknown end-members (Study 1).

At the same time, this thesis shows that groundwater mixing in less hydrogeologically complex aquifers can be assessed by means of a binary end-member mixing approach using noble gases. It was also shown that in such conceptually more constrained systems, groundwater mixing can be quantified equally well with a calibrated numerical model as with the tracer approach alone (Study 2).

This work also demonstrated that continuous (noble) gas analysis can reliably quantify the spatio-temporal dynamics of denitrification in riparian aquifers. This method provides the first efficient approach to analyze denitrification in groundwater with a high temporal resolution by means of on-site (noble) gas analysis (Study 3).

Overall, this thesis emphasizes the need for novel, more efficient measurement techniques (i.e., in-situ noble gas analysis) that yield spatially and temporally resolved data sets. Such data sets, in turn, provide a more accurate description of complex environmental systems. In conclusion, this thesis showed that a combination of novel tracer methods and complementary modeling approaches is a promising way forward to further advance the understanding of surface water–groundwater interactions.

8

RECOMMENDATIONS AND FUTURE RESEARCH

This thesis integrates a multitude of methods with in-situ (noble) gas analysis, i.e., the GE-MIMS system, representing the core method. The GE-MIMS has been proven useful for a variety of research questions as shown in this thesis. However, there are a few limitations to its application in groundwater studies, which became apparent during this thesis. Thus, several recommendations are given to prevent repeating previously failed approaches or those in need of further improvement: The GE-MIMS system (using the membrane module) is not suitable for studying groundwater systems on small scales (i.e., $<$10 m, depending on aquifer composition and groundwater sampling scheme) because the required pumping rate ($<$0.5L/min) to operate the GE-MIMS will inevitably disrupt the natural flow paths, which would lead to a biased assessment of small–scale flow and transport processes. Therefore, the use of the GE-MIMS is only recommended if no disruption of the system is guaranteed. Moreover, even though the scale might be large enough, the GE-MIMS cannot be deployed if the minimum pumping rate cannot be provided due to a low hydraulic conductivity or a too small piezometer/well screen length. Long-term, continuous analysis using the membrane modules can also be challenging as the membrane will eventually clog due to particles in the sampling water. Lastly, if the sampling water is warmer relative to the ambient air temperature, water will condensate in the module, which can lead to clogging of the capillary attached to the MS.

Despite some limitations, the GE-MIMS system is a very promising and powerful tool, which can help to shed light on a multitude of hydrology-related research fields. In the following, five promising research topics are presented, in which the application of in-situ noble gas analysis—ideally integrated with other methods—can contribute to further scientific advancement in emerging hydro(geo)logical research fields:

1. **High-altitude hydrogeology:**
   Climate change substantially alters the seasonality and quantity of surface water and groundwater resources, particularly in mountainous regions, e.g., by affecting snow accumulation, snow melting or river discharge patterns (e.g., Addor et al. 2014; T. R. Green et al. 2011; Maxwell et al. 2008). Such changes will inevitably affect groundwater recharge and storage. Therefore, an improved understanding of groundwater recharge and flow characteristics under a changing climate is needed to evaluate the implications of climate

change for a sustainable management of groundwater resources in mountainous regions (e.g., Holman 2006; Jasechko 2019).

Noble gases can potentially provide valuable insights into groundwater recharge conditions. They can be used to reconstruct groundwater recharge elevations in mountainous terrain if combined with other isotopic tracers (e.g., Jasechko 2019; Manning et al. 2003). Using noble gases to determine the recharge temperature is not straightforward because dissolved noble gas concentrations in water are a function of temperature, air pressure (i.e., recharge elevation) and salinity (neglectable in most mountainous environments). Since temperature and pressure are strongly correlated, they cannot be disentangled, which is why the recharge altitude has to be assumed to infer the recharge temperature (after accounting for excess air, e.g., Aeschbach-Hertig et al., 1999).

There are, however, methods available to constrain recharge elevations: the local atmospheric lapse (i.e., relationship between elevation and mean annual air temperature; Manning et al., 2003) or the isotopic lapse rate (i.e., relationship between depletion of heavy water isotopes in precipitation with increasing elevation; Friedman et al., 1964) determined by stable water isotopes (δ^2H and δ^{18}O) can be used to constrain recharge temperatures (obtained by noble gases) as recently demonstrated by Doyle et al. (2015) and Peters et al. (2018).

Using in-situ noble gas analysis would allow for a fast and wide screening of dissolved noble gases in groundwater and spring water in mountainous regions where data are usually scarce. Consequently, combined analyses of in-situ noble gas (e.g., Brennwald et al. 2016) and stable water isotope analyses (e.g., Herbstritt et al. 2019) would hone groundwater recharge estimates and allow to develop accurate projections of climate change impacts on groundwater replenishment in high-elevation areas.

2. **Spatio-temporal denitrification dynamics in groundwater:**
Data on denitrification are generally scarce since conventional methods to study this redox process are typically costly and labor-intensive. Thus, the spatio-temporal dynamics of denitrification remain poorly understood (Boyer et al. 2006; Davidson et al. 2006; Groffman et al. 2006; Kolbe et al. 2019). In Part iii of this thesis (Popp et al. 2020), in-situ (noble) gas analysis was introduced as a new, efficient approach to reliably quantify the end-product of denitrification, N_2, in groundwater. This method allows for large scale screening of groundwaters to assess nitrate contamination or to better understand the temporal dynamics of denitrification.

A combined analysis of in-situ dissolved (noble) gas analysis with other established methods to study denitrification (e.g., dual isotope approach, microbial investigations; Rivett et al., 2008) would allow to better understand nitrate sources and N-cycling in groundwaters, particularly in regions where nitrate contamination of groundwater is posing a threat to the aquatic environment (Mekonnen et al. 2015; Rockström et al. 2009).

3. **Spatio-temporal patterns of greenhouse-gas emissions in polar regions:**
   The disproportionate temperature increase observed in many polar areas due to global warming rapidly degrades organic matter and mobilizes stored carbon. These processes lead to the emission of large amounts of the greenhouse gases CO_2 and CH_4, which in turn accelerate climate feedback mechanisms (e.g., Elberling et al. 2013; IPCC 2013).

   There are many fragile systems facing the impacts of climate change such as thawing permafrost peat-lands as well as sediments of polar streams, lakes and wetlands that represent poorly understood feedback mechanisms of climate change (e.g., Comer-Warner et al. 2018; Yudhowijoyo et al. 2018). Despite multi-million dollar research in arctic environments (e.g., the SEARCH project, `https://www.searcharcticscience.org/`), there are still research gaps concerning the seasonal changes and the changing feedback mechanisms between greenhouse gas release, collapse and recovery of soils, soil moisture as well as vegetation growth and biomass accumulation, which require a more long-term and extended monitoring of polar ecosystems (Turetsky et al. 2019).

   For studying the spatio-temporal patterns of greenhouse-gases within these sensitive ecosystems, the MIMS (Brennwald et al. 2016) can be combined with a new membrane that can sniff gas directly in any medium such as unsaturated soil. At the same time, to quantify gas release, a portable gas diffusion flux meter can be deployed (e.g., West Systems 2019). These new technological advancements allow for relatively undisturbed and fast in-situ analyses of CO_2 and CH_4 and therefore, represent crucial technical advancements to observe and understand the mechanisms of greenhouse gas emissions in polar regions.

   An extended sampling of the spatio-temporal storage and release mechanisms of greenhouse gases ideally combined with various other methods such as the analysis of microbial activities (e.g., Jansson et al. 2014), geophysical or airborne methods, and more holistic modeling frameworks can illuminate key processes affecting

greenhouse gas release (as proposed by Turetsky et al., 2019). Ultimately, insights on the seasonal dynamics and spatial heterogeneity of greenhouse-gas emissions could enhance the prediction of climate change impacts by providing data to calibrate or validate existing regional- to global-scale models on greenhouse gas emissions.

4. **Catchment hydrology:**
   Helium-rich (i.e., old) groundwater in catchments can provide insights into groundwater residence and transit times (e.g., Cook et al. 2000; M. Sprenger et al. 2019). The GE-MIMS (Brennwald et al. 2016) could be used for widespread sampling of old, ^{4}He-rich groundwater in systems where a high spatial (and temporal) data resolution is required. High resolution ^{4}He data can help to illuminate process understanding, for instance, in hydrogeologically complex catchments with fault zones where deep groundwater up-welling can be expected or in high-latitude catchments which represent underexplored aquifer systems despite their high vulnerability to climate change effects (Jasechko 2019). Likewise, the GE-MIMS would allow to obtain high-resolution, long-term time series of dissolved (noble) gases (including ^{4}He) recorded in stream water at catchment outlets to improve the understanding of catchment dynamics and responses to snow melt or high discharge events.

   Such data-sets would help in gauging the vulnerability of groundwater resources to changes caused by extreme events such as floods or droughts. Moreover, different modeling approaches such as Bayesian mixing modeling (Popp et al. 2019) or numerical modeling can be applied to such data-sets to elucidate groundwater flow and transport. Finally, ^{4}He data—spatially or temporally resolved—can also assist in developing, calibrating, and validating realistic integrative groundwater flow models (Schilling et al. 2019; M. Sprenger et al. 2019).

5. **Shale gas development:**
   Conventional and unconventional (i.e., "fracking") shale gas extraction can lead to methane contamination of groundwater, which has widespread implications for drinking water supply as well as global warming since CO_4 can eventually be released to the atmosphere (e.g., Howarth 2019; McMahon et al. 2018a,b; Yudhowijoyo et al. 2018). The mobility and persistence of methane dissolved in groundwater is very heterogeneous and requires a high spatial and temporal resolution monitoring to detect groundwater contamination and leakages to the atmosphere (e.g., Cahill et al. 2017).

The application of the GE-MIMS would allow for such a high resolution real-time sampling and could thus enhance the understanding of potential environmental risks stemming from methane release due to shale gas extraction. Moreover, a combined analysis of noble gases and methane (e.g., $^4He/CH_4$) can be used as fingerprint to distinguish natural methane sources from anthropogenic contamination (e.g., Darrah et al. 2014).

A

APPENDIX

Apart from addressing the main research questions of my thesis, I worked together with colleagues on a variety of research topics during my PhD studies. The following articles result from these collaborations.

A.1 The Suitability of Using Dissolved Gases to Determine Groundwater Discharge to High Gradient Streams

This work has been published as: Gleeson, T., Manning, A.H., **Popp, A.**, Zane, M., Clark, J.F. (2018) The suitability of using dissolved gases to determine groundwater discharge to high gradient streams, *Journal of Hydrology*, 557, 561–572, doi:10.1016/j.jhydrol.2017.12.022.

Abstract

Determining groundwater discharge to streams using dissolved gases is known to be useful over a wide range of streamflow rates but the suitability of dissolved gas methods to determine discharge rates in high gradient mountain streams has not been sufficiently tested, even though headwater streams are critical as ecological habitats and water resources. The aim of this study is to test the suitability of using dissolved gases to determine groundwater discharge rates to high gradient streams by field experiments in a well-characterized, high gradient mountain stream and a literature review. At a reach scale (550 m) we combined stream and groundwater radon activity measurements with an in-stream SF_6 tracer test. By means of numerical modeling we determined gas exchange velocities and derived very low groundwater discharge rates ($\sim$15% of streamflow). These groundwater discharge rates are below the uncertainty range of physical streamflow measurements and consistent with temperature, specific conductance and streamflow measured at multiple locations along the reach. At a watershed-scale (4 km), we measured CFC-12 and $\delta^{18}O$ concentrations and determined gas exchange velocities and groundwater discharge rates with the same numerical model. The groundwater discharge rates along the 4 km stream reach were highly variable, but were consistent with the values derived in the detailed study reach. Additionally, we synthesized literature values of gas exchange velocities for different stream gradients which show an empirical relationship that will be valuable in

planning future dissolved gas studies on streams with various gradients. In sum, we show that multiple dissolved gas tracers can be used to determine groundwater discharge to high gradient mountain streams from reach to watershed scales.

A.2 Characterization of a Managed Aquifer Recharge System

This work has been published as: Moeck, C., Radny, D., **Popp, A.**, Brennwald, M., Stoll, S., Auckenthaler, A., Berg, M., Schirmer, M. (2017) Characterization of a managed aquifer recharge system using multiple tracers, *Science of the Total Environment*, 609, 701–714, doi:10.1016/j.scitotenv.2017.07.211

Abstract

Knowledge about the residence times of artificially infiltrated water into an aquifer and the resulting flow paths is essential to developing groundwater-management schemes. To obtain this knowledge, a variety of tracers can be used to study residence times and gain information about subsurface processes. Although a variety of tracers exists, their interpretation can differ considerably due to subsurface heterogeneity, underlying assumptions, and sampling and analysis limitations. The current study systematically assesses information gained from seven different tracers during a pumping experiment at a site where drinking water is extracted from an aquifer close to contaminated areas and where groundwater is artificially recharged by infiltrating surface water. We demonstrate that the groundwater residence times estimated using dye and heat tracers are comparable when the thermal retardation for the heat tracer is considered. Furthermore, major ions, acesulfame, and stable isotopes (δ^2H and δ^{18}O) show that mixing of infiltrated water and groundwater coming from the regional flow path occurred and a vertical stratification of the flow system exist. Based on the concentration patterns of dissolved gases (He, Ar, Kr, N_2, and O_2) and chlorinated solvents (e.g., tetrachloroethene), three temporal phases are observed in the ratio between infiltrated water and regional groundwater during the pumping experiment. Variability in this ratio is significantly related to changes in the pumping and infiltration rates. During constant pumping rates, more infiltrated water was extracted, which led to a higher dilution of the regional groundwater. An infiltration interruption caused however, the ratio to change and more regional groundwater is extracted, which led to an increase in all concentrations. The obtained results are discussed for each tracer considered and its strengths and limitations are illustrated. Overall, it is demonstrated that aquifer heterogeneity and various subsurface processes necessitate

application of multiple tracers to quantify uncertainty when identifying flow processes.

A.3 Reporting Negative Results in Hydrology

This work has been published as: van Emmerik, T., **Popp, A.**, Solcerova, A., Müller, H., Hut, R. (2018) Reporting negative results to stimulate experimental hydrology: discussion of "The role of experimental work in hydrological sciences—insights from a community survey", *Hydrological Sciences Journal*, 63(8), 1269–1272, doi:10.1080/02626667.2018.1493203

Abstract

Experimental work in hydrology is in decline. Based on a community survey, Blume et al. showed that the hydrological community associates experimental work with greater risks. One of the main issues with experimental work is the higher chance of negative results (defined here as when the expected or wanted result was not observed despite careful experimental design, planning and execution), resulting in a longer and more difficult publishing process. Reporting on negative results would avoid putting time and resources into repeating experiments that lead to negative results, and give experimental hydrologists the scientific recognition they deserve. With this commentary, we propose four potential solutions to encourage reporting on negative results, which might contribute to a stimulation of experimental hydrology.

A.4 Science Communication in Today's Media Landscape

This work has been published as: Lutz, S.R., **Popp, A.**, van Emmerik, T., Gleeson, T., Kalaugher, L., Möbius, K., Mudde, T., Walton, B., Hut, R., Savenije, H., Slater, L.J., Solcerova, A., Stoof, C.R., Zink, M. (2018) HESS opinions: science in today's media landscape—challenges and lessons from hydrologists and journalists, *Hydrology and Earth System Sciences*, 22(7), 3589–3599, doi:10.5194/hess-2018-13

Abstract

Media such as television, newspapers and social media play a key role in the communication between scientists and the general public. Communicating your science via the media can be positive and rewarding by providing the inherent joy of sharing your knowledge with a broader audience, promoting science as a fundamental part of culture and society, im-

pacting decision- and policy-makers, and giving you a greater recognition by institutions, colleagues and funders. However, the interaction between scientists and journalists is not always straightforward. For instance, scientists may not always be able to translate their work in to a compelling story, and journalists may sometimes misinterpret scientific output. In this paper, we present insights from hydrologists and journalists discussing the advantages and benefits as well as the potential pitfalls and aftermath of science–media interaction. As we perceive interacting with the media as a rewarding and essential part of our work, we aim to encourage scientists to participate in the diverse and evolving media landscape. With this paper, we call on the scientific community to support scientists who actively contribute to a fruitful science–media relationship.

A.5 Gender Inequality in the Earth and Space Sciences

This work has been published as: **Popp, A.L.**, Lutz, S., Khatami, S., van Emmerik, T., Knoben, W.J.M. (2019), A global survey on the perceptions and impacts of gender inequality in the Earth and space sciences, *Earth and Space Science*, 6, 1460–1468, doi:10.1029/2019EA000706.

Abstract

The *leaky pipeline* phenomenon refers to the disproportionate decline of female scientists at higher academic career levels and is a major problem in the natural sciences. Identifying the underlying causes is challenging, and thus solving the problem remains difficult. To better understand the reasons for the leaky pipeline, we assess the perceptions and impacts of gender bias and imbalance—two major drivers of the leakage—at different academic career levels with an anonymous survey in geoscience academia (n=1220). The survey results show that both genders view male geoscientists as substantially more gender-biased than female scientists. Moreover, female geoscientists are more than twice as likely to experience negative gender bias at their workplaces and scientific organizations compared to male geoscientists. There are also pronounced gender differences regarding (i) the relevance of role models, (ii) family-friendly working conditions and (iii) the approval of gender quotas for academic positions. Given the male dominance in senior career levels, our results emphasize that those feeling less impacted by the negative consequences of gender bias and imbalance are the ones in position to tackle the problem. We thus call for actions to better address gender biases and to ensure a balanced gender representation at decision-making levels to ultimately retain more women in geoscience academia.

A.6 The Relevance of the Hyporheic Zone

This work is has been published as: Lewandowski, J., Arnon, S., Banks, E., Batelaan, O., Betterle, A., Broecker, T., Coll, C., Drummond, J.D., Gaona Garcia, J, Galloway, J., Gomez-Velez, J., Grabowski, R.C., Herzog, S.P., Hinkelmann, R., Höhne, A., Hollender, J., Horn, M.A., Jaeger, A., Krause, S., Löchner Prats, A., Magliozzi, C., Meinikmann, K., Mojarrad, B.B., Mueller, B.M., Peralta-Maraver, I., **Popp, A.L.**, Posselt, M., Putschew, A., Radke, M., Raza, M., Riml, J., Robertson, A., Rutere, C., Schaper, J.L., Schirmer, M., Schulz, H., Shanafield, M., Singh, T., Ward, A.S., Wolke, P., Wörman, A. and Wu, L. (2019), Is the hyporheic zone relevant beyond the scientific community?, *Water*, 11(11), 2230, doi:10.3390/w11112230.

Abstract

Rivers are important ecosystems under continuous anthropogenic stresses. The hyporheic zone is a ubiquitous, reactive interface between the main channel and its surrounding sediments along the river network. For almost half a century, the main physical, biological and biogeochemical drivers and processes within the hyporheic zone have been studied by multiple scientific disciplines. These previous efforts have shown that the hyporheic zone is a modulator for most metabolic stream processes and serves as refuge and habitat for a diverse range of aquatic organisms. It also exerts a major control on river water quality by increasing the contact time with reactive environments which in turn results in retention and transformation of nutrients, trace organic compounds, fine suspended particles, and microplastics, among others. The aim of this review is to showcase the critical importance of the hyporheic zone both from a scientific and an applied perspective, its role in ecosystem services, and to identify major research gaps in our understanding of hyporheic processes. Finally, we highlight the potential of hyporheic restoration to efficiently manage and reactivate ecosystem functions and services in river corridors.

A.7 Subsurface Gas Migration in Northern British Columbia, Canada

This work is has been published as: Cahill, A.G., Ladd, B., Chao, J., Soares, J., Cary, T., Finke, N., Manning, C., **Popp, A.L.**, Chopra, C., Mayer, K.U., Black, A., Lauer, R., van Geloven, C., Welch, L., Crowe, S., Mayber, B., Beckie, R.D. (2020), Controlled Natural Gas Release Experiment in a Confined Aquifer, Northeastern British Columbia (NTS 094A/04): Activity Report 2018–2019, *Geoscience BC*, p. 145–160, ISSN 2562-2765

Abstract

This paper summarizes the past twelve months of a research program aimed at advancing knowledge on fugitive natural gas migration in groundwater. Research activities were carried out at the Hudson's Hope Field Research Station (HHFRS) located in northeastern British Columbia (BC; Figure 1). In the summer of 2018, natural gas was intentionally injected into the subsurface; the physical and biogeochemical conditions associated with this injection have been monitored ever since. The installation of HHFRS and previous activities at the site are described in Cahill et al. (2019a, b). Fugitive gas (FG) describes natural gas that has been unintentionally released in the subsurface in the context of energy resource development. Gas migration (GM) occurs when fugitive gas is released in the subsurface outside of an energy well casing and into the adjacent formation(s), as opposed to fugitive gas that leaks inside the well casing and manifests as surface casing vent flow (SCVF). Although both FG and GM were identified long ago (Chafin, 1994;Dusseault et al., 2000), significant knowledge gaps regarding gas migration, environmental impacts and environmental fate still exist, largely because of the complexity of the physical and biogeochemical processes involved, but also due to the distinct geological environments of the various resource plays. Consequently, there is a pressing need to address knowledge gaps related to FG and GM in north-eastern BC, particularly in light of the technological improvements in unconventional production methods in the last decade and the accompanying increase in exploration and development of petroleum resources (Council of Canadian Academies, 2014). A principal objective of this research program, and the Energy and Environment Research Initiative (EERI) at The University of British Columbia (UBC), is to provide the science knowledge base that can be used to inform the management of oil and gas development in BC. By conducting a controlled natural gas release experiment in an area of active oil and gas development, the aim is to 1) characterize the physical and biogeochemical processes that control subsurface gas migration and impact, and quantify the amount of natural gas that remains, degrades or leaves the subsurface; 2) test FG monitoring and detection methodologies; and 3) inform regulations to facilitate safe and sustainable development of natural gas resources.

B

CURRICULUM VITAE

Andrea Popp

Education

09/2015–10/2019 **Dr. Sc. nat.**, *ETH Zurich (CH).*

10/2012–08/2015 **M.Sc. Hydrology**, *University of Freiburg (DE).*

09/2014–02/2015 **EUCOR (The European Campus) student**, *University of Basel (CH).*

02/2011–03/2011 **Visiting student**, *University of Konstanz (DE).*

10/2009–09/2012 **B.Sc. Environmental Natural Sciences, minor in Hydrology**, *University of Freiburg (DE).*

Research Experience & Professional Appointments

09/2015–12/2019 **Scientific employee**, *Eawag (Swiss Federal Institute of Aquatic Science and Technology)*, Department of Water Resources and Drinking Water, Dübendorf (CH).

06/2019–07/2019 **Visiting scientist**, *University of Neuchâtel*, Centre d'Hydrogéologie et de Géothermie, Neuchâtel (CH).

07/2018–08/2018 **Visiting scientist**, *University of Laval*, Department of Geology and Geological Engineering, Quebec (CA).

05/2016–07/2016 **Visiting scientist**, *IGB (Leibniz-Institute of Freshwater Ecology and Inland Fisheries)*, Ecohydrology department, Berlin (DE).

07/2015–08/2015 **Visiting scholar**, *University of Victoria*, Civil Engineering Department, Victoria (CA).

10/2014–05/2015 **Visiting scholar**, *Eawag*, Department of Water Resources and Drinking Water, Dübendorf (CH).

11/2012–12/2014 **Research assistant**, *University of Freiburg*, Chair of Hydrology, Freiburg (DE).

07/2012–09/2012 **Internship**, *Agency for the Environment and Energy*, Groundwater Department, Basel (CH).

11/2011–06/2012 **Student assistant**, *University of Freiburg*, Chair of Hydrology, Freiburg (DE).

06/2011–10/2011 **Student assistant**, *University of Freiburg*, Chair of Physical Geography, Freiburg (DE).

03/2010–09/2010 **Commissioner for public relations**, *student union University of Freiburg*, Freiburg (DE).

Teaching & Supervision

09/2016–10/2017 **Group leader & tutor**, ETH Week "Challenging Water" and "Manufacturing the Future".

09/2015–02/2017 **Teaching assistant**, physics laboratory course for B.Sc. Environmental Sciences students at ETH.

Since 2015 **Student supervision**, Benjamin Plüss (M.Sc. Environmental Sciences, ETH), Wendelin Wild (B.Sc. Environmental Engineering, ETH).

BIBLIOGRAPHY

3M Liqui-Cel (2017). *A high level of consistency and control*. Wuppertal, Germany (cit. on pp. 35, 53, 75).

B. W. Abbott, V. Baranov, C. Mendoza-Lera, M. Nikolakopoulou, A. Harjung, T. Kolbe, M. N. Balasubramanian, T. N. Vaessen, F. Ciocca, A. Campeau, M. B. Wallin, P. Romeijn, M. Antonelli, J. Gonçalves, T. Datry, A. M. Laverman, J. R. de Dreuzy, D. M. Hannah, S. Krause, C. Oldham, and G. Pinay (2016). „Using multi-tracer inference to move beyond single-catchment ecohydrology." In: *Earth-Science Rev.* 160, pp. 19–42. DOI: 10.1016/j.earscirev.2016.06.014 (cit. on p. 31).

B. W. Abbott, K. Bishop, J. P. Zarnetske, C. Minaudo, F. S. Chapin, S. Krause, D. M. Hannah, L. Conner, D. Ellison, S. E. Godsey, S. Plont, J. Marçais, T. Kolbe, A. Huebner, R. J. Frei, T. Hampton, S. Gu, M. Buhman, S. Sara Sayedi, O. Ursache, M. Chapin, K. D. Henderson, and G. Pinay (2019). „Human domination of the global water cycle absent from depictions and perceptions." In: *Nat. Geosci.* 12.7, pp. 533–540. DOI: 10.1038/s41561-019-0374-y (cit. on p. 5).

N. Addor, O. Rössler, N. Köplin, M. Huss, R. Weingartner, and J. Seibert (2014). „Robust changes and sources of uncertainty in the projected hydrological regimes of Swiss catchments." In: *Water Resour. Res.* 50.10, pp. 7541–7562. DOI: 10.1002/2014WR015549 (cit. on pp. 48, 50, 99).

W. Aeschbach-Hertig, H. El-Gamal, M. Wieser, and L. Palcsu (2008). „Modeling excess air and degassing in groundwater by equilibrium partitioning with a gas phase." In: *Water Resour. Res.* 44.8, pp. 1–12. DOI: 10.1029/2007WR006454 (cit. on pp. 72, 76).

W. Aeschbach-Hertig and T. Gleeson (2012). „Regional strategies for the accelerating global problem of groundwater depletion." In: *Nat. Geosci.* 5.12, pp. 853–861. DOI: 10.1038/ngeo1617 (cit. on p. 5).

W. Aeschbach-Hertig, F. Peeters, U. Beyerle, and R. Kipfer (1999). „Interpretation of dissolved atmospheric noble gases in natural waters." In: *Water Resour. Res.* 35.9, pp. 2779–2792. DOI: 10.1029/1999WR900130 (cit. on pp. 6, 8, 71, 76, 87, 100).

W. Aeschbach-Hertig, F. Peeters, U. Beyerle, and R. Kipfer (2000). „Palaeotemperature reconstruction from noble gases in ground water taking into account equilibration with entrapped air." In: *Nature* 405.6790, pp. 1040–1044. DOI: 10.1038/35016542 (cit. on pp. 8, 76, 87).

Aquanty Inc. (2015). *HGS Reference Manual*. Waterloo (cit. on p. 49).

C. A. Arendt, S. M. Aciego, and E. A. Hetland (2015). „An open source Bayesian Monte Carlo isotope mixing model with applications in Earth

surface processes." In: *Geochemistry, Geophys. Geosystems* 16.5, pp. 1274–1292. DOI: 10.1002/2014GC005683 (cit. on p. 17).

AWEL (2012). *Zürcher Gewässer 2012 Ausblick, Entwicklung Zustand*. Zurich (cit. on p. 73).

AWEL (2018). *Stelle 177 : Chriesbach vor Glatt* (cit. on p. 73).

C. Ballentine and C. Hall (1999). „Determining paleotemperature and other variables by using an error-weighted, nonlinear inversion of noble gas concentrations in water." In: *Geochim. Cosmochim. Acta* 63.16, pp. 2315–2336. DOI: 10.1016/S0016-7037(99)00131-3 (cit. on p. 76).

R. Barthel and S. Banzhaf (2016). „Groundwater and Surface Water Interaction at the Regional-scale—A Review with Focus on Regional Integrated Models." In: *Water Resour. Manag.* 30.1, pp. 1–32. DOI: 10.1007/s11269-015-1163-z (cit. on p. 48).

F. K. Barthold, C. Tyralla, K. Schneider, K. B. Vaché, H. G. Frede, and L. Breuer (2011). „How many tracers do we need for end member mixing analysis (EMMA)? A sensitivity analysis." In: *Water Resour. Res.* 47.8, pp. 1–14. DOI: 10.1029/2011WR010604 (cit. on pp. 16, 22).

J. Batlle-Aguilar, E. W. Banks, O. Batelaan, R. Kipfer, M. S. Brennwald, and P. G. Cook (2017). „Groundwater residence time and aquifer recharge in multilayered, semi-confined and faulted aquifer systems using environmental tracers." In: *J. Hydrol.* 546, pp. 150–165. DOI: 10.1016/j.jhydrol.2016.12.036 (cit. on pp. 18, 21).

T. J. Battin and D. Sengschmitt (1999). „Linking Sediment Biofilms, Hydrodynamics, and River Bed Clogging: Evidence from a Large River." In: *Microb. Ecol.* 37.3, pp. 185–196 (cit. on p. 83).

J. Bear (1972). *Dynamics of Fluids in Porous Media*. New York: Dover publications, Inc., pp. 1–764 (cit. on p. 73).

S. Bernal, A. Butturini, and F. Sabater (2006). „Inferring nitrate sources through end member mixing analysis in an intermittent Mediterranean stream." In: *Biogeochemistry* 81.3, pp. 269–289. DOI: 10.1007/s10533-006-9041-7 (cit. on p. 22).

M. D. Besmer, J. Epting, R. M. Page, J. A. Sigrist, P. Huggenberger, and F. Hammes (2016). „Online flow cytometry reveals microbial dynamics influenced by concurrent natural and operational events in groundwater used for drinking water treatment." In: *Sci. Rep.* 6.November, pp. 1–10. DOI: 10.1038/srep38462 (cit. on p. 77).

U. Beyerle, W. Aeschbach-Hertig, D. Imboden, H. Baur, T. Graf, and R. Kipfer (2000). „A Mass Spectrometric System for the Analysis of Noble Gases and Tritium from Water Samples." In: *Environ. Sci. Technol.* 34.10, pp. 2042–2050. DOI: 10.1021/es990840h (cit. on p. 36).

U. Beyerle, W. Aeschbach-Hertig, M. Hofer, D. M. Imboden, H. Baur, and R. Kipfer (1999). „Infiltration of river water to a shallow aquifer investigated with 3H/3He, noble gases and CFCs." In: *J. Hydrol.* 220.3-4,

pp. 169–185. DOI: 10.1016/S0022-1694(99)00069-4 (cit. on pp. 16, 36).

W. H. Blake, P. Boeckx, B. C. Stock, H. G. Smith, S. Bodé, H. R. Upadhayay, L. Gaspar, R. Goddard, A. T. Lennard, I. Lizaga, D. A. Lobb, P. N. Owens, E. L. Petticrew, Z. Z. A. Kuzyk, B. D. Gari, L. Munishi, K. Mtei, A. Nebiyu, L. Mabit, A. Navas, and B. X. Semmens (2018). „A deconvolutional Bayesian mixing model approach for river basin sediment source apportionment." In: *Sci. Rep.* 8.1, p. 13073. DOI: 10.1038/s41598-018-30905-9 (cit. on p. 17).

R. V. Blau and F. Muchenberger (1997). *Grundlagen für Schutz und Bewirtschaftung der Grundwasser des Kantons Bern*. Tech. rep. Bern: Wasser- und Energiewirtschaftsamt des Kantons Bern, Geotechnisches Institut AG, pp. 1–105 (cit. on p. 49).

G. Blicher-Mathiesen, G. W. McCarty, and L. P. Nielsen (1998). „Denitrification and degassing in groundwater estimated from dissolved dinitrogen and argon." In: *J. Hydrol.* 208, pp. 16–24 (cit. on pp. 71, 80).

G. Blöschl, J. Hall, A. Viglione, R. A. P. Perdigão, J. Parajka, B. Merz, D. Lun, B. Arheimer, G. T. Aronica, A. Bilibashi, M. Boháč, O. Bonacci, M. Borga, I. Čanjevac, A. Castellarin, G. B. Chirico, P. Claps, N. Frolova, D. Ganora, L. Gorbachova, A. Gül, J. Hannaford, S. Harrigan, M. Kireeva, A. Kiss, T. R. Kjeldsen, S. Kohnová, J. J. Koskela, O. Ledvinka, N. Macdonald, M. Mavrova-Guirguinova, L. Mediero, R. Merz, P. Molnar, A. Montanari, C. Murphy, M. Osuch, V. Ovcharuk, I. Radevski, J. L. Salinas, E. Sauquet, M. Šraj, J. Szolgay, E. Volpi, D. Wilson, K. Zaimi, and N. Živković (2019). „Changing climate both increases and decreases European river floods." In: *Nature*. DOI: 10.1038/s41586-019-1495-6 (cit. on pp. 5, 48).

F. Boano, J. W. Harvey, A. Marion, A. I. Packman, R. Revelli, L. Ridolfi, and A. Wörman (2014). „Hyporheic flow and transport processes: Mechanisms, models, and biogeochemical implications." In: *Rev. Geophys.* 52.4, pp. 603–679. DOI: 10.1002/2012RG000417 (cit. on pp. 5, 48).

J. K. Böhlke, R. C. Antweiler, J. W. Harvey, A. E. Laursen, L. K. Smith, R. L. Smith, and M. A. Voytek (2009). „Multi-scale measurements and modeling of denitrification in streams with varying flow and nitrate concentration in the upper Mississippi River basin, USA." In: *Biogeochemistry* 93.1-2, pp. 117–141. DOI: 10.1007/s10533-008-9282-8 (cit. on pp. 71, 80).

S. Bourke, P. G. Cook, M. Shanafield, S. Dogramaci, and J. F. Clark (2014). „Characterisation of hyporheic exchange in a losing stream using radon-222." In: *J. Hydrol.* 519, pp. 94–105. DOI: 10.1016/j.jhydrol.2014.06.057 (cit. on p. 51).

H. Bouwer and R. C. Rice (1976). „A slug test for determining hydraulic conductivity of unconfined aquifers with completely or partially pen-

etrating wells." In: *Water Resour. Res.* 12.3, pp. 423–428. DOI: 10.1029/WR012i003p00423 (cit. on p. 74).

E. W. Boyer, R. B. Alexander, W. J. Parton, C. Li, K. Butterbach-Bahl, S. D. Donner, R. W. Skaggs, and S. J. D. Grosso (2006). „Modeling denitrification in terrestrial and aquatic ecosystems at regional scales." In: *Ecological Applications* 16.6, pp. 2123–2142. DOI: 10.1890/1051-0761(2006)016[2123:MDITAA]2.0.CO;2 (cit. on pp. 70, 71, 100).

M. S. Brennwald, M. Schmidt, J. Oser, and R. Kipfer (2016). „A portable and autonomous mass spectrometric system for on-site environmental gas analysis." In: *Environ. Sci. Technol.* acs.est.6b03669. DOI: 10.1021/acs.est.6b03669 (cit. on pp. 6, 7, 18, 35, 36, 48, 53, 72, 74, 75, 100–102).

M. J. Brewer, C. Soulsby, and S. M. Dunn (2002). „A Bayesian Model for Compositional Data Analysis." en. In: *Compstat*. Ed. by W. Härdle and B. Rönz. Physica-Verlag HD, pp. 105–110 (cit. on pp. 17, 54).

M. A. Briggs, F. D. Day-Lewis, J. P. Zarnetske, and J. W. Harvey (2015). „A physical explanation for the development of redox microzones in hyporheic flow." In: *Geophys. Res. Lett.* 42.11, pp. 4402–4410. DOI: 10.1002/2015GL064200 (cit. on p. 78).

P. Brunner and C. T. Simmons (2012). „HydroGeoSphere: A Fully Integrated, Physically Based Hydrological Model." In: *Ground Water* 50.2, pp. 170–176. DOI: 10.1111/j.1745-6584.2011.00882.x (cit. on p. 56).

P. Brunner, R. Therrien, P. Renard, C. T. Simmons, and H.-J. H. Franssen (2017). „Advances in understanding river-groundwater interactions." In: *Rev. Geophys.* 55.3, pp. 818–854. DOI: 10.1002/2017RG000556 (cit. on pp. 5, 6, 48).

A. G. Cahill, C. M. Steelman, O. Forde, O. Kuloyo, S. Emil Ruff, B. Mayer, K. Ulrich Mayer, M. Strous, M. Cathryn Ryan, J. A. Cherry, and B. L. Parker (2017). „Mobility and persistence of methane in groundwater in a controlled-release field experiment." In: *Nat. Geosci.* 10.4, pp. 289–294. DOI: 10.1038/ngeo2919 (cit. on p. 102).

B. Carpenter, A. Gelman, M. Hoffman, D. Lee, B. Goodrich, M. Betancourt, M. Brubaker, J. Guo, P. Li, and A. Riddell (2017). „Stan: A Probabilistic Programming Language." In: *Journal of Statistical Software, Articles* 76.1, pp. 1–32. DOI: 10.18637/jss.v076.i01 (cit. on p. 25).

J. Carrera, E. Vázquez-Suñé, O. Castillo, and X. Sánchez-Vila (2004). „A methodology to compute mixing ratios with uncertain end-members." In: *Water Resour. Res.* 40.12, pp. 1–11. DOI: 10.1029/2003WR002263 (cit. on pp. 16, 17, 22, 54).

N. Christophersen and R. P. Hooper (1992). „Multivariate Analysis of Stream Water Chemical Data' The Use of Principal Components Analysis for the End-Member Mixing Problem." In: *Water Resour. Res.* 28.1, pp. 99–107 (cit. on p. 16).

N. Christophersen, C. Neal, R. P. Hooper, R. D. Vogt, and S. Andersen (1990). „Modelling streamwater chemistry as a mixture of soilwater end-members—A step towards second-generation acidification models." In: *J. Hydrol.* 116.1-4, pp. 307–320. DOI: 10.1016/0022-1694(90)90130-P (cit. on pp. 16, 17, 22, 23).

S. A. Comer-Warner, P. Romeijn, D. C. Gooddy, S. Ullah, N. Kettridge, B. Marchant, D. M. Hannah, and S. Krause (2018). „Thermal sensitivity of CO_2 and CH_4 emissions varies with streambed sediment properties." In: *Nat. Commun.* 9.1. DOI: 10.1038/s41467-018-04756-x (cit. on p. 101).

P. Cook and S. Dogramaci (2019). „Estimating Recharge From Recirculated Groundwater With Dissolved Gases: An End-Member Mixing Analysis." In: *Water Resour. Res.* 55.7, pp. 5468–5486. DOI: 10.1029/2019WR025012 (cit. on p. 16).

P. Cook and A. L. Herczeg (2000). *Environmental Tracers in Subsurface Hydrology*. Vol. 53. 9. Springer Science+Business Media New York. DOI: 10.1017/CBO9781107415324.004 (cit. on pp. 9, 21, 48, 51, 52, 102).

M. J. Currell and I. Cartwright (2011). „Major-ion chemistry, δ13C and 87Sr/86Sr as indicators of hydrochemical evolution and sources of salinity in groundwater in the Yuncheng Basin, China." In: *Hydrogeol. J.* 19.4, pp. 835–850. DOI: 10.1007/s10040-011-0721-6 (cit. on p. 21).

T. H. Darrah, A. Vengosh, R. B. Jackson, N. R. Warner, and R. J. Poreda (2014). „Noble gases identify the mechanisms of fugitive gas contamination in drinking-water wells overlying the Marcellus and Barnett Shales." In: *Proc. Natl. Acad. Sci.* 111.39, pp. 14076–14081. DOI: 10.1073/pnas.1322107111 (cit. on p. 103).

E. A. Davidson and S. Seitzinger (2006). „The Enigma of Progress in Denitrification Research Denitrification." In: *Ecol. Appl.* 16.6, pp. 2057–2063 (cit. on pp. 70, 71, 100).

P. Davis, J. Syme, J. Heikoop, J. Fessenden-Rahn, G. Perkins, B. Newman, A. E. Chrystal, and S. B. Hagerty (2015). „Quantifying uncertainty in stable isotope mixing models." In: *J. Geophys. Res. Biogeosciences* 120.5, pp. 903–923. DOI: 10.1002/2014JG002839 (cit. on p. 17).

J. R. Delsman, G. H. Oude Essink, K. J. Beven, and P. J. Stuyfzand (2013). „Uncertainty estimation of end-member mixing using generalized likelihood uncertainty estimation (GLUE), applied in a lowland catchment." In: *Water Resour. Res.* 49.8, pp. 4792–4806. DOI: 10.1002/wrcr.20341 (cit. on pp. 16, 17, 25, 26, 37, 54).

Der Schweizerische Bundesrat (2018). *Gewässerschutzverordnung* (cit. on p. 62).

S. Dogramaci, G. Skrzypek, W. Dodson, and P. F. Grierson (2012). „Stable isotope and hydrochemical evolution of groundwater in the semi-arid

Hamersley Basin of subtropical northwest Australia." In: *J. Hydrol.* 475, pp. 281–293. DOI: 10.1016/j.jhydrol.2012.10.004 (cit. on p. 21).

J. M. Doyle, T. Gleeson, A. H. Manning, and K. U. Mayer (2015). „Using noble gas tracers to constrain a groundwater flow model with recharge elevations: A novel approach for mountainous terrain." In: *Water Resour. Res.* 51.10, pp. 8094–8113. DOI: 10.1002/2015WR017274 (cit. on p. 100).

DURRIDGE (2019). *Rad7 Electronic Radon Detector–User Manual*. Billerica, MA 01821 (cit. on p. 53).

D. Dwivedi, B. Arora, C. I. Steefel, B. Dafflon, and R. Versteeg (2018). „Hot Spots and Hot Moments of Nitrogen in a Riparian Corridor." In: *Water Resour. Res.* 54.1, pp. 205–222. DOI: 10.1002/2017WR022346 (cit. on p. 85).

B. Elberling, A. Michelsen, C. Schädel, E. A. G. Schuur, H. H. Christiansen, L. Berg, M. P. Tamstorf, and C. Sigsgaard (2013). „Long-term CO_2 production following permafrost thaw." In: *Nat. Clim. Chang.* 3.10, pp. 890–894. DOI: 10.1038/nclimate1955 (cit. on p. 101).

E. B. Erhardt and E. J. Bedrick (2013). „A Bayesian framework for stable isotope mixing models." In: *Environ. Ecol. Stat.* 20.3, pp. 377–397. DOI: 10.1007/s10651-012-0224-1 (cit. on p. 17).

W. Eschenbach, D. Budziak, J. Elbracht, H. Höper, L. Krienen, R. Kunkel, K. Meyer, R. Well, and F. Wendland (2018). „Possibilities and limitations of validating modelled nitrate inputs into groundwater at the macroscale using the N2/Ar-method." In: *Grundwasser* 23.2, pp. 125–139. DOI: 10.1007/s00767-018-0391-6 (cit. on pp. 71, 80).

European Union (1991). „Directive 91/676/CEE concerning the protection of waters against pollution caused by nitrates from agricultural sources." In: *Off. J. Eur. Communities* L, pp. 1–8. DOI: 10.1017/CBO9781107415324.004 (cit. on p. 70).

G. Ferguson and T. Gleeson (2012). „Vulnerability of coastal aquifers to groundwater use and climate change." In: *Nat. Clim. Chang.* 2.5, pp. 342–345. DOI: 10.1038/nclimate1413 (cit. on p. 5).

I. Friedman, A. C. Redfield, B. Schoen, and J. Harris (1964). „The variation of the deuterium content of natural waters in the hydrologic cycle." In: *Rev. Geophys.* 2.1, p. 177. DOI: 10.1029/RG002i001p00177 (cit. on p. 100).

W. P. Gardner, G. A. Harrington, D. K. Solomon, and P. G. Cook (2011). „Using terrigenic ^{4}He to identify and quantify regional groundwater discharge to streams." In: *Water Resour. Res.* 47.6, pp. 1–13. DOI: 10.1029/2010WR010276 (cit. on pp. 18, 21, 22, 52).

T. Gleeson, A. H. Manning, A. Popp, M. Zane, and J. F. Clark (2018). „The suitability of using dissolved gases to determine groundwater

discharge to high gradient streams." In: *J. Hydrol.* 557, pp. 561–572. DOI: 10.1016/j.jhydrol.2017.12.022 (cit. on pp. 48, 51).

C. T. Green, L. J. Puckett, J. K. Böhlke, B. A. Bekins, S. P. Phillips, L. J. Kauffman, J. M. Denver, and H. M. Johnson (2008). „Limited Occurrence of Denitrification in Four Shallow Aquifers in Agricultural Areas of the United States." In: *J. Environ. Qual.* 37.3, p. 994. DOI: 10.2134/jeq2006.0419 (cit. on pp. 71, 80).

T. R. Green, M. Taniguchi, H. Kooi, J. J. Gurdak, D. M. Allen, K. M. Hiscock, H. Treidel, and A. Aureli (2011). „Beneath the surface of global change: Impacts of climate change on groundwater." In: *J. Hydrol.* 405.3-4, pp. 532–560. DOI: 10.1016/j.jhydrol.2011.05.002 (cit. on pp. 48, 99).

P. M. Groffman, K. Butterbach-Bahl, R. W. Fulweiler, A. J. Gold, J. L. Morse, E. K. Stander, C. Tague, C. Tonitto, and P. Vidon (2009). „Challenges to incorporating spatially and temporally explicit phenomena (hotspots and hot moments) in denitrification models." In: *Biogeochemistry* 93.1-2, pp. 49–77. DOI: 10.1007/s10533-008-9277-5 (cit. on p. 70).

P. M. Groffman, M. A. Altabet, J. K. Böhlke, K. Butterbach-Bahl, M. B. David, M. K. Firestone, A. E. Giblin, T. M. Kana, L. P. Nielsen, and M. A. Voyteck (2006). „Methods for measuring denitrification: diverse approaches to a difficult problem." In: *Ecol. Appl.* 16.6, pp. 2091–2122. DOI: 10.1890/1051-0761(2006)016[2091:MFMDDA]2.0.CO;2 (cit. on pp. 70, 71, 100).

C. Gu, W. Anderson, and F. Maggi (2012). „Riparian biogeochemical hot moments induced by stream fluctuations." In: *Water Resour. Res.* 48.9, pp. 1–17. DOI: 10.1029/2011WR011720 (cit. on p. 70).

A. Hayakawa, M. Hatakeyama, R. Asano, Y. Ishikawa, and S. Hidaka (2013). „Nitrate reduction coupled with pyrite oxidation in the surface sediments of a sulfide-rich ecosystem." In: *J. Geophys. Res. Biogeosciences* 118.2, pp. 639–649. DOI: 10.1002/jgrg.20060 (cit. on pp. 72, 74).

T. H. E. Heaton and J. C. Vogel (1981). „"Excess air" in groundwater." In: *J. Hydrol.* 50, pp. 201–216. DOI: 10.1016/0022-1694(81)90070-6 (cit. on pp. 8, 51, 80, 87).

P. D. Henne, M. Bigalke, U. Büntgen, D. Colombaroli, M. Conedera, U. Feller, D. Frank, J. Fuhrer, M. Grosjean, O. Heiri, J. Luterbacher, A. Mestrot, A. Rigling, O. Rössler, C. Rohr, T. Rutishauser, M. Schwikowski, A. Stampfli, S. Szidat, J.-P. Theurillat, R. Weingartner, W. Wilcke, and W. Tinner (2018). „An empirical perspective for understanding climate change impacts in Switzerland." In: *Reg. Environ. Chang.* 18.1, pp. 205–221. DOI: 10.1007/s10113-017-1182-9 (cit. on p. 48).

B. Herbstritt, B. Gralher, and M. Weiler (2019). „Continuous, near-real-time observations of water stable isotope ratios during rainfall and

throughfall events." In: *Hydrol. Earth Syst. Sci.* 23.7, pp. 3007–3019. DOI: 10.5194/hess-23-3007-2019 (cit. on pp. 48, 100).

A. R. Hill, K. J. Devito, and P. G. Vidon (2014). „Long-term nitrate removal in a stream riparian zone." In: *Biogeochemistry* 121.2, pp. 425–439. DOI: 10.1007/s10533-014-0010-2 (cit. on p. 70).

E. Hoehn and H. R. Von Gunten (1989). „Radon in groundwater: A tool to assess infiltration from surface waters to aquifers." In: *Water Resour. Res.* 25.8, pp. 1795–1803. DOI: 10.1029/WR025i008p01795 (cit. on pp. 49, 51, 55).

E. Hoehn, H. R. Von Gunten, F. Stauffer, and T. Dracos (1992). „Radon-222 as a Groundwater Tracer. A Laboratory Study." In: *Environ. Sci. Technol.* 26.4, pp. 734–738. DOI: 10.1021/es00028a010 (cit. on p. 51).

I. P. Holman (2006). „Climate change impacts on groundwater recharge-uncertainty, shortcomings, and the way forward?" In: *Hydrogeol. J.* 14.5, pp. 637–647. DOI: 10.1007/s10040-005-0467-0 (cit. on pp. 5, 48, 100).

J. Holocher, F. Peeters, W. Aeschbach-Hertig, W. Kinzelbach, and R. Kipfer (2003). „Kinetic model of gas bubble dissolution in groundwater and its implications for the dissolved gas composition." In: *Environ. Sci. Technol.* 37.7, pp. 1337–1343. DOI: 10.1021/es025712z (cit. on pp. 8, 9, 71, 76, 80, 87).

R. P. Hooper (2003). „Diagnostic tools for mixing models of stream water chemistry." In: *Water Resour. Res.* 39.3, pp. 55–61. DOI: 10.1029/2002WR001528 (cit. on pp. 17, 18, 22, 54).

R. P. Hooper, N. Christophersen, and N. E. Peters (1990). „Modelling streamwater chemistry as a mixture of soilwater end-members - An application to the Panola Mountain catchment, Georgia, U.S.A." In: *J. Hydrol.* 116.1-4, pp. 321–343. DOI: 10.1016/0022-1694(90)90131-G (cit. on pp. 16, 17).

R. W. Howarth (2019). „Ideas and perspectives: is shale gas a major driver of recent increase in global atmospheric methane?" In: *Biogeosciences* 16.15, pp. 3033–3046. DOI: 10.5194/bg-16-3033-2019 (cit. on p. 102).

IPCC (2013). *Climate Change 2013: The Physical Science Basis. Contribution of Working Group I to the Fifth Assessment Report of the Intergovernmental Panel on Climate Change [Stocker, T.F., D. Qin, G.-K. Plattner, M. Tignor, S.K. Allen, J. Boschung, A. Nauels, Y. Xia, V. Bex and P.M. Midgley (eds.)].* Tech. rep. Cambridge University Press, Cambridge, United Kingdom and New York, NY, USA, p. 1535 (cit. on p. 101).

J. A. Izbicki, N. F. Teague, P. B. Hatzinger, J. K. Böhlke, and N. C. Sturchio (2015). „Groundwater movement, recharge, and perchlorate occurrence in a faulted alluvial aquifer in California (USA)." In: *Hydrogeol. J.* 23.3, pp. 467–491. DOI: 10.1007/s10040-014-1217-y (cit. on p. 71).

W. G. Jacoby (2000). „Loess: a nonparametric, graphical tool for depicting relationships between variables.“ In: *Elect. Stud.* 19.4, pp. 577–613. DOI: 10.1016/S0261-3794(99)00028-1 (cit. on p. 76).

J. K. Jansson and N. Taş (2014). „The microbial ecology of permafrost.“ In: *Nat. Rev. Microbiol.* 12.6, pp. 414–425. DOI: 10.1038/nrmicro3262 (cit. on p. 101).

S. Jasechko (2016). „Partitioning young and old groundwater with geochemical tracers.“ In: *Chem. Geol.* 427, pp. 35–42. DOI: 10.1016/j.chemgeo.2016.02.012 (cit. on p. 16).

S. Jasechko (2019). „Global isotope hydrogeology—Review.“ In: *Rev. Geophys.* 57. DOI: 10.1029/2018RG000627 (cit. on pp. 5, 48, 49, 100, 102).

T. Jonas, C. Marty, and J. Magnusson (2009). „Estimating the snow water equivalent from snow depth measurements in the Swiss Alps.“ In: *J. Hydrol.* 378.1-2, pp. 161–167. DOI: 10.1016/j.jhydrol.2009.09.021 (cit. on p. 56).

T. M. Kana, C. Darkangelo, M. D. Hunt, J. B. Oldham, G. E. Bennett, and J. C. Cornwell (1994). „Membrane Inlet Mass Spectrometer for Rapid High-Precision Determination of N_2, O_2, and Ar in Environmental Water Samples.“ In: *Anal. Chem.* 66.23, pp. 4166–4170. DOI: 10.1021/ac00095a009 (cit. on pp. 71, 80).

D. Käser and D. Hunkeler (2015). „Contribution of alluvial groundwater to the outflow of mountainous catchments.“ In: *Water Resour. Res.* 51, pp. 9127–9140. DOI: 10.1002/2014WR016259 (cit. on pp. 49, 50, 54).

D. Kavetski, G. Kuczera, and S. W. Franks (2006). „Bayesian analysis of input uncertainty in hydrological modeling: 1. Theory.“ In: *Water Resour. Res.* 42.3 (cit. on p. 23).

C. D. Kennedy, D. P. Genereux, D. R. Corbett, and H. Mitasova (2009). „Relationships among groundwater age, denitrification, and the coupled groundwater and nitrogen fluxes through a streambed.“ In: *Water Resour. Res.* 45.9, pp. 1–15. DOI: 10.1029/2008WR007400 (cit. on pp. 71, 80).

R. Kipfer, W. Aeschbach-Hertig, F. Peeters, and M. Stute (2002). „Noble Gases in Lakes and Ground Waters.“ In: *Rev. Miner. Geochemistry* 47.1, pp. 615–700. DOI: 10.2138/rmg.2002.47.14 (cit. on pp. 6–8, 36, 52, 71, 72, 80, 87).

S. Klump, O. A. Cirpka, H. Surbeck, and R. Kipfer (2008). „Experimental and numerical studies on excess-air formation in quasi-saturated porous media.“ In: *Water Resour. Res.* 44.5, pp. 1–15. DOI: 10.1029/2007WR006280 (cit. on pp. 9, 71, 76, 80).

S. Klump, Y. Tomonaga, P. Kienzler, W. Kinzelbach, T. Baumann, D. M. Imboden, and R. Kipfer (2007). „Field experiments yield new insights into gas exchange and excess air formation in natural porous media.“

In: *Geochim. Cosmochim. Acta* 71.6, pp. 1385–1397. DOI: 10.1016/j.gca.2006.12.006 (cit. on pp. 71, 72, 81).

T. Kolbe, J.-R. de Dreuzy, B. W. Abbott, L. Aquilina, T. Babey, C. T. Green, J. H. Fleckenstein, T. Labasque, A. M. Laverman, J. Marçais, S. Peiffer, Z. Thomas, and G. Pinay (2019). „Stratification of reactivity determines nitrate removal in groundwater." In: *Proc. Natl. Acad. Sci.* 116.7, pp. 2494–2499. DOI: 10.1073/pnas.1816892116 (cit. on pp. 70, 100).

S. F. Korom (1992). „Natural denitrification in the saturated zone: A review." In: *Water Resour. Res.* 28.6, pp. 1657–1668. DOI: 10.1029/92WR00252 (cit. on pp. 10, 70).

S. Krause, F. Boano, M. O. Cuthbert, J. H. Fleckenstein, and J. Lewandowski (2014). „Understanding process dynamics at aquifer-surface water interfaces: An introduction to the special section on new modeling approaches and novel experimental technologies." In: *Water Resour. Res.* 50.2, pp. 1847–1855. DOI: 10.1002/2013WR014755 (cit. on p. 48).

S. Krause, J. Lewandowski, N. B. Grimm, D. M. Hannah, G. Pinay, K. McDonald, E. Martí, A. Argerich, L. Pfister, J. Klaus, T. Battin, S. T. Larned, J. Schelker, J. Fleckenstein, C. Schmidt, M. O. Rivett, G. Watts, F. Sabater, A. Sorolla, and V. Turk (2017). „Ecohydrological interfaces as hot spots of ecosystem processes." In: *Water Resour. Res.* 53.8, pp. 6359–6376. DOI: 10.1002/2016WR019516 (cit. on pp. 70, 74).

S. Krishnaswami, W. C. Graustein, K. K. Turekian, and J. F. Dowd (1982). „Radium, thorium and radioactive lead isotopes in groundwaters: Application to the in situ determination of adsorption-desorption rate constants and retardation factors." In: *Water Resour. Res.* 18.6, pp. 1663–1675. DOI: 10.1029/WR018i006p01663 (cit. on p. 51).

J. K. Kruschke (2015). „Markov Chain Monte Carlo." In: *Doing Bayesian Data Analysis*. 2nd ed. Academic Press. Chap. 7, pp. 143–191. DOI: 10.1016/B978-0-12-405888-0.00007-6 (cit. on pp. 26, 37).

J. T. Kulongoski, D. R. Hilton, R. G. Cresswell, S. Hostetler, and G. Jacobson (2008). „Helium-4 characteristics of groundwaters from Central Australia: Comparative chronology with chlorine-36 and carbon-14 dating techniques." In: *J. Hydrol.* 348.1-2, pp. 176–194. DOI: 10.1016/j.jhydrol.2007.09.048 (cit. on pp. 18, 21).

A.-M. Kurth, C. Weber, and M. Schirmer (2015). „How effective is river restoration in re-establishing groundwater-surface water interactions?–A case study." In: *Hydrol. Earth Syst. Sci.* 19.6, pp. 2663–2672. DOI: 10.5194/hess-19-2663-2015 (cit. on pp. 73, 78).

L. Mächler, M. S. Brennwald, and R. Kipfer (2013a). „Argon concentration time-series as a tool to study gas dynamics in the hyporheic zone." In: *Environ. Sci. Technol.* 47.13, pp. 7060–7066. DOI: 10.1021/es305309b (cit. on pp. 6, 72).

L. Mächler, S. Peter, M. S. Brennwald, and R. Kipfer (2013b). „Excess air formation as a mechanism for delivering oxygen to groundwater." In: *Water Resour. Res.* 49.10, pp. 6847–6856. DOI: 10.1002/wrcr.20547 (cit. on p. 72).

L. Mächler, M. S. Brennwald, and R. Kipfer (2012). „Membrane inlet mass spectrometer for the quasi-continuous on-site analysis of dissolved gases in groundwater." In: *Environ. Sci. Technol.* 46.15, pp. 8288–8296. DOI: 10.1021/es3004409 (cit. on p. 48).

J. Magnusson, D. Gustafsson, F. Hüsler, and T. Jonas (2014). „Assimilation of point SWE data into a distributed snow cover model comparing two contrasting methods." In: *Water Resour. Res.* 50.10, pp. 7816–7835. DOI: 10.1002/2014WR015302 (cit. on p. 56).

A. H. Manning and D. K. Solomon (2003). „Using noble gases to investigate mountain-front recharge." In: *J. Hydrol.* 275.3-4, pp. 194–207. DOI: 10.1016/S0022-1694(03)00043-X (cit. on p. 100).

B. Marty, T. Torgersen, V. Meynier, R. K. O'Nions, and G. de Marsily (1993). „Helium isotope fluxes and groundwater ages in the Dogger Aquifer, Paris Basin." In: *Water Resour. Res.* 29.4, pp. 1025–1035. DOI: 10.1029/93WR00007 (cit. on p. 18).

R. M. Maxwell and S. J. Kollet (2008). „Interdependence of groundwater dynamics and land-energy feedbacks under climate change." In: *Nat. Geosci.* 1.10, pp. 665–669. DOI: 10.1038/ngeo315 (cit. on pp. 48, 99).

E. B. McAleer, C. E. Coxon, K. G. Richards, M. M. Jahangir, J. Grant, and P. E. Mellander (2017). „Groundwater nitrate reduction versus dissolved gas production: A tale of two catchments." In: *Sci. Total Environ.* 586, pp. 372–389. DOI: 10.1016/j.scitotenv.2016.11.083 (cit. on pp. 71, 80).

P. B. McMahon, J. C. Thomas, J. T. Crawford, M. M. Dornblaser, and A. G. Hunt (2018a). „Methane in groundwater from a leaking gas well, Piceance Basin, Colorado, USA." In: *Sci. Total Environ.* 634, pp. 791–801. DOI: 10.1016/j.scitotenv.2018.03.371 (cit. on p. 102).

P. B. McMahon, J. C. Thomas, J. T. Crawford, M. M. Dornblaser, and A. G. Hunt (2018b). „Methane in groundwater from a leaking gas well, Piceance Basin, Colorado, USA." In: *Sci. Total Environ.* 634, pp. 791–801. DOI: 10.1016/j.scitotenv.2018.03.371 (cit. on p. 102).

M. M. Mekonnen and A. Y. Hoekstra (2015). „Global Gray Water Footprint and Water Pollution Levels Related to Anthropogenic Nitrogen Loads to Fresh Water." In: *Environ. Sci. Technol.* 49.21, pp. 12860–12868. DOI: 10.1021/acs.est.5b03191 (cit. on pp. 69, 101).

C. Mendoza-Lera and T. Datry (2017). „Relating hydraulic conductivity and hyporheic zone biogeochemical processing to conserve and restore river ecosystem services." In: *Sci. Total Environ.* 579, pp. 1815–1821. DOI: 10.1016/j.scitotenv.2016.11.166 (cit. on pp. 70, 72, 73).

C. Mendoza-Lera, A. Frossard, M. Knie, L. L. Federlein, M. O. Gessner, and M. Mutz (2016). „Importance of advective mass transfer and sediment surface area for streambed microbial communities.“ In: *Freshw. Biol.* 62.1, pp. 133–145. DOI: 10.1111/fwb.12856 (cit. on pp. 74, 78).

L. Merill and D. J. Tonjes (2014). „A review of the hyporheic zone, stream restoration, and means to enhance denitrification.“ In: *Crit. Rev. Environ. Sci. Technol.* 44.21, pp. 2337–2379. DOI: 10.1080/10643389.2013.829769 (cit. on p. 70).

A. Michel, T. Brauchli, M. Lehning, B. Schaefli, and H. Huwald (2020). „Stream temperature and discharge evolution in Switzerland over the last 50 years: annual and seasonal behaviour.“ In: *Hydrol. Earth Syst. Sci.* 24.1, pp. 115–142. DOI: 10.5194/hess-24-115-2020 (cit. on pp. 48, 50).

C. Moeck, A. Affolter, D. Radny, H. Dressmann, A. Auckenthaler, P. Huggenberger, and M. Schirmer (2017a). „Improved water resource management for a highly complex environment using three-dimensional groundwater modelling.“ In: *Hydrogeol. J.* DOI: 10.1007/s10040-017-1640-y (cit. on p. 19).

C. Moeck, J. Molson, and M. Schirmer (2019). „Pathline density distributions in a Null-Space Monte Carlo approach to assess groundwater pathways.“ In: *Groundwater*. DOI: 10.1111/gwat.12900 (cit. on p. 19).

C. Moeck, D. Radny, A. Auckenthaler, M. Berg, J. Hollender, and M. Schirmer (2017b). „Estimating the spatial distribution of artificial groundwater recharge using multiple tracers.“ In: *Isotopes Environ. Health Stud.* 53.5, pp. 484–499. DOI: 10.1080/10256016.2017.1334651 (cit. on pp. 26, 32).

C. Moeck, D. Radny, P. Borer, J. Rothardt, A. Auckenthaler, M. Berg, and M. Schirmer (2016). „Multicomponent statistical analysis to identify flow and transport processes in a highly-complex environment.“ In: *J. Hydrol.* 542, pp. 437–449. DOI: 10.1016/j.jhydrol.2016.09.023 (cit. on pp. 18–20, 22, 30, 32).

C. Moeck, D. Radny, A. Popp, M. Brennwald, S. Stoll, A. Auckenthaler, M. Berg, and M. Schirmer (2017c). „Science of the Total Environment Characterization of a managed aquifer recharge system using multiple tracers.“ In: *Sci. Total Environ.* 609, pp. 701–714. DOI: 10.1016/j.scitotenv.2017.07.211 (cit. on pp. 18–20, 22, 30, 32).

T. Müller, K. Osenbrück, G. Strauch, S. Pavetich, K. S. Al-Mashaikhi, C. Herb, S. Merchel, G. Rugel, W. Aeschbach, and W. Sanford (2016). „Use of multiple age tracers to estimate groundwater residence times and long-term recharge rates in arid southern Oman.“ In: *Appl. Geochemistry* 74, pp. 67–83. DOI: 10.1016/j.apgeochem.2016.08.012 (cit. on pp. 18, 21).

M. E. Newcomer, S. S. Hubbard, J. H. Fleckenstein, U. Maier, C. Schmidt, M. Thullner, C. Ulrich, N. Flipo, and Y. Rubin (2018). „Influence of Hydrological Perturbations and Riverbed Sediment Characteristics on Hyporheic Zone Respiration of CO_2 and N_2." In: *J. Geophys. Res. Biogeosciences* 123.3, pp. 902–922. DOI: 10.1002/2017JG004090 (cit. on pp. 70, 78, 85).

S. Oana (1957). „Bestimmung von Argon in besonderem Hinblick auf gelöste Gase in natürlichen Gewässern." In: *J. Earth Sci. Nagoya Univ.* 5, pp. 103–105 (cit. on p. 71).

T. Oki and S. Kanae (2006). „Global hydrological cycles and world water resources." In: *Science* 313.5790, pp. 1068–1072. DOI: 10.1126/science.1128845 (cit. on p. 5).

M. Ozima and F. Podosek (1984). „Noble Gas Geochemistry." In: Cambridge University Press (cit. on p. 71).

A. I. Packman and M. Salehin (2003). „Relative roles of stream flow and sedimentary conditions in controlling hyporheic exchange." In: *Hydrobiologia* 494, pp. 291–297. DOI: 10.1023/A:1025403424063 (cit. on pp. 70, 73).

C. Paniconi and M. Putti (2015). „Physically based modeling in catchment hydrology at 50: Survey and outlook." In: *Water Resour. Res.* 51.9, pp. 7090–7129. DOI: 10.1002/2015WR017780 (cit. on p. 48).

A. Parnell and R. Inger (2019). *Stable Isotope Mixing Models in R with simmr*. Tech. rep. (cit. on p. 17).

D. Partington, P. Brunner, C. Simmons, R. Therrien, A. Werner, G. Dandy, and H. Maier (2011). „A hydraulic mixing-cell method to quantify the groundwater component of streamflow within spatially distributed fully integrated surface water–groundwater flow models." In: *Environ. Model. Softw.* 26.7, pp. 886–898. DOI: 10.1016/j.envsoft.2011.02.007 (cit. on p. 56).

F. Pelizardi, S. A. Bea, J. Carrera, and L. Vives (2017). „Identifying geochemical processes using End Member Mixing Analysis to decouple chemical components for mixing ratio calculations." In: *J. Hydrol.* 550, pp. 144–156. DOI: 10.1016/j.jhydrol.2017.04.010 (cit. on pp. 16, 17).

S. Peter, R. Rechsteiner, M. F. Lehmann, R. Brankatschk, T. Vogt, S. Diem, B. Wehrli, K. Tockner, and E. Durisch-Kaiser (2012). „Nitrate removal in a restored riparian groundwater system: Functioning and importance of individual riparian zones." In: *Biogeosciences* 9.11, pp. 4295–4307. DOI: 10.5194/bg-9-4295-2012 (cit. on p. 70).

E. Peters, A. Visser, B. Esser, and J. Moran (2018). „Tracers Reveal Recharge Elevations, Groundwater Flow Paths and Travel Times on Mount Shasta, California." In: *Water* 10.2, p. 97. DOI: 10.3390/w10020097 (cit. on p. 100).

A. M. Piper (1944). „A graphic procedure in the geochemical interpretation of water-analyses." In: *Trans. Am. Geophys. Union* 25.6, p. 914. DOI: 10.1029/TR025i006p00914 (cit. on p. 21).

A. L. Popp, C. C. Manning, M. S. Brennwald, and R. Kipfer (2020). „A new on-site method for tracing denitrification in riparian groundwater." In: *Environ. Sci. Technol.* DOI: 10.1021/acs.est.9b05393 (cit. on pp. 54, 63, 100).

A. L. Popp, A. Scheidegger, C. Moeck, M. S. Brennwald, and R. Kipfer (2019). „Integrating Bayesian groundwater mixing modeling with on-site helium analysis to identify unknown water sources." In: *Water Resour. Res.* 55. DOI: 10.1029/2019WR025677 (cit. on pp. 54, 102).

E. Prest, F. Hammes, S. Kötzsch, M. van Loosdrecht, and J. Vrouwenvelder (2013). „Monitoring microbiological changes in drinking water systems using a fast and reproducible flow cytometric method." In: *Water Res.* 47.19, pp. 7131–7142. DOI: 10.1016/j.watres.2013.07.051 (cit. on pp. 74, 92).

M. Price, P. K. Swart, and R. M. Price (2003). „Use of tritium and helium to define groundwater flow conditions in Everglades National Park." In: *Water Resour. Res.* 39.9, pp. 1–12. DOI: 10.1029/2002WR001929 (cit. on p. 18).

R Core Team (2018). *R: A Language and Environment for Statistical Computing*. R Foundation for Statistical Computing. Vienna, Austria (cit. on p. 26).

A. J. Ranalli and D. L. Macalady (2010). „The importance of the riparian zone and in-stream processes in nitrate attenuation in undisturbed and agricultural watersheds—A review of the scientific literature." In: *J. Hydrol.* 389.3-4, pp. 406–415. DOI: 10.1016/j.jhydrol.2010.05.045 (cit. on p. 70).

M. O. Rivett, S. R. Buss, P. Morgan, J. W. N. Smith, and C. D. Bemment (2008). „Nitrate attenuation in groundwater: a review of biogeochemical controlling processes." In: *Water Res.* 42.16, pp. 4215–32. DOI: 10.1016/j.watres.2008.07.020 (cit. on pp. 70, 72, 74, 83, 101).

J. Rockström, W. Steffen, K. Noone, Å. Persson, F. S. Chapin, E. F. Lambin, T. M. Lenton, M. Scheffer, C. Folke, H. J. Schellnhuber, B. Nykvist, C. A. de Wit, T. Hughes, S. van der Leeuw, H. Rodhe, S. Sörlin, P. K. Snyder, R. Costanza, U. Svedin, M. Falkenmark, L. Karlberg, R. W. Corell, V. J. Fabry, J. Hansen, B. Walker, D. Liverman, K. Richardson, P. Crutzen, and J. A. Foley (2009). „A safe operating space for humanity." In: *Nature* 461.7263, pp. 472–475. DOI: 10.1038/461472a (cit. on pp. 69, 101).

O. Rössler, N. Addor, L. Bernhard, S. Figura, N. Köplin, D. Livingstone, M. Schädler, J. Seibert, and R. Weingartner (2014). *Hydrological Responses To Climate Change : River Runoff and Groundwater* (cit. on p. 48).

O. Rössler, B. Diekkrüger, and J. Löffler (2012). „Potential drought stress in a Swiss mountain catchmentEnsemble forecasting of high mountain soil moisture reveals a drastic decrease, despite major uncertainties.“ In: *Water Resour. Res.* 48.4, pp. 1–19. DOI: 10.1029/2011WR011188 (cit. on p. 48).

J. Rueedi, R. Purtschert, U. Beyerle, C. Alberich, and R. Kipfer (2005). „Estimating groundwater mixing ratios and their uncertainties using a statistical multi parameter approach.“ In: *J. Hydrol.* 305, pp. 1–14. DOI: 10.1016/j.jhydrol.2004.06.044 (cit. on pp. 16, 17).

M. E. Sanborn, A. K. Souders, J. Wimpenny, Q.-Z. Yin, and M. Young (2016). „Bayesian nitrate source apportionment to individual groundwater wells in the Central Valley by use of elemental and isotopic tracers.“ In: *Water Resour. Res.* Pp. 1–21. DOI: 10.1002/2015WR018523 (cit. on p. 16).

D. L. Saunders and J. Kalff (2001). „Denitrification Rates in the Sediments of Lake Memphremagog, Canada-USA.“ In: *Water Res.* 35.8, pp. 1897–1904 (cit. on p. 70).

O. S. Schilling, P. G. Cook, and P. Brunner (2019). „Beyond Classical Observations in Hydrogeology: The Advantages of Including Exchange Flux, Temperature, Tracer Concentration, Residence Time, and Soil Moisture Observations in Groundwater Model Calibration.“ In: *Rev. Geophys.* 57.1, pp. 146–182. DOI: 10.1029/2018RG000619 (cit. on pp. 6, 48, 102).

O. S. Schilling, C. Gerber, D. J. Partington, R. Purtschert, M. S. Brennwald, R. Kipfer, D. Hunkeler, and P. Brunner (2017). „Advancing Physically-Based Flow Simulations of Alluvial Systems Through Atmospheric Noble Gases and the Novel ^{37}Ar Tracer Method.“ In: *Water Resour. Res.* 53.12, pp. 10465–10490. DOI: 10.1002/2017WR020754 (cit. on pp. 48, 54–56, 61).

P. Shuai, M. B. Cardenas, P. S. Knappett, P. C. Bennett, and B. T. Neilson (2017). „Denitrification in the banks of fluctuating rivers: The effects of river stage amplitude, sediment hydraulic conductivity and dispersivity, and ambient groundwater flow.“ In: *Water Resour. Res.* 53.9, pp. 7951–7967. DOI: 10.1002/2017WR020610 (cit. on p. 85).

E. Sinha, A. M. Michalak, and V. Balaji (2017). „Eutrophication will increase during the 21st century as a result of precipitation changes.“ In: *Science* 357.6349, pp. 405–408. DOI: 10.1126/science.aan2409 (cit. on pp. 69, 70).

G. Skrzypek, S. Dogramaci, and P. F. Grierson (2013). „Geochemical and hydrological processes controlling groundwater salinity of a large inland wetland of northwest Australia.“ In: *Chem. Geol.* 357, pp. 164–177. DOI: 10.1016/j.chemgeo.2013.08.035 (cit. on p. 21).

R. L. Smith, B. L. Howes, and J. H. Duff (1991). „Denitrification in nitrate-contaminated groundwater: Occurrence in steep vertical geochemical gradients." In: *Geochim. Cosmochim. Acta* 55.7, pp. 1815–1825. DOI: 10.1016/0016-7037(91)90026-2 (cit. on p. 70).

C. Soulsby, J. Petry, M. Brewer, S. Dunn, B. Ott, and I. Malcolm (2003). „Identifying and assessing uncertainty in hydrological pathways: a novel approach to end member mixing in a Scottish agricultural catchment." In: *J. Hydrol.* 274.1-4, pp. 109–128. DOI: 10.1016/S0022-1694(02)00398-0 (cit. on pp. 17, 26).

I. Spottke, E. Zechner, and P. Huggenberger (2005). „The southeastern border of the Upper Rhine Graben: A 3D geological model and its importance for tectonics and groundwater flow." In: *Int. J. Earth Sci.* 94.4, pp. 580–593. DOI: 10.1007/s00531-005-0501-4 (cit. on pp. 18, 19, 22).

C. Sprenger, G. Lorenzen, I. Hülshoff, G. Grützmacher, M. Ronghang, and A. Pekdeger (2011). „Vulnerability of bank filtration systems to climate change." In: *Sci. Total Environ.* 409.4, pp. 655–663. DOI: 10.1016/j.scitotenv.2010.11.002 (cit. on p. 5).

M. Sprenger, C. Stumpp, M. Weiler, W. Aeschbach, S. T. Allen, P. Benettin, M. Dubbert, A. Hartmann, M. Hrachowitz, J. W. Kirchner, J. J. McDonnell, N. Orlowski, D. Penna, S. Pfahl, M. Rinderer, N. Rodriguez, M. Schmidt, and C. Werner (2019). „The demographics of water: A review of water ages in the critical zone." In: *Rev. Geophys.* 2018RG000633. DOI: 10.1029/2018RG000633 (cit. on pp. 6, 48, 49, 61, 102).

R. Stenger, J. C. Clague, U. Morgenstern, and T. J. Clough (2018). „Vertical stratification of redox conditions, denitrification and recharge in shallow groundwater on a volcanic hillslope containing relict organic matter." In: *Sci. Total Environ.* 639, pp. 1205–1219. DOI: 10.1016/j.scitotenv.2018.05.122 (cit. on p. 71).

C. J. Stevens (2019). „Nitrogen in the environment." In: *Science* 363.6427, pp. 578–580. DOI: 10.1126/science.aav8215 (cit. on p. 69).

M. Stute, C. Sonntag, J. Deák, and P. Schlosser (1992a). „Helium in deep circulating groundwater in the Great Hungarian Plain: Flow dynamics and crustal and mantle helium fluxes." In: *Geochim. Cosmochim. Acta* 56.5, pp. 2051–2067. DOI: 10.1016/0016-7037(92)90329-H (cit. on p. 33).

M. Stute, P. Schlosser, J. F. Clark, and W. S. Broecker (1992b). „Paleotemperatures in the Southwestern United States Derived from Noble Gases in Ground Water." In: *Science* 256.5059, pp. 1000–1003. DOI: 10.1126/science.256.5059.1000 (cit. on p. 80).

B. Szymczycha, K. D. Kroeger, J. Crusius, and J. F. Bratton (2017). „Depth of the vadose zone controls aquifer biogeochemical conditions and extent of anthropogenic nitrogen removal." In: *Water Res.* 123, pp. 794–801. DOI: 10.1016/j.watres.2017.06.048 (cit. on pp. 71, 80).

D. Tetzlaff, J. Buttle, S. K. Carey, K. McGuire, H. Laudon, and C. Soulsby (2015). „Tracer-based assessment of flow paths, storage and runoff generation in northern catchments: a review." In: *Hydrol. Process.* 29.16, pp. 3475–3490. DOI: 10.1002/hyp.10412 (cit. on pp. 31, 33).

I. Tolstikhin and I. Kamenskiy (1969). „Determination of Groundwater Ages by the T-^{3}He Method." In: *Geochemistry Int.* 6, pp. 810–811 (cit. on p. 36).

M. R. Turetsky, B. W. Abbott, M. C. Jones, K. Walter Anthony, D. Olefeldt, E. A. G. Schuur, C. Koven, A. D. McGuire, G. Grosse, P. Kuhry, G. Hugelius, D. M. Lawrence, C. Gibson, and A. B. K. Sannel (2019). „Permafrost collapse is accelerating carbon release." In: *Nature* 569.7754, pp. 32–34. DOI: 10.1038/d41586-019-01313-4 (cit. on pp. 101, 102).

C. Turnadge and B. D. Smerdon (2014). „A review of methods for modelling environmental tracers in groundwater: Advantages of tracer concentration simulation." In: *J. Hydrol.* 519, pp. 3674–3689. DOI: 10.1016/j.jhydrol.2014.10.056 (cit. on p. 16).

UNEA (2017). *Towards a Pollution-Free Planet*. Kenya (cit. on p. 70).

S. Uyanik, S. Demirel, N. Dursun, A. Kilic, O. Cinar, and E. Sahinkaya (2011). „Simultaneous heterotrophic and sulfur-oxidizing autotrophic denitrification process for drinking water treatment: Control of sulfate production." In: *Water Res.* 45.20, pp. 6661–6667. DOI: 10.1016/j.watres.2011.09.056 (cit. on pp. 72, 74).

J. F. Valder, A. J. Long, A. D. Davis, and S. J. Kenner (2012). „Multivariate statistical approach to estimate mixing proportions for unknown end members." In: *J. Hydrol.* 460-461, pp. 65–76. DOI: 10.1016/j.jhydrol.2012.06.037 (cit. on pp. 16, 17, 22).

J. C. Vogel, A. S. Talma, and T. H. Heaton (1981). „Gaseous nitrogen as evidence for denitrification in groundwater." In: *J. Hydrol.* 50.C, pp. 191–200. DOI: 10.1016/0022-1694(81)90069-X (cit. on pp. 71, 80).

A. S. Ward and A. I. Packman (2018). „Advancing our predictive understanding of river corridor exchange." In: *Wiley Interdiscip. Rev. Water* 6.1, e1327. DOI: 10.1002/wat2.1327 (cit. on p. 70).

West Systems (2019). *High resolution Methane and Carbon Dioxide diffuse flux meter*. Tech. rep. Firenze, Italy, pp. 1–4 (cit. on p. 101).

D. Weymann, R. Well, H. Flessa, C. V. D. Heide, M. Deurer, K. Meyer, C. Konrad, W. Walther, T. Drive, P. North, and N. Zealand (2008). „Groundwater N_2O emission factors of nitrate-contaminated aquifers as derived from denitrification progress and N_2O accumulation." In: *Biogeosciences* 5, pp. 1215–1226 (cit. on pp. 71, 80).

WHO (2011). „Guidelines for Drinking-water Quality." In: *World Heal. Organ.* 4 (cit. on p. 70).

G. B. Wilson, J. N. Andrews, and A. H. Bath (1990). „Dissolved gas evidence for denitrification in the Lincolnshire Limestone groundwaters,

eastern England." In: *J. Hydrol.* 113.1-4, pp. 51–60. DOI: 10.1016/0022-1694(90)90166-U (cit. on pp. 71, 80, 85).

T. C. Winter (1995). „Recent advances in understanding the interaction of groundwater and surface water." In: *Rev. Geophys.* 33.2 S, pp. 985–994. DOI: 10.1029/95RG00115 (cit. on pp. 5, 48).

T. C. Winter (1999). „Relation of streams, lakes, and wetlands to groundwater flow systems." In: *Hydrogeol. J.* 7.1, pp. 28–45. DOI: 10.1007/s100400050178 (cit. on p. 5).

T. C. Winter, J. W. Harvey, O. L. Franke, and W. M. Alley (1998). „Ground Water and Surface Water: A Single Resource." In: *U.S. Geol. Surv.* (Cit. on p. 48).

M. Würsten (1991). *GWB–Hydrogeologische Untersuchungen Aeschau: Schlussbericht*. Tech. rep. Zurich: Geotechnisches Institut (cit. on p. 49).

C. Yu, X. Huang, H. Chen, H. C. J. Godfray, J. S. Wright, J. W. Hall, P. Gong, S. Ni, S. Qiao, G. Huang, Y. Xiao, J. Zhang, Z. Feng, X. Ju, P. Ciais, N. C. Stenseth, D. O. Hessen, Z. Sun, L. Yu, W. Cai, H. Fu, X. Huang, C. Zhang, H. Liu, and J. Taylor (2019). „Managing nitrogen to restore water quality in China." In: *Nature* 567.7749, pp. 516–520. DOI: 10.1038/s41586-019-1001-1 (cit. on p. 70).

A. Yudhowijoyo, R. Rafati, A. Sharifi Haddad, M. S. Raja, and H. Hamidi (2018). „Subsurface methane leakage in unconventional shale gas reservoirs: A review of leakage pathways and current sealing techniques." In: *J. Nat. Gas Sci. Eng.* 54, pp. 309–319. DOI: 10.1016/j.jngse.2018.04.013 (cit. on pp. 101, 102).